El 59

UDC 621.313.33 : 519.62/.64

ACTA POLYTECHNICA SCANDINAVICA

ELECTRICAL ENGINEERING SERIES No. 59

Analysis of Induction Motors Based on the Numerical Solution of the Magnetic Field and Circuit Equations

ANTERO ARKKIO

Helsinki University of Technology
Laboratory of Electromechanics
SF-02150 Espoo, Finland

Thesis for the degree of Doctor of Technology to be presented with due permission for public examination and criticism in Auditorium S4 at Helsinki University of Technology, Otaniemi, Finland, on the 18th of December, 1987, at 12 o'clock noon.

HELSINKI 1987

Arkkio, A., **Analysis of induction motors based on the numerical solution of the magnetic field and circuit equations.** Acta Polytechnica Scandinavica, Electrical Engineering Series No. 59, Helsinki 1987, 97 pp. ISBN 951-666-250-1. ISSN 0001-6845. UDC 621.313.33 : 519.62/.64
Keywords: Induction motors, finite element analysis

ABSTRACT

A method for the analysis of induction motors is presented. The analysis is based on the combined solution of the magnetic field equations and the circuit equations of the windings. The equations are discretized by the finite element method. The magnetic field is assumed to be two-dimensional. The three-dimensional features i.e. the skew of the rotor slots and the end-region fields are taken into account within the two-dimensional formulation. The general time-dependence of the field and the motion of the rotor are modelled correctly in a step-by-step solution. The amount of computation is reduced significantly if the time-dependence is assumed to be sinusoidal and phasor quantities are used in the solution.

The method is applied to the calculation of a cage rotor motor and of a solid rotor motor. The sinusoidal approximation gives good results in the computation of steady-state locked-rotor quantities, but it does not model the motion of the rotor properly. The step-by-step method is used for computing machine quantities in steady and transient states. For instance the operation of the solid rotor motor supplied by a static frequency converter is simulated. The results obtained by the method agree well with the measured ones.

PREFACE

This work was carried out at the Laboratory of Electromechanics, Helsinki University of Technology. The work is part of a research project concerning the effects of magnetic saturation on the performance properties of induction motors.

I wish to express my gratitude to Professor Tapani Jokinen, Head of the Laboratory of Electromechanics, for his encouragement and advice during the course of the work, and to Dr Jorma Luomi, Associate professor of Electromechanics, for advice and discussions about numerical methods and the theory of electrical machines.

I also wish to thank Mr Alpo Hauru, Mr Asko Niemenmaa, Mr Antti Suontausta and the other members of the research group for helpful discussions and the technical staff of the Laboratory for assistance in the measurements. Mr Alpo Hauru put at my disposal the measurement and plotting routines used for recording the waveforms of machine quantities.

I am obliged to Mrs Ruth Vilmi for revision of the language.

Financial support by the Academy of Finland and by the Foundation of Technology in Finland is gratefully acknowledged.

Espoo, September 1987
Antero Arkkio

CONTENTS

LIST OF SYMBOLS

Boldface symbols are used for vectors and matrices. Symbols of complex quantities are underlined.

$\mathbf{A}$	vector potential
A	z-component of $\mathbf{A}$
$\mathbf{a}$	column vector of the nodal values of vector potential
a_i	i^{th} element of $\mathbf{a}$
a	number of parallel paths
$\mathbf{B}$	magnetic flux density
$\mathbf{D}$	electric flux density
$\mathbf{D}^r$	matrix defined in Eq. (75)
$\mathbf{D}^s$	matrix defined in Eq. (63)
$\mathbf{E}$	electric field strength
$\mathbf{e}_z$	unit vector parallel to the z-axis
$\mathbf{H}$	magnetic field strength
$\underline{h}$	periodicity factor
I	current
$\mathbf{i}^r$	column vector of the rotor bar currents
$\mathbf{i}^s$	column vector of the currents of the stator winding
i_+	positive phase-sequence current
$\mathbf{J}$	current density
J	z-component of $\mathbf{J}$
J_m	moment of inertia
$\mathbf{K}$	connection matrix associated with the stator winding
L_b	end-winding inductance
l	length of a conductor/length of the core region
l_b	average length of the winding overhang
N	shape function in the finite element method
N_c	number of turns in series in a coil
N_n	number of nodes in a finite element mesh
N_s	number of symmetry sectors in a machine
$\mathbf{M}$	connection matrix associated with the rotor cage
P_{in}	input power of a motor
P_{out}	output (shaft) power of a motor
P_{res}	resistive losses in a winding
p	number of pole pairs
Q	number of slots
q	number of slots per pole and phase

R	resistance
R_s	resistance of a stator phase winding
R_r	resistance of a rotor bar
r,φ,z	coordinates of a circular cylindrical coordinate system
S	integration surface
S_n	cross sectional area of coil side n
s	slip
T	period of time of an AC cycle
T_e	electromagnetic torque
T_s	shaft torque
t	time
U	scalar potential difference
$\mathbf{u}^r$	column vector of the potential differences of the rotor bars
$\mathbf{u}^s$	column vector of the potential differences of the stator winding
u_+	positive phase-sequence voltage
V	volume
$\mathbf{v}$	velocity
$\mathbf{v}^s$	column vector of the line voltages
W	weight function in Galerkin's method
W_{em}	energy of the electromagnetic field
x,y,z	cartesian coordinates
$\underline{\mathbf{Z}}_{be}$	impedance matrix of the ends of the rotor bars
$\underline{\mathbf{Z}}_{sc}$	impedance matrix of the end rings of a cage winding
β^r_n	function defined in Eq. (73)
β^s_n	function defined in Eq. (60)
Γ	integration path
γ	angle of a symmetry sector
ϕ	electric scalar potential
λ_b	parameter related to the end-winding inductance
μ	permeability
μ_0	permeability of vacuum
ν	reluctivity
ν_{ef}	effective reluctivity
σ	conductivity
Ψ	flux linkage
Ω	integration surface
Ω_m	mechanical angular frequency
ω	electrical angular frequency

1 INTRODUCTION

1.1 The need for field analysis

The design of an electrical machine is based on the knowledge of the magnetic field in the machine. The exact field distribution may be solved from Maxwell's equations. The complicated geometries of electrical machines and the nonlinearity due to the saturation of the iron core, however, make the solution of the field equations very laborious. Furthermore, the field equations are coupled to the voltage equations of the windings and the motion equation of the rotor. The equations should be solved together as a system of equations.

In the conventional design of an induction motor the field is known only approximately. The dimensioning of the iron core and the evaluation of the machine characteristics are based on a rough idea of the field distribution in the core. These methods usually give satisfactory results for steady-state operation near the synchronous speed of the machine, but for locked-rotor or transient operation the results are unreliable.

Conventional calculation routines have usually been designed for the analysis of cage or wound-rotor induction motors supplied by sinusoidal voltages. They are not directly applicable to the analysis of motors supplied by static frequency converters or motors of special construction, e.g. solid rotor induction motors.

More reliable calculation methods are needed especially in the design of large machines, as it is very expensive to construct full-size prototypes to test the validity of the design. It is also important to know the transient performance of high-power induction motors accurately, e.g. in starting, in order to be able to determine the requirements imposed on the power supply.

During the last decades a lot of research work has been done associated with the numerical field analysis. The development of solution methods and the growth of computer capacities have made it possible to solve more and more involved magnetic field problems. In particular, the finite element method has proven to be efficient when dealing with complicated geometries. The solution of the three-dimensional time-dependent magnetic field of an induction motor is, however, still too large a task. The problem must be simplified by assuming the magnetic field to be two-dimensional, independent of the coordinate parallel to the shaft of the machine.

In this work numerical field analysis is applied to the calculation of induction motors. The evaluation of machine characteristics is based on the finite element solution of the magnetic field. The field is assumed to be two-dimensional. The three-dimensionality of the machine, i.e. the end-region fields and the effect of skewed rotor bars, is taken into account within the two-dimensional model. The aim is to develop methods and to construct computation routines that can be applied to the analysis of induction motors in steady and transient states.

1.2 Equations of the electromagnetic field

In this section the differential equations of the scalar and vector potentials are derived from Maxwell's equations. The aim is to give the basic field theoretical material for the next two sections that contain the discretization of the field equations by the finite element method and a short review of the numerical field analysis of induction motors.

The induction motor is treated as a quasi-static magnetic system. The field quantities satisfy the equations

$$\nabla \times \mathbf{E} = -\frac{\partial \mathbf{B}}{\partial t} \tag{1}$$

$$\nabla \times \mathbf{H} = \mathbf{J} \tag{2}$$

and the material equations

$$\mathbf{H} = \nu \mathbf{B} \tag{3}$$

$$\mathbf{J} = \sigma \mathbf{E} \tag{4}$$

where $\mathbf{E}$ is the electric field strength
$\mathbf{B}$ is the magnetic flux density
t is time
$\mathbf{H}$ is the magnetic field strength
$\mathbf{J}$ is the current density
ν is the reluctivity of the material
σ is the conductivity of the material.

The polarization and displacement currents are assumed to be small compared with the conductive currents in the conductors

$$\frac{\partial \mathbf{D}}{\partial t} << \mathbf{J} \tag{5}$$

where **D** is the electric flux density. At the frequencies encountered in electrical machines this is a good approximation. The reluctivity ν of the laminated iron core of an electrical machine is field-dependent. This leads to nonlinear field equations. An isotropic core material is assumed in the two-dimensional model.

Using the magnetic vector potential **A**

$$\mathbf{B} = \nabla \times \mathbf{A} \tag{6}$$

and the electric scalar potential ϕ we obtain from Eqs. (1) - (3)

$$\mathbf{E} = -\frac{\partial \mathbf{A}}{\partial t} - \nabla \phi \tag{7}$$

$$\nabla \times (\nu \nabla \times \mathbf{A}) = \mathbf{J} \tag{8}$$

The current density is given by

$$\mathbf{J} = -\sigma \frac{\partial \mathbf{A}}{\partial t} - \sigma \nabla \phi \tag{9}$$

It satisfies the continuity equation

$$\nabla \cdot \mathbf{J} = 0 \tag{10}$$

The equations for the vector and scalar potentials are obtained by substituting Eq. (9) in Eqs. (8) and (10)

$$\nabla \times (\nu \nabla \times \mathbf{A}) + \sigma \frac{\partial \mathbf{A}}{\partial t} + \sigma \nabla \phi = 0 \tag{11}$$

$$\nabla \cdot \left(\sigma \frac{\partial \mathbf{A}}{\partial t}\right) + \nabla \cdot (\sigma \nabla \phi) = 0 \tag{12}$$

The uniqueness of the solution requires that a value must be given to the divergence of the vector potential. The "Coulomb's gauge" condition

$$\nabla \cdot \mathbf{A} = 0 \tag{13}$$

is commonly used.

In a general three-dimensional case there are four unknown quantities (components of the vector potential and the scalar potential) in Eqs. (11) - (13). The unknown quantities depend on the three spatial coordinates and time. Because of the complicated geometry of an induction motor and the nonlinearity of iron the solution of Eqs. (11) - (13) is usually beyond the capacities of present-day computers. The problem must be simplified.

The solution of the field equations becomes much easier if it is possible to use a two-dimensional model in which the geometry and the material quantities are independent of e.g. the z-coordinate, and the vector potential and the current density are given by

$$\begin{aligned} \mathbf{A} &= A(x,y,t)\, \mathbf{e}_z \\ \mathbf{J} &= J(x,y,t)\, \mathbf{e}_z \end{aligned} \tag{14}$$

where x and y are the cartesian spatial coordinates
$\mathbf{e}_z$ is the unit vector parallel to the z-axis.

The expressions in Eq. (14) give satisfactory approximations for the field and current density inside the core region of an unskewed electrical machine. When this model is used in the calculation of a skewed induction motor, the effects of end-region fields and skewed rotor conductors must be taken into account separately (Chapter 2). The end of this section is devoted to the two-dimensional equations.

When Eqs. (14) are substituted in Eq. (9) it is seen that the scalar potential must be a linear function of the z-coordinate in a two-dimensional conductor

$$\phi = \phi_1 z + \phi_0 \tag{15}$$

If there are several conductors in a two-dimensional field region and the conductors are separated from each other by dielectric materials, the linear dependence on the z-coordinate is valid in every conductor separately. There may be potential differences between the conductors. The continuity of the scalar potential implies that the potential is also x- and y-dependent in the dielectric

regions. As a potential difference causes no currents in a dielectric medium, the exact solution of the scalar potential is not needed in these regions.

When the two-dimensional model is used to calculate a straight conductor of length l, the scalar potential difference between the ends of the conductor is given by

$$U = \int_{\Gamma} -\nabla \phi \cdot d\mathbf{l} = -\phi_1 \, l \tag{16}$$

A relation between the potential difference and the total current of the conductor is obtained by integrating the current density over the cross section S of the conductor

$$I = \int_S \mathbf{J} \cdot d\mathbf{S} = \int_S \left(-\sigma \frac{\partial \mathbf{A}}{\partial t} - \sigma \nabla \phi \right) \cdot d\mathbf{S}$$

$$= -\int_S \sigma \frac{\partial \mathbf{A}}{\partial t} \cdot d\mathbf{S} + U \frac{1}{l} \int_S \sigma \, dS \tag{17}$$

If symbol R is used for the DC resistance of the conductor

$$R = \frac{l}{\int_S \sigma \, dS} \tag{18}$$

the voltage equation of the conductor becomes

$$U = R\, I + R \int_S \sigma \frac{\partial \mathbf{A}}{\partial t} \cdot d\mathbf{S} \tag{19}$$

Three basic cases may be encountered in the solution of the magnetic field induced by a single two-dimensional conductor. If the current density of the conductor is known a priori, the vector potential can be solved directly from Eq. (8). This case is strictly valid only if there is no time-dependence. If the potential difference between the ends of the conductor is known, the equation for the vector potential is

$$\nabla \times (\nu \nabla \times \mathbf{A}) + \sigma \frac{\partial \mathbf{A}}{\partial t} = \frac{\sigma}{l} U \mathbf{e}_z \tag{20}$$

If the total current of the conductor is taken as the source of the field, the vector potential satisfies the integrodifferential equation

$$\nabla \times (\nu \nabla \times \mathbf{A}) + \sigma \frac{\partial \mathbf{A}}{\partial t} - \frac{\sigma R}{l} \int_S \sigma \frac{\partial \mathbf{A}}{\partial t} \cdot d\mathbf{S}\, \mathbf{e}_z = \frac{\sigma R}{l} I \mathbf{e}_z \tag{21}$$

An alternative method for the last case is to solve the voltage equation (19) and the field equation (20) together as a system of two equations.

In a more general case there are several conductors in the solution region. The conductors are connected in series and in parallel and they are fed from voltage and current sources. In this case the voltage equations of the conductors must always be solved together with the field equation of the whole system. A detailed treatment of the solution of the voltage and field equations of an induction motor is given in Section 2.3.

The time-coordinate must usually be discretized in the solution of time-dependent field equations. If the system under consideration consists of stationary, magnetically linear materials only, a sinusoidally varying source (potential difference or current) induces a sinusoidally varying magnetic field. In this special case the time-dependence can be eliminated from the equations by using complex field quantities. The physical quantities are obtained as the real parts of the complex variables. In the two-dimensional case the vector potential and the current density are

$$\begin{aligned} \mathbf{A} &= \mathrm{Re}\{ \underline{A}(x,y)\, e^{j\omega t}\}\, \mathbf{e}_z \\ \mathbf{J} &= \mathrm{Re}\{ \underline{J}(x,y)\, e^{j\omega t}\}\, \mathbf{e}_z \end{aligned} \tag{22}$$

where ω is the angular frequency of the time variation. In the assumption of sinusoidal time variation Eq. (20), for example, becomes

$$\nabla \times (\nu \nabla \times \underline{\mathbf{A}}) + j\sigma\omega \underline{\mathbf{A}} = \frac{\sigma}{l} \underline{U}\, \mathbf{e}_z \tag{23}$$

The assumption of sinusoidal time variation is valid only in steady state. If there are nonlinear materials present, a sinusoidally time varying source does not

induce a sinusoidally varying magnetic field. However, in order to simplify the solution procedure, the sinusoidal approximation is often used also in nonlinear cases.

If the true time-dependence of the field quantities in a nonlinear system is needed, the field equations must be solved by a step-by-step method evaluating the variation of the field in short time intervals Δt. In the Crank-Nicholson method the vector potential at a time step k+1 is approximated

$$\mathbf{A}_{k+1} = \frac{1}{2}\left\{ \frac{\partial \mathbf{A}}{\partial t}\Big|_{k+1} + \frac{\partial \mathbf{A}}{\partial t}\Big|_{k} \right\} \Delta t + \mathbf{A}_k \tag{24}$$

When Eq. (20) is written at time steps k+1 and k and the equations obtained are added together, the equation

$$\nabla \times (\nu_{k+1} \nabla \times \mathbf{A}_{k+1}) + \nabla \times (\nu_k \nabla \times \mathbf{A}_k) + \sigma \left\{ \frac{\partial \mathbf{A}}{\partial t}\Big|_{k+1} + \frac{\partial \mathbf{A}}{\partial t}\Big|_{k} \right\}$$

$$= \frac{\sigma}{l} \{U_{k+1} + U_k\} \mathbf{e}_z \tag{25}$$

is obtained. When the sum of derivatives in Eq. (24) is substituted in Eq. (25) and the terms corresponding to the time step k are transferred to the right hand side of the equation, Eq. (25) becomes

$$\nabla \times (\nu_{k+1} \nabla \times \mathbf{A}_{k+1}) + \frac{2\sigma}{\Delta t} \mathbf{A}_{k+1}$$

$$= \frac{\sigma}{l} U_{k+1} \mathbf{e}_z - \left\{ \nabla \times (\nu_k \nabla \times \mathbf{A}_k) - \frac{2\sigma}{\Delta t} \mathbf{A}_k - \frac{\sigma}{l} U_k \mathbf{e}_z \right\} \tag{26}$$

All terms on the right hand side of Eq. (26), the vector potential at the previous time step k and the source potential differences, are known quantities. Thus Eq. (26) is a spatial coordinate dependent, partial differential equation for the vector potential at time $t = t_{k+1}$. Starting from the initial values and evaluating successively the vector potentials of the next time steps the true time variation of the field is worked out. This procedure, however, requires much computation time because e.g. in the solution of an induction motor every period of line frequency must be divided into hundreds of time intervals in order to get accurate results (Chapter 3).

The boundary and initial values of the vector potential must be known in the solution of the field equations. The solution region should be chosen accordingly.

In the field analysis of an induction motor it is usually assumed that the outer surface of the machine is an equipotential surface of the vector potential. This assumption means that no flux penetrates through the outer surface of the machine.

1.3 Finite element solution of the field equations

The finite element method (FEM) is commonly used in the solution of magnetic fields. Nothing new about FEM is presented in this section. The equations used in the Newton-Raphson iteration method are derived because the same matrix elements are needed in Section 2.3 for the solution of the coupled field and circuit equations. The details of FEM can be found e.g. in Zienkiewicz (1983).

There are two commonly used formulations for the solution of a field problem by FEM. An energy related functional may be formed from the field quantities. The solution of the field equations is given as a stationary point of the functional. Chari et al. (1982) derived a functional associated with Eqs. (11) and (12) in a general three-dimensional case. The other alternative is to use a method of weighted residuals e.g. Galerkin's method. In this work Galerkin's method is used in the discretization of the two-dimensional field equation (26).

In order to shorten the notation Eq. (26) is written in the form

$$\nabla \times (\nu \nabla \times \mathbf{A}) + \frac{2\sigma}{\Delta t}\mathbf{A} = g\,\mathbf{e}_z \tag{27}$$

where the vector $g\,\mathbf{e}_z$ denotes the right hand side of Eq. (26) and the indices of time steps are neglected. In a method of weighted residuals Eq. (27) is multiplied by a weight function vector $\mathbf{We}_z$ and integrated over the volume V of the solution region

$$\int_V \left\{ [\nabla \times (\nu \nabla \times \mathbf{A})] \cdot \mathbf{We}_z + \frac{2\sigma}{\Delta t}\mathbf{A} \cdot \mathbf{We}_z - g\,W \right\} dV = 0 \tag{28}$$

In the two-dimensional model **A** is parallel to the z-axis. Eq. (28) can be transformed to the form

$$\int_V \left\{ -\nabla \cdot (\nu \nabla A)\,W + \frac{2\sigma}{\Delta t} A\,W - g\,W \right\} dV = 0 \tag{29}$$

Using the identity

$$\nabla \cdot (\nu \nabla A)\, W = \nabla \cdot (W \nu \nabla A) - \nu\, \nabla W \cdot \nabla A \tag{30}$$

and Gauss's theorem the higher derivatives are eliminated from Eq. (29)

$$\int_V \left\{ \nu \nabla A \cdot \nabla W + \frac{2\sigma}{\Delta t} A W - g W \right\} dV = \oint_S \nu W \frac{\partial A}{\partial n} dS \tag{31}$$

The surface integral on the right hand side of the equation is taken over the boundary S of the solution region. Because there is no z-dependence and the surface integral in Eq. (31) vanishes on the end surfaces of the integration cylinder V, the volume integral can be changed to a surface integral over the cross section of the machine by integrating over the z-coordinate

$$\int_\Omega \left\{ \nu \nabla A \cdot \nabla W + \frac{2\sigma}{\Delta t} A W - g W \right\} d\Omega = \oint_\Gamma \nu W \frac{\partial A}{\partial n} d\Gamma \tag{32}$$

where Ω denotes the two-dimensional solution region and Γ the boundary of Ω.

In the finite element method the approximation of the vector potential is

$$\tilde{A} = \sum_{j=1}^{N_n} a_j N_j(x,y) \tag{33}$$

where a_j is a nodal value associated with the node j of the finite element mesh
N_j is a shape function associated with the node j
N_n is the number of nodes in the finite element mesh.

In the sinusoidal approximation the nodal values a_j are complex variables. The shape function N_j is a real valued function having a value different from zero only in those elements that are connected to the mesh point j. The summation index j in Eq. (33) runs over all the node points of the mesh including also the points of fixed nodal values on the boundary. In the following derivation the nodes for which the nodal values are unknown are called free nodes.

When Galerkin's method and the finite element method are combined, the vector potential is approximated by Eq. (33) and the shape functions connected to the free nodes are used one by one as the weight function. Thus the number of equations

is equal to the number of unknown nodal values in the approximation. The equation for a node i is

$$\int_{\Omega} \left\{ \nu \left(\sum_{j=1}^{N_n} a_j \nabla N_j \right) \cdot \nabla N_i + \frac{2\sigma}{\Delta t} \left(\sum_{j=1}^{N_n} a_j N_j \right) N_i - g N_i \right\} d\Omega$$

$$= \oint_{\Gamma} \nu N_i \left(\sum_{j=1}^{N_n} a_j \frac{\partial N_j}{\partial n} \right) d\Gamma \qquad (34)$$

In the analysis of an electrical machine the nodal values are fixed to a constant value e.g. zero on the outer surface of the machine. The line integral over this boundary (Γ) in Eq. (34) vanishes as the index i runs over the free nodes inside the solution region and the shape functions associated with these nodes are zero on the boundary. The equation can be written

$$\int_{\Omega} \left\{ \sum_{j=1}^{N_n} \left(\nu \nabla N_i \cdot \nabla N_j + \frac{2\sigma}{\Delta t} N_i N_j \right) a_j - g N_i \right\} d\Omega = 0 \qquad (35)$$

If the number of free nodes is N, there are N nonlinear equations for the solution of N nodal values a_j. The Newton-Raphson iteration method is used for the solution. If we write Eq. (35) in short

$$f_i(a_1, \ldots, a_N) = 0 \qquad i = 1, \ldots, N \qquad (36)$$

and denote by **f** the column vector of the residual functions f_i, the Newton-Raphson iteration method is given by the equations

$$\mathbf{P}(\mathbf{a}^n)\, \Delta\mathbf{a}^n = -\mathbf{f}(\mathbf{a}^n)$$

$$\mathbf{a}^{n+1} = \mathbf{a}^n + \Delta\mathbf{a}^n \qquad (37)$$

where **P** is the Jacobian of the system of equations
n is an index denoting an iteration step
$\mathbf{a}^n$ is the column vector of nodal values at the iteration step n
$\Delta\mathbf{a}^n$ is the correction added to $\mathbf{a}^n$ at the iteration step n.

The elements of the Jacobian are the derivatives of the residual functions

$$P_{lm}(\mathbf{a}^n) = \frac{\partial f_l(a_1^n, \ldots, a_N^n)}{\partial a_m^n} \tag{38}$$

When the Newton-Raphson method is applied to Eq. (35), the elements of the residual vector **f** and the Jacobian **P** are

$$f_i(a_{k+1}) = \int_\Omega \left\{ \sum_{j=1}^{N_n} \left(\nu(a_{k+1})\ \nabla N_i \cdot \nabla N_j + \frac{2\sigma}{\Delta t}\ N_i N_j \right) a_{j|k+1} - \frac{\sigma}{l} N_i U_{k+1} \right\} d\Omega$$

$$+ \int_\Omega \left\{ \sum_{j=1}^{N_n} \left(\nu(a_k)\ \nabla N_i \cdot \nabla N_j - \frac{2\sigma}{\Delta t}\ N_i N_j \right) a_{j|k} - \frac{\sigma}{l} N_i U_k \right\} d\Omega \tag{39}$$

$$P_{lm}(a_{k+1}) = \int_\Omega \left\{ \sum_{j=1}^{N_n} \left(\frac{\partial \nu(a_{k+1})}{\partial a_{m|k+1}} \nabla N_l \cdot \nabla N_j\ a_{j|k+1} \right) \right.$$

$$\left. + \nu(a_{k+1}) \nabla N_l \cdot \nabla N_m + \frac{2\sigma}{\Delta t} N_l N_m \right\} d\Omega \tag{40}$$

where the index k denotes a time step and the indices j, l and m denote nodes.

If the assumption of sinusoidal time variation is made, the elements of the complex residual vector **f** obtained from the discretization of Eq. (23) are

$$\underline{f}_i(\underline{\mathbf{a}}) = \int_\Omega \left\{ \sum_{m=1}^{N_n} (\nu \nabla N_i \cdot \nabla N_m + j\sigma\omega N_i N_m)\ \underline{a}_m - \frac{\sigma}{l} N_i\ \underline{U} \right\} d\Omega \tag{41}$$

If the source of the field is a current, the component i of the complex residual vector corresponding to the integrodifferential equation (21) is

$$f_i(\underline{a}) = \int_\Omega \left\{ \sum_{m=1}^{N_n} (\nu \nabla N_i \cdot \nabla N_m + j\sigma\omega N_i N_m)\, \underline{a}_m \right.$$

$$\left. - \frac{j\sigma\omega R}{l} N_i \int_\Omega \sigma \left(\sum_{m=1}^{N_n} \underline{a}_m N_m \right) d\Omega - \frac{\sigma R}{l} N_i \underline{I} \right\} d\Omega \qquad (42)$$

1.4 A short review of the field analysis of induction motors

The first efforts to solve magnetic field problems by the finite element method were made in the late 1960's. In the analysis of electrical machines the finite element method was first applied to synchronous machines (Chari & Silvester 1971a) and DC-machines (Chari & Silvester 1971b) because the operation of these machine types can be approximately modelled by stationary fields. Even nowadays most of the research work concerning the magnetic field analysis of electrical machines deals with the modelling of synchronous machines. They have been analyzed by using step-by-step methods to solve the time-dependence (Tandon et al. 1983) and by three-dimensional finite element formulations (Chari et al. 1982).

The field of an induction motor has to be solved with a method that takes the time-dependence into account. Probably the difficulties connected with the solution of time-dependent nonlinear fields have postponed the numerical analysis of induction motors. The first publications dealing with this problem appeared at the beginning of the 1980's. For the present only two-dimensional formulations have been used.

Ito et al. (1981) computed the nonlinear field of an induction motor using an eddy-current formulation and assuming sinusoidal time variation. The end rings of the rotor cage were assumed to form ideal short circuits so that the ends of rotor bars were all in the same potential. The vector potential in the rotor bars satisfies Eq. (23) with the potential difference $\underline{U}$ equal to zero. The rotor was assumed to be pseudostationary (Section 2.2.3). The method was used to study various properties of induction motors and some suggestions were made to improve the design of the motors.

Andresen & Müller (1983) made the same assumptions as above, but they used the finite difference method to solve the field equations. The field solution was used for obtaining the locked-rotor current and torque of an induction motor. The

effects of different slot shapes on the locked-rotor characteristics were studied.

Williamson & Ralph (1982 and 1983) have connected conventional calculation methods and numerical field analysis in their work. The basis of their model is Eq. (8) and the assumption of sinusoidal time variation. Current densities in the conductors are assumed to be constants so that skin effect is not taken into account when solving the field equations. The rotor currents are solved from the air gap flux (vector potential) induced by the stator currents with the aid of rotor bar impedances. The method is quite versatile. The effects of harmonic components and skewed rotor slots are taken into account. The skin effect may be included in the values of rotor bar impedances. A drawback of the method is the time consumption in the iterations needed in the solution of the winding currents. The method was used to compute the properties of a shaded pole motor.

Bouillault & Razek (1983) and Brunelli et al. (1983) used time-stepping methods to calculate the time variation of magnetic fields in induction motors. Both papers deal with solid rotor induction motors. It is assumed that the ends of the rotor are equipotential surfaces of the scalar potential so that the rotor field can be solved from Eq. (26) with the potential differences equal to zero.

The voltage equations of the windings of an induction motor are coupled to the field equation. In earlier publications the currents of the stator winding have been taken as the sources of the field (e.g. Andresen & Müller 1983) or the solution is obtained in a double iteration process in which the voltage equations of the stator winding are solved in an outer iteration and the solution of the field equation forms an inner iteration. A more efficient method is obtained if the discretized field and voltage equations are solved in the same iteration loop. Brandl et al. (1975) computed steady-state operating characteristics of a synchronous machine by solving the coupled field and voltage equations together in the same matrix equation. Nakata & Takahashi (1982) used the method to analyze an induction motor in steady-state and Brunelli et al. (1983) used a related method in the step-by-step solution of a solid rotor induction motor.

If the impedances associated with the end rings and bar ends of the rotor cage are included in the model, voltage equations have to be formed for the cage winding. Konrad (1982) and Weiss & Csendes (1982) have presented eddy current formulations that can be applied to the solution of magnetically coupled multiconductor systems, when the currents of the conductors are known. This is not far from the solution of the field and voltage equations of a rotor cage.

Strangas & Theis (1985) have computed the field of an induction motor using a method in which the field equation and the voltage equations of the stator and rotor windings are solved together. They present a quite general two-dimensional step-by-step formulation for the evaluation of the operating characteristics of a shaded pole motor. The nodal values of the vector potential and the currents and potential differences of the windings are solved in the same matrix equation. In an other paper Strangas (1985) applies the formulation to the analysis of a cage induction motor. No computed results of the operating characteristics are presented, but the method seems to be quite generally applicable to the analysis of induction motors. For instance the possibility to rotate the rotor is included in the method.

Shen et al. (1985) and Shen & Meunier (1986) present a formulation for sinusoidally varying field quantities that is very similar to that given by Strangas for general time-dependence. The voltage equations of the stator and rotor windings are written in matrix form. After the elimination of the currents from the voltage equations and from the discretized field equation a global matrix equation is obtained that connects the nodal values of the vector potential and the potential differences. The equations are derived for sinusoidally varying quantities, but the same principles are valid for general time-dependence. The advantage of the matrix notation in the treatment of the voltage equations is obvious.

1.5 Previous and present works associated with this study

A part of the computation routines used in this work has been constructed in earlier research projects of the Laboratory of Electromechanics. Numerical field analysis was first applied to the design of an acyclic motor having superconducting field windings (Luomi 1984). The static axisymmetric field of the machine was solved by the finite element method or by a combined finite element - boundary element method. The computation routines used for the analysis of the acyclic motor were later transformed and applied to the analysis of induction motors at the no-load condition (Wallenius 1983). The sinusoidal approximation was used for the computation of no-load currents. A finite element mesh generator was made for the generation of two-dimensional, first-order finite element meshes of induction motors.

In the present study the computation programs have been further developed in order to be able to analyze a cage induction motor in a general operation state. For this purpose the sinusoidal eddy-current formulation was first implemented

in the routines. The voltage equation of the rotor and stator windings were added to the matrix equations of the finite element method, and routines for the evaluation of machine properties from the field solution were constructed. The methods used in the sinusoidal approximation were transformed to a step-by-step formulation in order to be able to solve the general time dependence. The possibility to rotate the rotor in a step-by-step solution was implemented in order to be able to simulate rotor motion and to check the validity of the approximate methods used for modelling the motion.

Associated with this work the use of the sinusoidal approximation and effective reluctivity in the analysis of induction motors was studied by comparing the results of the sinusoidal approximation with the results of a step-by-step method (Luomi et al. 1986, Niemenmaa 1986). At present a new research project has been started, the aim of which is to develop methods for the calculation of iron losses in electrical machines. The field solution routines constructed will be applied to the loss analysis of induction motors.

2 FIELD ANALYSIS OF CAGE INDUCTION MOTORS

2.1 Geometry of the problem

Periodic symmetry

Figure 1 shows the cross sectional geometry of an induction machine in a plane perpendicular to the shaft. The equipotential lines of the vector potential induced by a current in the three-phase stator winding are also shown. The number of pole pairs is two and the number of slots per pole and phase is three. The figure consists of four sectors that have identical geometries. Because of the symmetry it has been enough to compute the field in one of the sectors. The three other sectors have been copied by the plotting routine. The phase belts can be distinguished from the shadings of the coil sides.

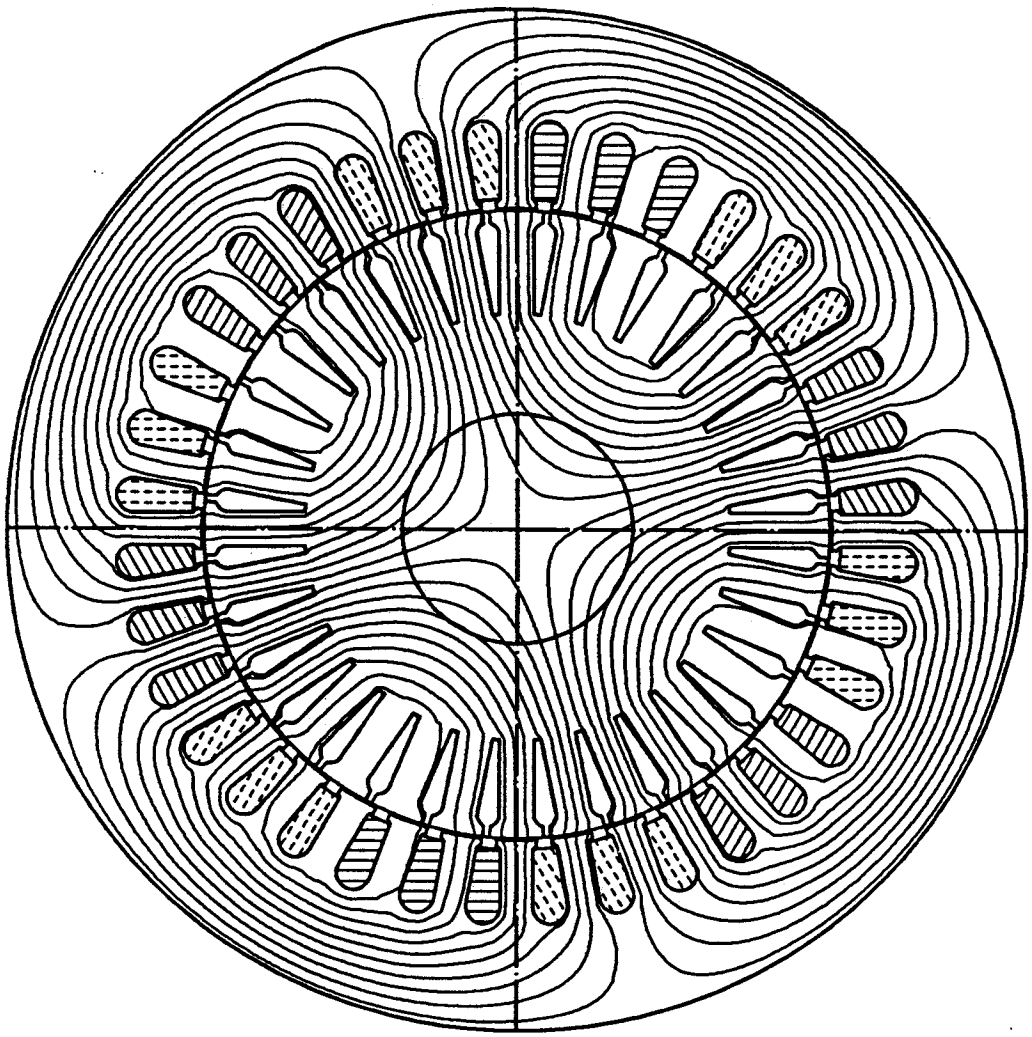

Figure 1. The cross section of an induction machine. The vector potential induced by a three-phase stator current is shown as equipotential lines.

It is assumed that no flux penetrates the outer surface of the machine. This means that the vector potential has a constant value on the boundary. The central node of the shaft is fixed to the same value in order to prevent a circulating net flux around the axis.

Periodic boundary conditions are used on the sides of a solution sector. The values of vector potential at corresponding nodes on the periodic boundaries are related by a periodicity factor $\underline{h}$

$$\mathbf{A}' = \underline{h}\,\mathbf{A} = e^{-jp\gamma}\mathbf{A} \tag{43}$$

where γ is the angle of the solution sector
p is the number of pole pairs of the machine.

A complex periodicity factor is associated with the sinusoidal approximation. In the step-by-step solution only the real values are valid. The implementation of the periodic boundary condition follows the lines given by Silvester et al. (1973) for real valued periodicity factors. When a complex periodicity factor is used, the real and imaginary parts of the vector potential nodal values are connected non-symmetrically to each other in the Jacobian of the Newton-Raphson method. The vector potential was fixed to a constant value on the outer surface of the machine. As the periodicity condition has to be satisfied also on the outer surface, the constant value is usually equal to zero.

The symmetry of the system is determined by the numbers of stator and rotor slots and by the number of poles. An induction motor is usually so designed that the symmetry sector contains two poles. This choice is made in order to minimize the effects of harmonic components on the operation of the machine. If the symmetry sector contains two pole pitches, and the number of slots per pole and phase is large, a lot of computer capacity is required in the solution of the discretized field equation.

In order to reduce the size of the problem the number of rotor slots must sometimes be changed so that a smaller solution region is obtained (Williamson & Ralph 1983). If the symmetry sector of the true machine is two pole pitches wide, there are three possibilities to get a higher symmetry. The reduced symmetry sector may contain one pole pitch, one phase belt or one slot pitch. The last two cases can only be used in the approximation of sinusoidal time variation. The change of slot numbers causes errors in the computed results, but the savings in computation time and memory requirements are significant. The

effects of the change of symmetry are discussed further in Chapter 3.

The finite element mesh

A mesh generator was constructed that forms the meshes of common induction motor geometries from data containing the necessary dimensions, slot numbers and slot geometry codes. The routine deduces the smallest symmetry sector and forms an element mesh in the sector. Finite element meshes consisting of isoparametric first-, second- or third-order triangular elements can be produced. Figure 2 shows a typical finite element mesh used in the analysis. The mesh consists of 904 isoparametric second-order elements and contains 1851 nodes.

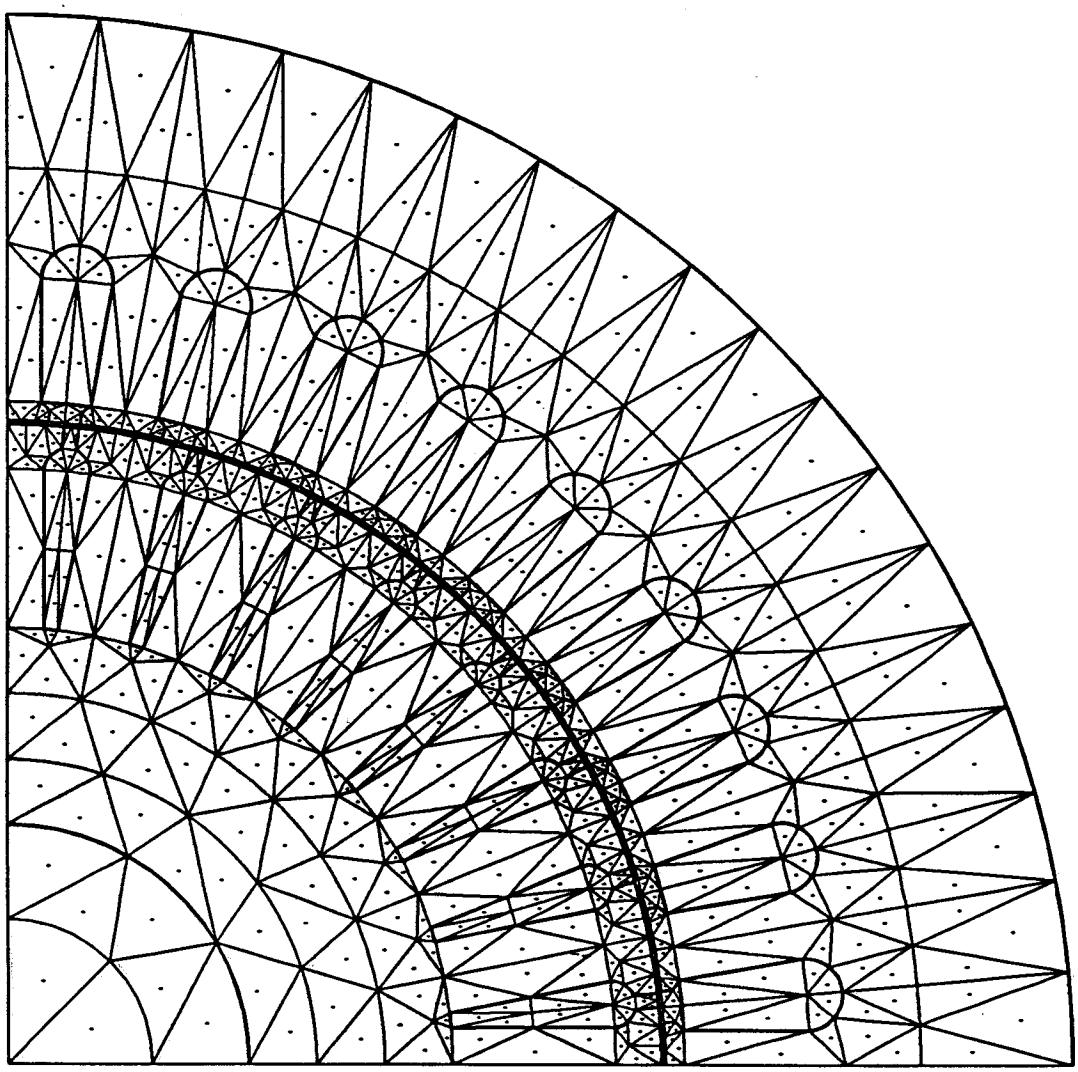

Figure 2. A typical finite element mesh used in the analysis of an induction motor. The mesh contains 904 isoparametric second-order elements and 1851 nodes.

Practice has shown that there should be a detailed finite element mesh in the air gap region in order to get accurate results. One possibility is to use a special air gap element (Abdel-Razek et al. 1982). The shape functions of an air gap element are analytical series expressions that satisfy the Laplace equation in the air gap. If the vector potential were known accurately on the boundaries, the air gap element would give an exact solution. However, the amount of computation is increased considerably if an air gap element is used instead of a normal finite element mesh. This is because the coefficient matrix associated with the air gap element is a full matrix whose elements are computed from slowly convergent series expansions. A typical air gap element in the field analysis of induction motors contains about 300 nodes. A large full sub-matrix in the Jacobian of the Newton-Raphson method also increases the time needed in the solution of the matrix equation.

The effect of rotor motion on the finite element mesh

When the true time variations of machine quantities of a running induction motor are studied, the field has to be solved with a time-stepping method, in which the rotor is rotated at each time step by an angle corresponding to the angular velocity of the rotor. The field equations for the stator and the rotor are written in their own coordinate systems and the solutions are matched with each other in the air gap.

One possibility is to use the air gap element to connect the stator and the rotor fields. The rotation is obtained by calculating a new coefficient matrix for the air gap element at each time step. A lot of computation is needed if an air gap element is used to rotate the rotor.

Another possibility to rotate the rotor is to change the finite element mesh in the air gap at every time step. This is done by dividing the mesh into two separate parts. The first mesh contains the stator and the air gap and the second mesh contains the rotor. The nodes on the inner surface of the air gap are connected to the corresponding nodes on the rotor surface by periodic boundary conditions. The motion is accomplished by changing the form of the elements in the air gap and by changing the correspondence of nodes on the periodic boundaries. The criterion in the formation of the air gap meshes is to keep the sides of the elements as short as possible. Related methods have been shortly described by Davat et al. (1985) and by Strangas & Theis (1985).

2.2 Simplifying assumptions

Several simplifying assumptions have to be made in the analysis. Actually, there are so many approximations that it is difficult to check the effect of a given approximation by comparing computed and measured results. The assumption of a two-dimensional field probably causes the largest errors, but there are also simplifications related to the time-dependence and to the modelling of iron properties that cause inaccuracy in the results. The main simplifications are discussed below.

2.2.1 Two-dimensional model

A complete three-dimensional formulation should be used in the calculation of the magnetic field of an induction machine. Three-dimensional finite element formulations have been developed for the analysis of time-dependent magnetic fields (e.g. Chari et al. 1982), but their practical applications are still restricted to relatively simple geometries. A two-dimensional model is used in this work. The three-dimensional effects, such as the skew of rotor slots and end-region fields, must be taken into account within the two-dimensional model.

End windings

Currents in the end windings of a machine induce components to the flux linkages of the stator and rotor windings that are not included in the fluxes computed from the two-dimensionally modelled region. These additional flux linkages must be taken into account in the voltage equations.

Probably the easiest way to add the effect of end-region fields into the voltage equations is to model the end windings as resistances and constant inductances, whose values are determined by simplifying analytical methods or by measurements (Barnes 1951, Richter 1954, Vogt 1983). The end-winding inductance of a stator winding in a three-phase induction motor is often written in the form

$$L_b = 2\mu_0 \, p \left(\frac{q N_c}{a} \right)^2 \lambda_b \, l_b \tag{44}$$

where μ_0 is the permeability of free space
p is the number of pole pairs
q is the number of slots per pole and phase

N_c is the number of turns in series in a coil
a is the number of parallel paths
λ_b is a semi-empirical parameter
l_b is the average length of the overhang.

The value of the parameter λ_b depends on the geometry of the end-winding region. Usually λ_b is so defined that it also includes the effect of the rotor end winding reduced to the stator. The values of λ_b have been tabulated for different stator and rotor configurations e.g. by Richter (1954).

Eq. (44) gives only a rough estimate for the value of the end-winding inductance. In more accurate methods the magnetic scalar potential is solved in a somewhat simplified end-region geometry (Reece & Pramanik 1965) or the end-region field is integrated numerically using current elements and image sources for modelling the iron surfaces (Lawrenson 1970). Recently, methods based on the numerical solution of field equations in the end-region geometry have become popular. There are formulations based on the magnetic scalar potential (Davey & King 1981), magnetic scalar and electric vector potentials (Sikora et al. 1986) and magnetic vector potential (Ito et al. 1980).

The results of Chapter 3 have been computed using the end-winding inductances obtained from Eq. (44). The end-winding inductance has only a small effect on no-load characteristics, but in the locked-rotor condition 5 - 15 % of the stator voltage is due to the end-winding inductance. Thus an inaccuracy in its value may have a significant effect on the accuracy of computed locked-rotor currents and torques.

The resistances of the ends of the rotor bars and of the end-ring segments are calculated from the dimensions of the conductors by simplified analytical models. The skin effect is neglected. The resistance of the stator end winding is taken into account in the total resistance of the stator winding.

Skewed rotor slots

The rotor slots of an induction motor are usually skewed, i.e. the rotor slots are not parallel to the shaft and the stator slots. In the conventional calculation of an induction machine the effect of skewing is treated with a skew factor that affects the magnetic coupling between the stator and rotor windings.

The use of a skew factor in a two-dimensional finite element formulation

complicates the solution procedure. This is because the flux linkage of a given winding has to be divided into two parts that are treated differently in the voltage equations. The first part is the flux linkage induced by windings that are unskewed in relation to the winding under consideration. The second part is the flux linkage due to skewed windings. The solution of these separate flux linkages leads to multiple field solutions and time-consuming iterations in the solution of the voltage equations. A method for modelling skew in a two-dimensional formulation using skew factors is given by Williamson & Ralph (1983).

A somewhat different method is attained if a skewed machine is thought to be made up of several slices that have been cut from an ideal two-dimensional machine by planes perpendicular to the shaft. The rotors of adjacent slices have been rotated by an angle corresponding to the skew. The winding currents are assumed to be continuous from slice to slice. The magnetic field of each slice is solved separately using a two-dimensional formulation. The voltages of the windings are added together from the potential differences induced in the slices and in the end windings. The method is discussed further in connection with the solution of voltage equations in Section 2.3.4.

The average core saturation level of a loaded skewed induction motor varies along the shaft direction (Binns et al. 1971). Thus a skewed machine saturates somewhat differently from an unskewed machine. The slice model takes into account the variation of the saturation level in the axial direction. The effect cannot be treated properly with a simple skew factor.

Currents in the iron core

The core of an electrical AC machine is made up of thin electrical steel sheets. An insulation layer on the sheets isolates them from each other. The losses due to eddy-currents in the sheets are minimized by making the sheets as thin as practical.

The punching of the core sheets breaks the insulation layer at the edges of the sheets. This may lead to galvanic contacts between adjacent sheets and further to eddy-currents that flow from sheet to sheet. It is difficult to take these eddy-currents into account in the analysis because of their statistical nature. Punching also affects the magnetic properties of the sheet edges.

The rotor bars of an induction machine are usually in galvanic contact with the surrounding electrical steel sheets. A potential difference between two rotor bars

induces a current that flows through the sheets from one bar to the other. Currents along the iron sheets are not consistent with the two-dimensional approximation. It is possible to treat these currents in a roughly simplified manner within the slice method used to model the skew. There are, however, difficulties in the determination of the contact resistances between rotor bars and sheets. Thus all currents in the electrical steel sheets are neglected. The laminated iron core is treated as a non-conducting, magnetically nonlinear medium.

2.2.2 The nonlinearity of iron

The nonlinear magnetization of iron complicates the solution of magnetic fields in electrical machines. In numerical solution routines saturation leads to time-consuming iterations. Iron also has significant hysteresis in its B,H-characteristics. The reluctivity is not a single-valued function of e.g. flux density, but depends on the history of the system.

In principle it is possible to take both hysteresis and saturation into account in a step-by-step solution. The difficulty lies in the lack of a phenomenological model for the magnetization that is easy to implement and fast to use in a computer routine and still gives the material properties accurately. Both the magnitude and the direction of a flux density vector in a machine core vary. The points of flux density vectors trace very complicated curves, especially in teeth at the air gap region. A good hysteresis model should be able to treat an arbitrary magnetic field exitation. Such a model contains very much information that has to be gathered experimentally before the parameters of the model can be determined.

In the time-stepping method a single-valued monotonic reluctivity curve for the core material is used. The curves are prepared from the peak value magnetization curves given by the producers of electrical steel sheets. The treatment of nonlinearity in the approximation of sinusoidal time variation is discussed below.

Hysteresis and eddy-currents in core sheets are not included in the model. This means that iron losses are totally neglected in the analysis. In the conventional analysis of electrical machines the iron losses are calculated by models based on loss measurements in fields varying unidirectionally at the rated frequency of the machine. Such models could also be implemented in the numerical field solution routines. It is believed, however, that a more general loss model is needed e.g. in the calculation of the air gap region where the time variation of the field

quantities is very complicated.

Iron losses have an influence on the no-load characteristics of an induction motor. In the locked-rotor condition the effect of iron losses is small compared with other loss components in the machine.

The approximation of sinusoidal time variation

As already discussed in Chapter 1 the time variation of fields in an electrical machine is practically never sinusoidal. The nonlinearity of iron and the rotation of the rotor require the use of a step-by-step method in the solution of the magnetic field. This is very time-consuming. If the time-dependence of the field is assumed to be sinusoidal, the computation time can be reduced radically. Therefore the assumption of sinusoidal time variation is commonly used in the literature.

The vector potential of a sinusoidally varying two-dimensional magnetic field observed in the stator coordinate system and written as a Fourier-series in cylindrical coordinates is

$$\underline{A} = \sum_{n=-\infty}^{\infty} \left\{ \underline{A}_n(r)\, e^{-j(n\varphi - \omega t)} \right\} \mathbf{e}_z \tag{45}$$

where r and φ are circular cylindrical coordinates

$\underline{A}_n$ is a complex r-dependent Fourier-coefficient

ω is the angular frequency.

It is seen from Eq. (45) that all space harmonics that vary at the line frequency are included in the approximation, but there are no time harmonic components. Thus e.g. the time harmonics due to saturation that vary at higher frequencies are not included in the sinusoidal approximation.

The assumption of sinusoidal time variation is made in order to eliminate the time-dependence from the field equations. This means that the reluctivity used in the approximation must be independent of time. Because the approximation of sinusoidal time variation is reasonable only when calculating effective values in a steady state, it is an obvious choice to define the reluctivity as a function of the effective value of the flux density

$$B_{ef} = \frac{1}{\sqrt{2}} \sqrt{\left(\frac{\partial A_R}{\partial x}\right)^2 + \left(\frac{\partial A_R}{\partial y}\right)^2 + \left(\frac{\partial A_I}{\partial x}\right)^2 + \left(\frac{\partial A_I}{\partial y}\right)^2} \tag{46}$$

where A_R and A_I are the real and imaginary parts of the vector potential. Actually the reluctivity curves used in the computer routines are cubic spline approximations and functions of a variable equal to twice the square of B_{ef}. This is because of computational efficiency (Silvester et al. 1973).

There is an unlimited number of possibilities to define an effective reluctivity. The definition that gives the best results for the effective values of current , torque and other machine characteristics is the best definition in that special case. Results computed using various effective reluctivities have been compared with the results of a time-stepping method (Luomi et al. 1986). The comparison was done for several induction motors. Among others the following definitions were studied

$$\nu_{B3} = \frac{1}{T} \int_0^T \frac{H(t)}{\hat{B} \sin\left(\frac{2\pi t}{T}\right)} \, dt \tag{47}$$

$$\nu_{B4} = \left\{ \frac{1}{T} \int_0^T \left\{ \frac{H(t)}{\hat{B} \sin\left(\frac{2\pi t}{T}\right)} \right\}^2 dt \right\}^{\frac{1}{2}} \tag{48}$$

$$\nu_{H2} = \frac{\hat{H}}{\frac{2}{T} \int_0^T B(t) \sin\left(\frac{2\pi t}{T}\right) dt} \tag{49}$$

$$\nu_{H4} = \left\{ \frac{1}{T} \int_0^T \left\{ \frac{\hat{H} \sin\left(\frac{2\pi t}{T}\right)}{B(t)} \right\}^2 dt \right\}^{\frac{1}{2}} \tag{50}$$

where T is the period of time of the AC cycle. The same subscripts have been used

for the reluctivities as in the reference.

In the first two equations it is assumed that the flux density varies sinusoidally and unidirectionally. The field strength is taken from the peak value magnetization curve of the material. In Eq. (47) the effective reluctivity is obtained as the time average of the ratio of the field strength and the flux density. The RMS value of the instantaneous reluctivity is calculated in Eq. (48).

In the last two equations it is assumed that the field strength varies sinusoidally and the flux density is taken from the peak value magnetization curve of the material. In Eq. (49) the reluctivity is defined as the ratio of the fundamentals of the field strength and the flux density. The RMS value of the instantaneous reluctivity is calculated in Eq. (50). In the comparison with the results of the step-by-step method (Luomi et al. 1986) the best agreement was obtained by the effective reluctivity defined by Eq. (47). This effective reluctivity has been used when computing machine characteristics by the sinusoidal approximation (Chapter 3).

The trace of the point of a flux density vector is an ellipse in the sinusoidal approximation and a more general curve in true time variation. The producers of electrical steel sheets give magnetization curves measured in an experiment in which the magnetic field varies unidirectionally. The peak value curves used in the calculation of the effective reluctivities do not contain information about the behavior of iron in a rotary magnetic field.

2.2.3 The motion of the rotor

In a general step-by-step solution of the magnetic field of a running induction machine the field equations for rotor and stator fields are written in their own coordinate systems. The solutions of the two field equations are matched with each other in the air gap. The rotor is rotated at each time step by an angle corresponding to the mechanical angular frequency. This means that a new finite element mesh in the air gap and a new Jacobian matrix has to be constructed at each time step. The problem of taking the motion into account in a finite element formulation is discussed e.g. by Davat et al. (1985).

In some special cases it is possible to find a coordinate system in which the material properties reluctivity $\nu(x,y,t)$ and conductivity $\sigma(x,y)$ are not directly affected by the motion of the bodies. If there is such a coordinate system, it is worth solving the field equations in this system. Transformation equations for

the field quantities are needed. If a coordinate system O' moves with a velocity **v** measured from an other coordinate system O, the transformation equations for the quasi-static magnetic system are (Melcher 1981, Van Bladel 1984)

$$\begin{aligned} \mathbf{B}' &= \mathbf{B} \\ \mathbf{E}' &= \mathbf{E} + \mathbf{v} \times \mathbf{B} \\ \mathbf{H}' &= \mathbf{H} \\ \mathbf{J}' &= \mathbf{J} \end{aligned} \tag{51}$$

where the quantities observed from the coordinate system O' are marked by apostrophes. Eqs. (51) are valid at velocities much smaller than the velocity of light.

The vector potential in the moving media observed from the stationary coordinate system O satisfies the equation

$$\nabla \times (\nu \nabla \times \mathbf{A}) + \sigma \left\{ \frac{\partial \mathbf{A}}{\partial t} - \mathbf{v} \times \nabla \times \mathbf{A} \right\} + \sigma \nabla \phi = 0 \tag{52}$$

In a linear case the assumption of sinusoidal time variation can be used together with the coordinate transformation. In this case the complex vector potential satisfies the equation

$$\nabla \times (\nu \nabla \times \underline{\mathbf{A}}) + \sigma (j\omega \underline{\mathbf{A}} - \mathbf{v} \times \nabla \times \underline{\mathbf{A}}) + \sigma \nabla \underline{\phi} = 0 \tag{53}$$

Nonlinear materials can be modelled approximately by using an effective reluctivity. In Chapter 3 this method is used in the analysis of an induction motor having a homogeneous solid iron rotor. The slotting of rotor and stator cores limits the use of coordinate transformations in the analysis of cage induction motors.

The time-dependence of the field quantities is far from sinusoidal in the teeth and coil region, when the stator and rotor teeth are moving passed each other. However, the assumption of sinusoidal time-dependence is often made. The easiest method to take the rotor motion into account in the sinusoidal approximation is to treat the rotor as quasi- or pseudostationary. The rotor field observed in the stator coordinate system is calculated from the equation

$$\nabla \times (\nu_{ef} \nabla \times \underline{\mathbf{A}}) + j\sigma s\omega \underline{\mathbf{A}} = \frac{\sigma}{l} \underline{U} \mathbf{e}_z \tag{54}$$

where s is the slip. In the pseudostationary approximation the rotor is fixed and the motion is modelled by multiplying the conductivities of rotor conductors by the factor s.

The shortages of the pseudostationary approximation become clear when the method is used to analyze a conducting cylinder rotating in a transverse magnetic field (Appendix A). The approximation only gives a correct result at the slip value 1. If the magnetic field only contains the first space harmonic component, the method gives correct values at all slip values.

The effect of higher space harmonics is treated more accurately in the method used by Williamson & Ralph (1983). As already discussed in Section 1.4 the harmonic currents in the rotor are solved from the flux (vector potential) distribution in the air gap using a circuit theoretical model for the rotor cage. The torques due to each harmonic component can be calculated separately and the total torque is obtained as a sum of the torque components.

2.3 Solution of the coupled field and circuit equations

The stator winding of an induction motor is usually connected to a line voltage. A potential difference equal to the line voltage is induced in the winding. Thus, the line voltage is the actual source of the magnetic field. The source terms are imposed into the finite element formulation through the voltage equations of the stator winding. The magnetic coupling between the rotor and stator windings causes the rotor currents. If the effect of the rotor end windings is included in the model, voltage equations must also be constructed for the rotor winding.

The potential differences, currents and vector potential are coupled to each other in the voltage equations and in the field equations. Because of the nonlinearity of the core materials the system of equations must be solved iteratively. Practice has shown that the equations should be solved simultaneously in the same iteration loop, if a fast convergence and a short solution time are wanted.

2.3.1 Voltage equations of the stator winding

The scalar potential difference induced in a phase of the stator winding should be calculated from the equation

$$U = \int_\Gamma -\nabla \phi \cdot \mathbf{dl} = \int_\Gamma \left\{ \frac{1}{\sigma}\mathbf{J} + \frac{\partial \mathbf{A}}{\partial t} \right\} \cdot \mathbf{dl} \qquad (55)$$

where Γ is an integration path along the phase winding. There are two difficulties connected with the use of Eq. (55). Firstly, the vector potential and current density distributions are unknown in the end windings. Secondly, if Eq. (55) is used, every conductor in a slot must be separately solved from Eq. (20). This means that every conductor must have a detailed finite element mesh. Such a mesh constructed for the cross section of an induction machine soon becomes too large to be solved.

The number of elements needed in a stator slot is reduced if a circuit theoretical approach is taken. It is assumed that the stator winding consists of infinitely thin conductors with no skin effect. The potential difference of a phase winding is obtained from the equation

$$U = \frac{\partial \Psi}{\partial t} + R\, I \tag{56}$$

where Ψ is the flux linkage of the phase winding
R is the total resistance of the phase winding.

In a coil side of the stator winding the vector potential satisfies Eq. (8) with a constant current density

$$\mathbf{J} = \frac{N_{cn}\, I}{S_n}\, \mathbf{e}_z \tag{57}$$

where N_{cn} is the number of turns in series in the coil side n
S_n is the cross sectional area of the coil side n.

In order to reduce eddy-current losses the conductors of a stator winding are usually made so thin that Eqs. (56) and (57) are good approximations. However, if the effects of eddy-currents are studied e.g. in an inverter driven motor, every conductor of a slot should be modelled using Eq. (20).

The flux linkage in Eq. (56) is the sum of two components. The flux linkage associated with the two-dimensionally modelled core region is obtained as a surface integral of the vector potential over the coil sides of the phase winding. The flux linkage component of the end windings is modelled by a constant end-winding inductance. The expression for the potential difference of the phase winding becomes

$$U = N_s \left\{ \sum_{n=1}^{N_1} \frac{l\, N_{cn}}{S_n} \int_{S_n} \frac{\partial A}{\partial t}\, dS - \sum_{n=1}^{N_2} \frac{l\, N_{cn}}{S_n} \int_{S_n} \frac{\partial A}{\partial t}\, dS \right\} + R\, I + L_b \frac{dI}{dt} \qquad (58)$$

where N_s is the number of symmetry sectors that the machine contains

N_1 is the number of positively oriented coil sides of the phase winding in the solution sector

N_2 is the number of negatively oriented coil sides of the phase winding in the solution sector

L_b is the end-winding inductance of the phase winding.

It is assumed in Eq. (58) that the number of parallel paths is one and that the solution region contains an integer number of poles.

In the time-stepping formulation the time derivatives of the vector potential and the current are approximated by first-order difference ratios

$$\frac{\tilde{A}_{k+1} - \tilde{A}_k}{\Delta t} \rightarrow \frac{\partial A}{\partial t}$$

$$\frac{i^s_{k+1} - i^s_k}{\Delta t} \rightarrow \frac{dI}{dt} \qquad (59)$$

A more compact form is obtained for the voltage equation if a function $\beta^s{}_n$ is introduced

$$\beta^s_n(x,y) = \begin{cases} \dfrac{N_{cn}}{S_n} & \text{if point (x,y) belongs to a positively oriented coil side of the winding n} \\ -\dfrac{N_{cn}}{S_n} & \text{if point (x,y) belongs to a negatively oriented coil side of the winding n} \\ 0 & \text{otherwise.} \end{cases} \qquad (60)$$

After the substitution of the approximations (59) and the functions $\beta^s{}_n$ the voltage equation for the n^{th} phase winding becomes

$$\frac{u^s_{n|k+1} + u^s_{n|k}}{2} = N_s\, l \int_\Omega \beta^s_n \left\{ \sum_{j=1}^{N_n} \frac{a_{j|k+1} - a_{j|k}}{\Delta t} N_j \right\} d\Omega$$

$$+ \frac{R_s}{2} (i^s_{n|k+1} + i^s_{n|k}) + L_b \frac{i^s_{n|k+1} - i^s_{n|k}}{\Delta t} \qquad (61)$$

where u^s_n is the potential difference induced in the n^{th} phase winding
i^s_n is the current of the n^{th} phase winding
R_s is the resistance of the phase winding
Ω is the cross section of the machine
k denotes a time step.

The difference ratios approximate the time derivatives at time $t = (t_k + t_{k+1})/2$. In accordance the average values of the current and the potential difference at the time steps k and k+1 are used to approximate the true current and potential difference.

If column vectors $\mathbf{u}^s$ and $\mathbf{i}^s$, whose components are the potential differences and currents of the stator phase windings, are defined, a voltage equation in matrix form is obtained for the stator winding

$$\mathbf{D}^s \mathbf{a}_{k+1} - \frac{R_s \Delta t + 2 L_b}{2 N_s l} \mathbf{i}^s_{k+1}$$

$$+ \left\{ -\mathbf{D}^s \mathbf{a}_k - \frac{R_s \Delta t - 2 L_b}{2 N_s l} \mathbf{i}^s_k + \frac{\Delta t}{2 N_s l} (\mathbf{u}^s_{k+1} + \mathbf{u}^s_k) \right\} = 0 \qquad (62)$$

The terms in the parentheses only contain known quantities. It is assumed in Eq. (62) that all the phase windings have equal resistances and end-winding inductances. The components of the matrix $\mathbf{D}^s$ are

$$D^s_{ij} = -\int_\Omega \beta^s_i N_j \, d\Omega \qquad (63)$$

If sinusoidal time variation is assumed, the time derivatives in Eq. (58) are substituted by

$$j\,\omega\,\underline{\tilde{A}} \rightarrow \frac{\partial A}{\partial t}$$

$$j\,\omega\,\underline{i}_n^s \rightarrow \frac{dI}{dt} \tag{64}$$

The potential difference induced in the n^{th} phase winding is given by

$$\underline{u}_n^s = j\,\omega\,l\,N_s \int_\Omega \beta_n^s \left\{ \sum_{j=1}^{N_n} \underline{a}_j\,N_j \right\} d\Omega + (R_s + j\omega\,L_b)\,\underline{i}_n^s \tag{65}$$

The voltage equation of the stator winding written in matrix form is

$$\mathbf{D}^s\,\underline{\mathbf{a}} - \frac{R_s + j\,\omega L_b}{j\,\omega\,l\,N_s}\,\mathbf{i}^s + \frac{1}{j\,\omega\,l\,N_s}\,\underline{\mathbf{u}}^s = 0 \tag{66}$$

where $\mathbf{D}^s$ is the same matrix as in the step-by-step formulation.

Equations (62) and (66) give the relations between the vector potential and the currents and potential differences of the stator windings. The source of the electromagnetic field in the machine is, however, the line voltage of a polyphase system. The delta and star connections are the two commonly used ways to connect the stator windings. In the delta connection the potential differences induced in the stator windings are equal to the line voltages. In this case Eqs. (62) and (66) are directly applicable. A similar situation exists in the star connection, when the star point is connected. The potential differences of the stator windings are equal to the phase voltages.

In the star connection, when the star point is not connected, the situation is a little more complicated. There is an additional constraint to the stator currents

$$\sum_{i=1}^{m} i_i^s = 0 \tag{67}$$

where m is the number of phases. So there are only m-1 independent stator currents. If a column vector $\mathbf{i}^{s\,\prime}$ that contains the m-1 independent stator currents is defined, the relation between the two current vectors is

$$\mathbf{i}^s = \begin{bmatrix} 1 & 0 & 0 & \dots & 0 \\ 0 & 1 & 0 & \dots & 0 \\ 0 & 0 & 1 & \dots & 0 \\ . & . & . & \dots & . \\ . & . & . & \dots & . \\ . & . & . & \dots & 1 \\ -1 & -1 & -1 & \dots & -1 \end{bmatrix} \mathbf{i}^{s'} = \mathbf{K}^T \mathbf{i}^{s'} \tag{68}$$

where the dimensions of $\mathbf{K}^T$ are m × m-1.

If $\mathbf{v}^s$ denotes the line voltage vector and $\mathbf{u}^s$ the column vector of the potential differences of the stator winding, a relation between the vectors can be written in matrix form

$$\mathbf{K}\mathbf{u}^s = \begin{bmatrix} 1 & 0 & 0 & \dots & 0 & -1 \\ 0 & 1 & 0 & \dots & 0 & -1 \\ 0 & 0 & 1 & \dots & 0 & -1 \\ . & . & . & \dots & . & . \\ . & . & . & \dots & . & . \\ . & . & . & \dots & . & . \\ 0 & 0 & 0 & \dots & 1 & -1 \end{bmatrix} \mathbf{u}^s = - \begin{bmatrix} 0 & 0 & 0 & \dots & 0 & 1 \\ 1 & 0 & 0 & \dots & 0 & 1 \\ 1 & 1 & 0 & \dots & 0 & 1 \\ . & . & . & \dots & . & . \\ . & . & . & \dots & . & . \\ . & . & . & \dots & . & . \\ 1 & 1 & 1 & \dots & 0 & 1 \end{bmatrix} \mathbf{v}^s = \mathbf{Q}\mathbf{v}^s \tag{69}$$

where the dimensions of $\mathbf{Q}$ are m-1 × m .

When Eq. (62) is multiplied by the matrix $\mathbf{K}$ and Eq. (68) is substituted in the equation obtained, the voltage equation for the star connected stator winding is

$$\mathbf{K}\mathbf{D}^s \mathbf{a}_{k+1} - \frac{R_s \Delta t + 2 L_b}{2 N_s l} \mathbf{K}\mathbf{K}^T \mathbf{i}^{s'}_{k+1} + \left\{ -\mathbf{K}\mathbf{D}^s \mathbf{a}_k - \frac{R_s \Delta t - 2 L_b}{2 N_s l} \mathbf{K}\mathbf{K}^T \mathbf{i}^{s'}_k + \frac{\Delta t}{2 N_s l} \mathbf{Q} (\mathbf{v}^s_{k+1} + \mathbf{v}^s_k) \right\} = 0 \tag{70}$$

The current of the m^{th} stator winding is obtained from Eq. (68) if the m-1 independent currents are known. In the discussion of the solution of the coupled field and voltage equations both Eqs. (62) and (70) are expressed by the equation

$$\mathbf{K}\mathbf{D}^s \mathbf{a}_{k+1} + \mathbf{G}^s \mathbf{i}^s_{k+1} + \{ -\mathbf{K}\mathbf{D}^s \mathbf{a}_k + \mathbf{H}^s \mathbf{i}^s_k + \mathbf{C}^s (\mathbf{v}^s_{k+1} + \mathbf{v}^s_k) \} = 0 \tag{71}$$

It should be kept in mind, however, that the definitions of the matrices and the column vector $\mathbf{i}^s$ are different for different connections of the stator winding.

2.3.2 Voltage equations of the rotor cage

In order to shorten the expressions, the voltage equations of the rotor are derived for sinusoidally varying quantities. The derivation follows the lines given by Shen & Meunier (1986), but a more general rotor cage is considered. The same solution method is applicable in the case of general time variation, but the equations are considerably longer. The results are given for both cases.

The scalar potential is a continuous single-valued function. Thus the line integral in Eq. (55) along a closed path must be zero. This gives the condition needed in the construction of the voltage equations for the rotor cage. The potential differences of the rotor bars are calculated from Eq. (19). Using the complex variables the scalar potential difference $\underline{u}^r_n$ induced in the n^{th} rotor bar is given by

$$\underline{u}^r_n = R_r \underline{i}^r_n + j\, s\, \omega\, R_r \int_\Omega \beta^r_n \sigma \left\{ \sum_{j=1}^{N_n} \underline{a}_j N_j \right\} d\Omega \tag{72}$$

where the function β is defined

$$\beta^r_n(x,y) = \begin{cases} 1 & \text{if point (x,y) belongs to rotor bar n} \\ 0 & \text{otherwise.} \end{cases} \tag{73}$$

The slip s is included in Eq. (72) because of the assumption of a pseudostationary rotor.

When the column vectors $\underline{\mathbf{u}}^r$ and $\underline{\mathbf{i}}^r$ are formed from the potential differences and the currents of the rotor bars, the matrix equation

$$\mathbf{D}^r \underline{\mathbf{a}} + \frac{j}{s\,\omega\, l} \underline{\mathbf{i}}^r - \frac{j}{s\,\omega\, l\, R_r} \underline{\mathbf{u}}^r = 0 \tag{74}$$

is obtained. The elements of $\mathbf{D}^r$ are

$$D^r_{ij} = -\frac{1}{l} \int_\Omega \beta^r_i \sigma N_j \, d\Omega \tag{75}$$

Figure 3 shows the circuit and notations used in the derivation of the voltage equations for the rotor cage. In a symmetric cage the currents and potential differences in the corresponding segments of the two end rings are equal in magnitude but opposite in direction. Impedance matrices associated with the bar ends and end-ring segments are defined

$$\mathbf{Z}_{be} = 2\,\underline{Z}_{be}\,\mathbf{1}$$
$$\mathbf{Z}_{sc} = 2\,\underline{Z}_{sc}\,\mathbf{1} \tag{76}$$

where $\mathbf{1}$ denotes the diagonal unit matrix. If the rotor cage is nonsymmetric, more complicated impedance matrices must be defined, but the derivation of the voltage equations remains essentially the same. The total potential difference vector of the rotor bars including also the bar ends outside the two-dimensionally modelled core region is

$$\mathbf{u}^{r\,\prime} = \mathbf{u}^{r} + \mathbf{Z}_{be}\,\mathbf{i}^{r} \tag{77}$$

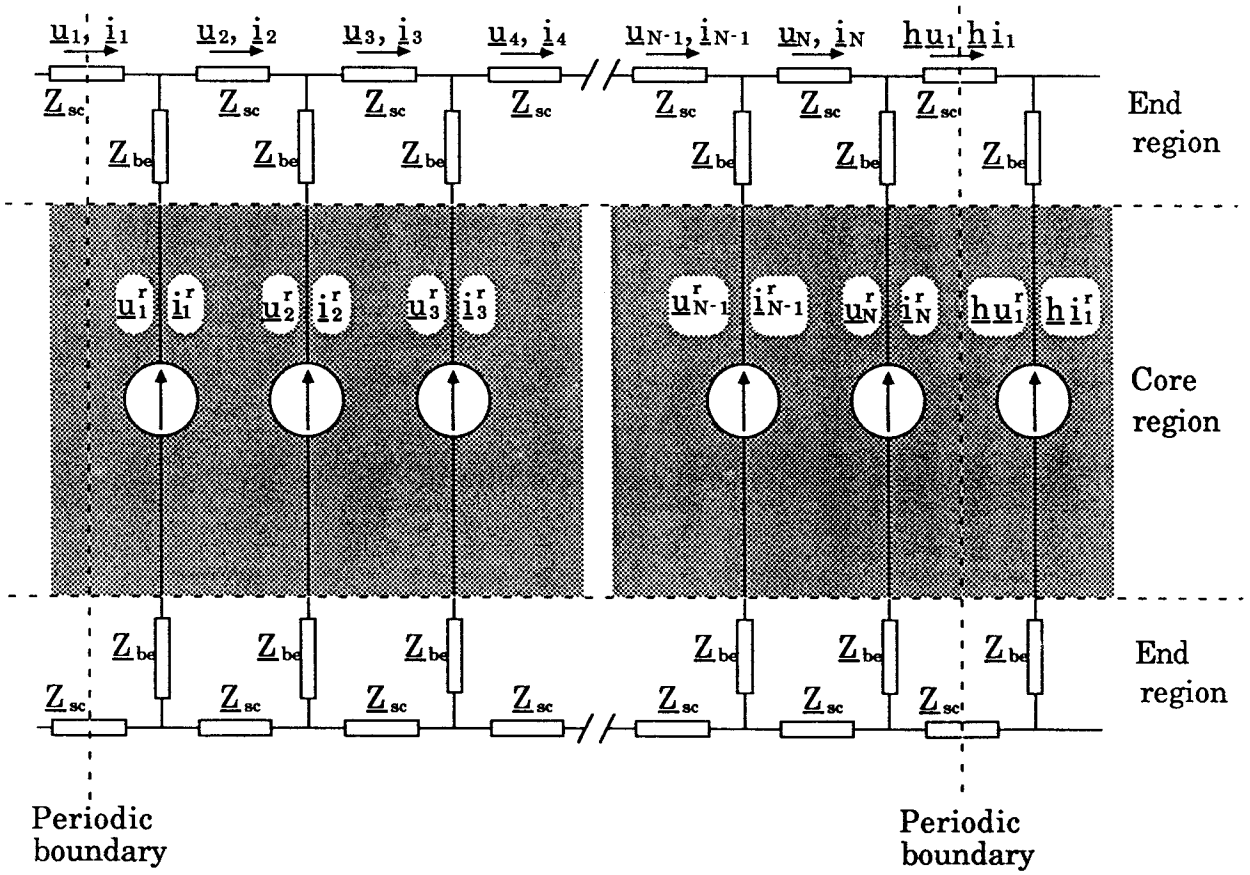

Figure 3. A circuit theoretical model of the rotor cage.

From Kirchhoff 's second law applied to the circuit of Figure 3 a relation between the potential difference vectors is obtained

$$2\,\underline{\mathbf{u}} = \begin{bmatrix} 1 & 0 & 0 & \cdots & -\underline{h} \\ -1 & 1 & 0 & \cdots & 0 \\ 0 & -1 & 1 & \cdots & 0 \\ \cdot & \cdot & \cdot & \cdots & \cdot \\ \cdot & \cdot & \cdot & \cdots & \cdot \\ \cdot & \cdot & \cdot & \cdots & \cdot \\ 0 & 0 & 0 & -1 & 1 \end{bmatrix} \underline{\mathbf{u}}^{r\,'} = \underline{\mathbf{M}}\,\underline{\mathbf{u}}^{r\,'} \tag{78}$$

where $\underline{\mathbf{u}}$ is the column vector of the end-ring potential differences. The periodicity factor $\underline{h}$ is included in the connection matrix $\underline{\mathbf{M}}$ because the currents and potential differences satisfy the same periodicity conditions as the vector potential in Eq. (43). Kirchhoff 's first law gives the equation

$$\underline{\mathbf{i}}^{r} = \begin{bmatrix} -1 & 1 & 0 & \cdots & 0 \\ 0 & -1 & 1 & \cdots & 0 \\ 0 & 0 & -1 & \cdots & 0 \\ \cdot & \cdot & \cdot & \cdots & \cdot \\ \cdot & \cdot & \cdot & \cdots & \cdot \\ \cdot & \cdot & \cdot & \cdots & 1 \\ \underline{h} & 0 & 0 & \cdots & -1 \end{bmatrix} \underline{\mathbf{i}} = -\underline{\mathbf{M}}^{T}\,\underline{\mathbf{i}} \tag{79}$$

where $\underline{\mathbf{i}}$ is the column vector of the end-ring currents. The potential differences in the end-ring segments between adjacent rotor bars are given by

$$2\,\underline{\mathbf{u}} = \underline{\mathbf{Z}}_{sc}\,\underline{\mathbf{i}} \tag{80}$$

Combining Eqs. (76) - (80) we obtain the relation between the rotor bar currents and the potential differences of the bars induced in the core region

$$(1 + \underline{\mathbf{M}}^{T}\,\underline{\mathbf{Z}}_{sc}^{-1}\,\underline{\mathbf{M}}\,\underline{\mathbf{Z}}_{be})\,\underline{\mathbf{i}}^{r} = -(\underline{\mathbf{M}}^{T}\,\underline{\mathbf{Z}}_{sc}^{-1}\,\underline{\mathbf{M}})\,\underline{\mathbf{u}}^{r} \tag{81}$$

The determinant of the connection matrix $\underline{\mathbf{M}}$ is

$$\det(\underline{\mathbf{M}}) = 1 - \underline{h} \tag{82}$$

This means that the product of matrices on the right hand side of Eq. (81) is singular if the periodicity factor is equal to one, i.e. if the symmetry sector contains an integer number of pole pairs. The singularity of the connection

matrix is the outcome of the physical fact that the addition of an extra potential to all the potential differences has no effect on the bar currents. In the singular case Eq. (81) does not define the potential difference vector $\underline{\mathbf{u}}^r$ uniquely as a function of the bar currents. If the periodicity factor differs from one, the periodicity condition gives an additional constraint to the system making the solution of the vector $\underline{\mathbf{u}}^r$ as a function of the currents possible.

Independently of the periodicity factor the potential differences $\underline{\mathbf{u}}^r$ define the currents of the rotor cage uniquely

$$\mathbf{i}^r = -(\mathbf{1} + \underline{\mathbf{M}}^T\, \underline{\mathbf{Z}}_{sc}^{-1}\, \underline{\mathbf{M}}\, \underline{\mathbf{Z}}_{be})^{-1}\, (\underline{\mathbf{M}}^T\, \underline{\mathbf{Z}}_{sc}^{-1}\, \underline{\mathbf{M}})\, \underline{\mathbf{u}}^r \tag{83}$$

When the current vector $\mathbf{i}^r$ is substituted in Eq. (74), the voltage equation of the rotor cage is obtained

$$\mathbf{D}^r\, \underline{\mathbf{a}} - \frac{j}{s\,\omega\,l\,R_r} \left\{ \mathbf{1} + R_r\, (\mathbf{1} + \underline{\mathbf{M}}^T\, \underline{\mathbf{Z}}_{sc}^{-1}\, \underline{\mathbf{M}}\, \underline{\mathbf{Z}}_{be})^{-1}\, (\underline{\mathbf{M}}^T\, \underline{\mathbf{Z}}_{sc}^{-1}\, \underline{\mathbf{M}}) \right\} \underline{\mathbf{u}}^r = 0 \tag{84}$$

When the equation is used at zero slip, a small positive value is given to the variable s in order to avoid overflows in the computer routines.

The derivation of the voltage equations for the rotor cage in the time-stepping formulation follows the lines given above. Only the results are given here. The equations corresponding to Eqs. (72), (83) and (84) are

$$\frac{1}{2}\,(u^r_{n|k+1} + u^r_{n|k}) = \frac{1}{2}\, R_r\, (i^r_{n|k+1} + i^r_{n|k}) + R_r \int_\Omega \beta^r_n\, \sigma \left\{ \sum_{j=1}^{N_n} \frac{a_{j|k+1} - a_{j|k}}{\Delta t}\, N_j \right\} d\Omega \tag{85}$$

$$\mathbf{i}^r_{k+1} = -\left\{ \left(R_{sc} + 2\,\frac{L_{sc}}{\Delta t} \right) \mathbf{1} + \left(R_{be} + 2\,\frac{L_{be}}{\Delta t} \right) \mathbf{M}^T\mathbf{M} \right\}^{-1} \left\{ \frac{1}{2}\, \mathbf{M}^T\mathbf{M}\, (\mathbf{u}^r_{k+1} + \mathbf{u}^r_k) + \left[\left(R_{sc} - 2\,\frac{L_{sc}}{\Delta t} \right) \mathbf{1} + \left(R_{be} - 2\,\frac{L_{be}}{\Delta t} \right) \mathbf{M}^T\mathbf{M} \right] \mathbf{i}^r_k \right\} \tag{86}$$

$$\mathbf{D}^r \mathbf{a}_{k+1} + \frac{\Delta t}{2\,l\,R_r}\left\{\mathbf{1} + \frac{R_r}{2}\left[\left(R_{sc} + 2\frac{L_{sc}}{\Delta t}\right)\mathbf{1} + \left(R_{be} + 2\frac{L_{be}}{\Delta t}\right)\mathbf{M}^T\mathbf{M}\right]^{-1}\mathbf{M}^T\mathbf{M}\right\}\mathbf{u}^r_{k+1}$$

$$-\mathbf{D}^r \mathbf{a}_k + \frac{\Delta t}{2\,l\,R_r}\left\{\mathbf{1} + \frac{R_r}{2}\left[\left(R_{sc} + 2\frac{L_{sc}}{\Delta t}\right)\mathbf{1} + \left(R_{be} + 2\frac{L_{be}}{\Delta t}\right)\mathbf{M}^T\mathbf{M}\right]^{-1}\mathbf{M}^T\mathbf{M}\right\}\mathbf{u}^r_k$$

$$-\frac{\Delta t}{2\,l}\left\{\mathbf{1} - \left[\left(R_{sc} + 2\frac{L_{sc}}{\Delta t}\right)\mathbf{1} + \left(R_{be} + 2\frac{L_{be}}{\Delta t}\right)\mathbf{M}^T\mathbf{M}\right]^{-1} \cdot \left[\left(R_{sc} - 2\frac{L_{sc}}{\Delta t}\right)\mathbf{1} + \left(R_{be} - 2\frac{L_{be}}{\Delta t}\right)\mathbf{M}^T\mathbf{M}\right]\right\}\mathbf{i}^r_k = 0 \qquad (87)$$

For further use Eq. (87) is written in a shorter form

$$\mathbf{D}^r \mathbf{a}_{k+1} + \mathbf{C}^r \mathbf{u}^r{}_{k+1} + \{-\mathbf{D}^r \mathbf{a}_k + \mathbf{C}^r \mathbf{u}^r{}_k + \mathbf{G}^r \mathbf{i}^r{}_k\} = 0 \qquad (88)$$

2.3.3 Solution of the field and voltage equations

In Section 1.3 the field equation with a potential difference as the source term was discretized using the finite element method. If all the conductors of an induction machine are taken into account, the two-dimensional field equation becomes

$$\nabla \times (\nu \nabla \times \mathbf{A}) + \sigma \frac{\partial \mathbf{A}}{\partial t} - \left\{\frac{1}{l}\sum_{j=1}^{Q_r} \sigma\, \beta^r_j\, u^r_j + \sum_{j=1}^{m} \beta^s_j\, i^s_j\right\}\mathbf{e}_z = 0 \qquad (89)$$

where the β functions defined in Eqs. (60) and (73) are used to define the current regions. Q_r denotes the number of rotor bars in the solution sector and m is the number of phases. Not only the vector potential but also the rotor potential differences and stator currents are unknown. Following the lines of Section 1.3 a residual vector $\mathbf{f}^f$ is obtained after the finite element discretization. The i^{th} element of the residual vector is

$$f_i^f(\mathbf{a}_{k+1},\mathbf{u}^r_{k+1},\mathbf{i}^s_{k+1}) = \int_\Omega \left\{ \sum_{j=1}^{N_n} \left(\nu(\mathbf{a}_{k+1})\ \nabla N_i \cdot \nabla N_j + \frac{2\sigma}{\Delta t}\ N_i N_j \right) a_{j|k+1} \right\} d\Omega$$

$$- \int_\Omega \left\{ N_i \frac{1}{l} \sum_{j=1}^{Q_r} \sigma\, \beta_j^r\, u_{j|k+1}^r + N_i \sum_{j=1}^{m} \beta_j^s\, i_{j|k+1}^s \right\} d\Omega$$

$$+ \int_\Omega \left\{ \sum_{j=1}^{N_n} \left(\nu(\mathbf{a}_k)\ \nabla N_i \cdot \nabla N_j - \frac{2\sigma}{\Delta t}\ N_i N_j \right) a_{j|k} \right\} d\Omega$$

$$- \int_\Omega \left\{ N_i \frac{1}{l} \sum_{j=1}^{Q_r} \sigma\, \beta_j^r\, u_{j|k}^r + N_i \sum_{j=1}^{m} \beta_j^s\, i_{j|k}^s \right\} d\Omega \qquad (90)$$

If the connection of the stator winding is taken into account using a connection matrix **K**, the discretized field equation becomes

$$\mathbf{f}^f(\mathbf{a}_{k+1},\mathbf{u}^r_{k+1},\mathbf{i}^s_{k+1}) = \mathbf{S}(\mathbf{a}_{k+1})\,\mathbf{a}_{k+1} + [\mathbf{D}^r]^T\,\mathbf{u}^r_{k+1} + [\mathbf{D}^s]^T\,\mathbf{K}^T\,\mathbf{i}^s_{k+1}$$
$$+ \{\mathbf{S}'(\mathbf{a}_k)\,\mathbf{a}_k + [\mathbf{D}^r]^T\,\mathbf{u}^r_k + [\mathbf{D}^s]^T\,\mathbf{K}^T\,\mathbf{i}^s_k\} = 0 \qquad (91)$$

In the delta connection **K** is a diagonal unit matrix. In the star connection with the disconnected star point **K** is given by Eq. (68) and the stator current vector $\mathbf{i}^s_{k+1}$ contains only the m-1 independent components.

Combining Eq. (91) with the voltage equations (88) and (71) a system of coupled equations is obtained

$$\mathbf{f}^f(\mathbf{a}_{k+1},\mathbf{u}^r_{k+1},\mathbf{i}^s_{k+1}) = \mathbf{S}(\mathbf{a}_{k+1})\,\mathbf{a}_{k+1} + [\mathbf{D}^r]^T\,\mathbf{u}^r_{k+1} + [\mathbf{D}^s]^T\,\mathbf{K}^T\,\mathbf{i}^s_{k+1}$$
$$+ \{\mathbf{S}'(\mathbf{a}_k)\,\mathbf{a}_k + [\mathbf{D}^r]^T\,\mathbf{u}^r_k + [\mathbf{D}^s]^T\,\mathbf{K}^T\,\mathbf{i}^s_k\} = 0$$

$$\mathbf{f}^r(\mathbf{a}_{k+1},\mathbf{u}^r_{k+1}) = \mathbf{D}^r\,\mathbf{a}_{k+1} + \mathbf{C}^r\,\mathbf{u}^r_{k+1} + \{-\mathbf{D}^r\,\mathbf{a}_k + \mathbf{C}^r\,\mathbf{u}^r_k + \mathbf{G}^r\,\mathbf{i}^r_k\} = 0 \qquad (92)$$

$$\mathbf{f}^s(\mathbf{a}_{k+1},\mathbf{i}^s_{k+1}) = \mathbf{K}\,\mathbf{D}^s\,\mathbf{a}_{k+1} + \mathbf{G}^s\,\mathbf{i}^s_{k+1}$$
$$+ \{-\mathbf{K}\,\mathbf{D}^s\,\mathbf{a}_k + \mathbf{H}^s\,\mathbf{i}^s_k + \mathbf{C}^s\,(\mathbf{v}^s_{k+1} + \mathbf{v}^s_k)\} = 0$$

It is possible to eliminate the rotor potential differences $\mathbf{u}^r_{k+1}$ and the stator currents $\mathbf{i}^s_{k+1}$ from the system of equations by solving them in matrix form from the last two equations and substituting in the first equation of Eq. (92). This leads to a small reduction in the number of unknown variables. However, after the

elimination all the nodal values associated with a stator phase winding or with a rotor bar are connected to each other by a full sub-matrix in the coefficient matrix of the system of equations. It was found in tests made for sinusoidally varying quantities that the solution of the reduced system of equations requires more computation time and memory than the solution of the nonreduced system of equations. Therefore, the nodal values of the vector potential, the rotor potential differences and the stator currents are solved together in the same matrix equation.

Because of the nonlinearity of the core material the matrix **S** in the discretized field equation depends on the nodal values of the vector potential. The Newton-Raphson iteration method is used for the solution. Corresponding to Eq. (37) the correction vector at the iteration step n is solved from the equation

$$\begin{bmatrix} \mathbf{P}(\mathbf{a}^n_{k+1}) & (\mathbf{D}^r)^T & (\mathbf{D}^s)^T\,\mathbf{K}^T \\ \mathbf{D}^r & \mathbf{C}^r & \mathbf{0} \\ \mathbf{K}\,\mathbf{D}^s & \mathbf{0} & \mathbf{G}^s \end{bmatrix} \cdot \begin{bmatrix} \Delta\mathbf{a}^n_{k+1} \\ \Delta\mathbf{u}^{r\,n}_{k+1} \\ \Delta\mathbf{i}^{s\,n}_{k+1} \end{bmatrix} = - \begin{bmatrix} \mathbf{f}^f(\mathbf{a}^n_{k+1}, \mathbf{u}^{r\,n}_{k+1}, \mathbf{i}^{s\,n}_{k+1}) \\ \mathbf{f}^r(\mathbf{a}^n_{k+1}, \mathbf{u}^{r\,n}_{k+1}) \\ \mathbf{f}^s(\mathbf{a}^n_{k+1}, \mathbf{i}^{s\,n}_{k+1}) \end{bmatrix} \tag{93}$$

The elements of the sub-matrix **P** are given in Eq. (40).

The choice of the algorithm used for the solution of the correction vector depends on the symmetry of the Jacobian. It is seen from Eq. (93) that the off-diagonal sub-matrices form a symmetric system. The defining equation (40) shows that **P**(**a**) is symmetric. The sub-matrix $\mathbf{C}^r$ has the same structure as the complex coefficient matrix

$$\begin{aligned} \underline{\mathbf{C}}^r &= -\frac{j}{s\,\omega\,l\,R_r}\{\mathbf{1} + R_r\,(\mathbf{1} + \mathbf{M}^T\,\mathbf{Z}_{sc}^{-1}\,\mathbf{M}\mathbf{Z}_{be})^{-1}\,\mathbf{M}^T\,\mathbf{Z}_{sc}^{-1}\mathbf{M}\} \\ &= -\frac{j}{s\,\omega\,l\,R_r}\{\mathbf{1} + R_r[\mathbf{Z}_{be}^{-1} - (\mathbf{Z}_{be} + \mathbf{Z}_{be}\,\mathbf{M}^T\,\mathbf{Z}_{sc}^{-1}\,\mathbf{M}\mathbf{Z}_{be})^{-1}]\} \end{aligned} \tag{94}$$

in Eq. (84). Thus the symmetry of $\mathbf{C}^r$ may be analyzed by studying the symmetry of the more general matrix $\underline{\mathbf{C}}^r$. It is easy to show, by transposing the matrix on the last row of Eq. (94), that $\underline{\mathbf{C}}^r$ is symmetric if the impedance matrices are symmetric. This is true e.g. for a symmetric rotor cage. From the derivations of Eqs. (62) and (70) it can be deduced that $\mathbf{G}^s$ is symmetric for delta and star connected polyphase windings.

Although the Jacobian is symmetric, it is not positive or negative definite. It can

be seen by studying the voltage equations (62), (70) and (71) of the stator winding that the matrix $\mathbf{G}^s$ is negative definite. On the other hand, e.g. for non-conducting linear materials, the quadratic matrix form $^1/_2\,\mathbf{a}^T\mathbf{P}\,\mathbf{a}$ is an estimate of the energy of the magnetic field. As the energy is a positive quantity, the matrix $\mathbf{P}$ is not negative definite. As the Jacobian contains the sub-matrix $\mathbf{P}$ that is not negative definite and the sub-matrix $\mathbf{G}^s$ that is negative definite, the Jacobian is not positive or negative definite. Computer routines designed for positive definite coefficient matrices cannot be used in the solution of Eq. (93).

For a sinusoidally varying magnetic field the equation corresponding to Eq. (89) is

$$\nabla \times (\nu_{ef}\nabla \times \mathbf{A}) + j\,s\omega\sigma\,\mathbf{A} - \left\{ \frac{1}{l}\sum_{j=1}^{Q_r} \sigma\,\beta_j^r\,\underline{u}_j^r + \sum_{j=1}^{m} \beta_j^s\,\underline{i}_j^s \right\} \mathbf{e}_z = 0 \tag{95}$$

where the variable s is equal to the slip in rotor elements, but equal to one in stator elements. In this case the discretized field equation is

$$\mathbf{f}^f(\underline{\mathbf{a}},\underline{\mathbf{u}}^r,\underline{\mathbf{i}}^s) = \underline{\mathbf{S}}(\underline{\mathbf{a}})\,\underline{\mathbf{a}} + [\mathbf{D}^r]^T\,\underline{\mathbf{u}}^r + [\mathbf{D}^s]^T\,\mathbf{K}^T\,\underline{\mathbf{i}}^s = 0 \tag{96}$$

where the elements of the matrix $\underline{\mathbf{S}}(\underline{\mathbf{a}})$ are

$$\mathbf{S}_{il}(\underline{\mathbf{a}}) = \int_{\Omega} \{\nu_{ef}(\underline{\mathbf{a}})\ \nabla N_i \cdot \nabla N_l + j\,s\omega\sigma\,N_i\,N_l\}\,d\Omega \tag{97}$$

When Eq. (96) is combined with the voltage equations (84) and (66), and the connection of the stator winding is taken into account in Eq. (66), a system of equations is obtained that can be written in matrix form

$$\begin{bmatrix} \mathbf{f}^f \\ \mathbf{f}^r \\ \mathbf{f}^s \end{bmatrix} = \begin{bmatrix} \underline{\mathbf{S}}(\underline{\mathbf{a}}) & (\mathbf{D}^r)^T & (\mathbf{D}^s)^T\mathbf{K}^T \\ \mathbf{D}^r & \underline{\mathbf{C}}^r & \mathbf{0} \\ \mathbf{K}\mathbf{D}^s & \mathbf{0} & \underline{\mathbf{G}}^s \end{bmatrix} \cdot \begin{bmatrix} \underline{\mathbf{a}} \\ \underline{\mathbf{u}}^r \\ \underline{\mathbf{i}}^s \end{bmatrix} + \begin{bmatrix} \mathbf{0} \\ \mathbf{0} \\ \underline{\mathbf{h}}(\underline{\mathbf{v}}^s) \end{bmatrix} = \begin{bmatrix} \mathbf{0} \\ \mathbf{0} \\ \mathbf{0} \end{bmatrix} \tag{98}$$

The real matrices in Eq. (98) are the same matrices as in Eq. (93) for the time-stepping method. The matrix $\underline{\mathbf{C}}^r$ is given in Eq. (94). The matrix $\underline{\mathbf{G}}^s$ is

$$\underline{\mathbf{G}}^s = -\frac{R_s + j\,\omega\,L_b}{j\,\omega\,l\,N_s}\,\mathbf{K}\mathbf{K}^T \tag{99}$$

for a symmetric stator winding, and the source vector is

$$\underline{\mathbf{h}}(\underline{\mathbf{Y}}^s) = \frac{1}{j\,\omega\,l\,N_s}\,\mathbf{Q}\,\underline{\mathbf{Y}}^s \tag{100}$$

where **K** is the connection matrix of the stator winding
Q is the diagonal unit matrix in the delta connection and the matrix defined in Eq. (69) in the star connection
$\underline{\mathbf{Y}}^s$ is the column vector of the line voltages.

If the system under consideration is magnetically linear, the matrix $\underline{\mathbf{S}}$ is independent of the vector potential and the equations are linear. The column vector of the unknown quantities can be solved directly from Eq. (98). It can be shown as above that the coefficient matrix in Eq. (98) is symmetric for machines with symmetric rotor cages.

In a nonlinear case the solution has to be found iteratively. The use of the Newton-Raphson iteration method is a little more complicated than in the step-by-step formulation because the real valued reluctivity is not differentiable with respect to the complex nodal values. The difficulty is avoided if the real and imaginary parts of Eq. (98) are separated and the larger system of equations of real variables is solved with the Newton-Raphson method. The correction vector at the iteration step n is solved from the equation

$$\begin{bmatrix}
\mathbf{P}^1(a_R^n,a_I^n) & \mathbf{R}(a_R^n,a_I^n) & (\mathbf{D}^r)^T & 0 & (\mathbf{D}^s)^T\mathbf{K}^T & 0 \\
-\mathbf{T}(a_R^n,a_I^n) & -\mathbf{P}^2(a_R^n,a_I^n) & 0 & -(\mathbf{D}^r)^T & 0 & -(\mathbf{D}^s)^T\mathbf{K}^T \\
\mathbf{D}^r & 0 & \mathbf{C}_R^r & -\mathbf{C}_I^r & 0 & 0 \\
0 & -\mathbf{D}^r & -\mathbf{C}_I^r & -\mathbf{C}_R^r & 0 & 0 \\
\mathbf{K}\mathbf{D}^s & 0 & 0 & 0 & \mathbf{G}_R^s & -\mathbf{G}_I^s \\
0 & -\mathbf{K}\mathbf{D}^s & 0 & 0 & -\mathbf{G}_I^s & -\mathbf{G}_R^s
\end{bmatrix}
\cdot
\begin{bmatrix}
\Delta a_R^n \\ \Delta a_I^n \\ \Delta u_R^{r\,n} \\ \Delta u_I^{r\,n} \\ \Delta i_R^{s\,n} \\ \Delta i_I^{s\,n}
\end{bmatrix}
= -
\begin{bmatrix}
f_R^f \\ -f_I^f \\ f_R^r \\ -f_I^r \\ f_R^s \\ -f_I^s
\end{bmatrix} \tag{101}$$

where the subscript R denotes the real part of a matrix or a vector and the subscript I denotes the imaginary part. The rows containing the imaginary parts of the residual vectors have been multiplied by -1. This gives a symmetric Jacobian matrix in magnetically linear cases. The elements of the matrices $\mathbf{P}^1$, $\mathbf{P}^2$, **R** and **T** are

$$\mathbf{P}^1_{lm}(\mathbf{a}_R,\mathbf{a}_I) = \frac{\partial}{\partial a_{R\,m}} \left\{ \int_\Omega \left\{ \sum_{j=1}^{N_n} [\nu_{ef}(\mathbf{a}_R,\mathbf{a}_I)\ \nabla\ N_l \cdot \nabla\ N_j]\ a_{Rj} \right\} d\Omega \right\}$$

$$\mathbf{P}^2_{lm}(\mathbf{a}_R,\mathbf{a}_I) = \frac{\partial}{\partial a_{I\,m}} \left\{ \int_\Omega \left\{ \sum_{j=1}^{N_n} [\nu_{ef}(\mathbf{a}_R,\mathbf{a}_I)\ \nabla\ N_l \cdot \nabla\ N_j]\ a_{Ij} \right\} d\Omega \right\} \qquad (102)$$

$$\mathbf{R}_{lm}(\mathbf{a}_R,\mathbf{a}_I) = \frac{\partial}{\partial a_{I\,m}} \left\{ \int_\Omega \left\{ \sum_{j=1}^{N_n} [\nu_{ef}(\mathbf{a}_R,\mathbf{a}_I)\ \nabla\ N_l \cdot \nabla\ N_j\ a_{Rj} - s\omega\sigma\ N_l\ N_j\ a_{Ij}] \right\} d\Omega \right\}$$

$$\mathbf{T}_{lm}(\mathbf{a}_R,\mathbf{a}_I) = \frac{\partial}{\partial a_{R\,m}} \left\{ \int_\Omega \left\{ \sum_{j=1}^{N_n} [\nu_{ef}(\mathbf{a}_R,\mathbf{a}_I)\ \nabla\ N_l \cdot \nabla\ N_j\ a_{Ij} + s\omega\sigma\ N_l\ N_j\ a_{Rj}] \right\} d\Omega \right\}$$

If the effective reluctivity is a function of the vector potential, the matrix **R** is not the transposed matrix of **-T**. This means that the Jacobian is nonsymmetric in magnetically nonlinear cases. The nonsymmetry increases the computation time and the size of the computer memory required in the solution of the equations.

The integrals in the expressions of the Jacobian matrix and the residual vector are calculated element by element. Isoparametric triangular elements are used and the integrals are computed using numerical quadrature formulas (Laursen & Gellert 1978) in the local normalized coordinate system associated with the isoparametric mapping. The reluctivity curve of the core material is approximated by cubic splines, the square of the flux density as the independent variable (Silvester et al. 1973).

The Jacobian of the Newton-Raphson method is a sparse matrix. A library of computer routines (Chu et al. 1984) is used for the solution of the matrix equations. The solution is based on the Gaussian elimination and various ordering methods are available for symmetric and nonsymmetric matrices. Tests have shown that the shortest solution times are usually obtained by a method that uses a variant of the minimum degree algorithm. About 40 - 50 % of the total computation time is spent in the solution of the matrix equation, when second-order isoparametric elements are used. The computation of the elements of the Jacobian matrix and the residual vector takes almost as much time as the solution.

The relatively long time constants associated with the windings of induction motors complicate the use of the step-by-step method in the simulation of

steady-state operation. If the zero field is taken as the initial state, tens of periods of the line frequency have to be simulated before a steady state is reached. The results of the sinusoidal approximation can be used to find an initial state that is nearer to the steady state. A saturated field computed using an effective reluctivity is not, however, a physically correct state of the machine. If the step-by-step method is started from such a field, oscillations will occur in the solution. The problem is avoided by computing a DC field whose sources are the instantaneous values of the currents in the sinusoidal approximation. The same peak value reluctivity curve is used for the solution of the initial state as in the step-by-step method. When the simulation is started from the DC field and the instantaneous currents, a steady state good enough is usually reached in a couple of simulated periods.

2.3.4 Modelling a skewed rotor

As mentioned in Section 2.2 the effect of skewed rotor slots can be taken into account if the machine is thought to be made up of several slices that have been cut from an ideal two-dimensional machine by planes perpendicular to the shaft. The rotors of the adjacent slices have been rotated by an angle corresponding to the skew. The winding currents are assumed to be continuous from slice to slice. The magnetic field of each slice is solved separately using a two-dimensional formulation.

In principle the field and voltage equations of a skewed machine could be solved with the Newton-Raphson iteration method as it was done for an unskewed machine above. However, as each slice has its own discretized field equation, and there should be several slices to model the skew properly, the matrix equation becomes too large to be solved efficiently. This is particularly true for sinusoidally varying fields as their matrix equations contain twice as many unknown variables as the equations in the step-by-step method.

Williamson & Begg (1985) have used an iteration method that is easy to apply to the solution of a sliced machine. The method is based on the idea of an impedance matrix $\mathbf{Z}$ that gives the relation between the potential differences $\underline{\mathbf{u}}$ and the currents $\underline{\mathbf{i}}$ of the windings

$$\underline{\mathbf{u}} = \mathbf{Z}\,\underline{\mathbf{i}} \tag{103}$$

The problem is to find the current vector and the impedance matrix that give the potential differences corresponding to the line voltage vector $\underline{\mathbf{y}}^s$. If the system is

nonlinear, the impedance matrix is current-dependent. The current vector is searched iteratively by constructing the impedance matrix $\underline{\mathbf{Z}}_n$ corresponding to a trial current vector $\mathbf{i}_n$

$$\underline{\mathbf{u}}_n = \underline{\mathbf{Z}}_n \mathbf{i}_n \tag{104}$$

A new corrected current vector is obtained by replacing the potential difference vector by the line voltage vector and solving for the current

$$\mathbf{i}_{n+1} = \underline{\mathbf{Z}}_n^{-1} \underline{\mathbf{y}}^s \tag{105}$$

When the method is applied to a skewed machine, the impedance matrix is constructed from the impedance matrices of the slices and the end windings. The column vectors of the stator and rotor potential differences induced in the slice m are written

$$\begin{aligned} \underline{\mathbf{u}}^s_m &= \underline{\mathbf{Z}}^{ss}_m \mathbf{i}^s + \underline{\mathbf{Z}}^{sr}_m \mathbf{i}^r \\ \underline{\mathbf{u}}^r_m &= \underline{\mathbf{Z}}^{rs}_m \mathbf{i}^s + \underline{\mathbf{Z}}^{rr}_m \mathbf{i}^r \end{aligned} \tag{106}$$

The coupling matrices in Eq. (106) are current-dependent because of the nonlinearity of the core material. Thus the matrices correspond to a certain operation state of the machine. In order to separate the couplings between the windings the system must be linearized in this state. This is done by fixing the reluctivities in the elements to the values that prevail in the total field induced by all the currents together.

The elements of the j^{th} column of the coupling matrices are evaluated by feeding a current to the j^{th} winding (a stator winding or a rotor bar) and solving the magnetic field of the linearized slice. Because a current is used as the source, the field in the rotor bars is solved from Eq. (21). The potential differences induced in the conductors are calculated from Eqs. (65) and (72). The resistances and the end-winding inductances of the stator winding are, however, neglected at this stage. The matrix element between e.g. two rotor bars is given by

$$\underline{Z}^{rr}_{m|ij} = \frac{\underline{u}^r_{m|i}}{\underline{i}^r_j} = \frac{1}{N_s}\left\{ R_r \delta_{ij} + \frac{j s \omega R_r}{\underline{i}^r_j} \int_{\Omega_m} \beta^r_i \sigma \left(\sum_{j=1}^{N_n} \underline{a}_j N_j \right) d\Omega \right\} \tag{107}$$

where N_s is the number of slices and δ_{ij} is the Kronecker delta. The total potential

differences induced in the core region are obtained by adding the potential differences of the slices together

$$\underline{\mathbf{u}}^{s} = \sum_{m=1}^{N_s} \underline{\mathbf{Z}}_m^{ss}\,\underline{\mathbf{i}}^{s} + \sum_{m=1}^{N_s} \underline{\mathbf{Z}}_m^{sr}\,\underline{\mathbf{i}}^{r} = \underline{\mathbf{Z}}^{ss}\,\underline{\mathbf{i}}^{s} + \underline{\mathbf{Z}}^{sr}\,\underline{\mathbf{i}}^{r}$$
$$\underline{\mathbf{u}}^{r} = \sum_{m=1}^{N_s} \underline{\mathbf{Z}}_m^{rs}\,\underline{\mathbf{i}}^{s} + \sum_{m=1}^{N_s} \underline{\mathbf{Z}}_m^{rr}\,\underline{\mathbf{i}}^{r} = \underline{\mathbf{Z}}^{rs}\,\underline{\mathbf{i}}^{s} + \underline{\mathbf{Z}}^{rr}\,\underline{\mathbf{i}}^{r} \tag{108}$$

The voltage equation of the stator winding is obtained by adding the terms containing the resistance and the end-winding inductance to the first equation. To get the voltage equation of the rotor cage the equations derived for the circuit of Figure 3 are used. Combining Eqs. (77) and (78) the equation

$$\underline{\mathbf{M}}\,\underline{\mathbf{u}}^{r} + \underline{\mathbf{M}}\,\underline{\mathbf{Z}}_{be}\,\underline{\mathbf{i}}^{r} - 2\,\underline{\mathbf{u}} = 0 \tag{109}$$

is obtained. In order to use the impedance method the end-ring potential difference vector $\underline{\mathbf{u}}$ must be expressed as a function of the bar current vector $\underline{\mathbf{i}}^{r}$. If the connection matrix $\underline{\mathbf{M}}$ has an inverse matrix, the potential difference vector is eliminated using Eqs. (80) and (79)

$$2\,\underline{\mathbf{u}} = \underline{\mathbf{Z}}_{sc}\,\underline{\mathbf{i}} = -\underline{\mathbf{Z}}_{sc}\,(\underline{\mathbf{M}}^{T})^{-1}\,\underline{\mathbf{i}}^{r} \tag{110}$$

and substituting back to Eq. (109)

$$\underline{\mathbf{M}}\,\underline{\mathbf{u}}^{r} + \{\underline{\mathbf{M}}\,\underline{\mathbf{Z}}_{be} + \underline{\mathbf{Z}}_{sc}\,(\underline{\mathbf{M}}^{T})^{-1}\}\,\underline{\mathbf{i}}^{r} = 0 \tag{111}$$

However, as discussed above, the connection matrix is singular if the periodicity factor is equal to one. In this case we need an additional constraint that is obtained by studying the potential differences of the end rings. If the periodicity factor is equal to one, the sum of the end-ring potential differences is zero

$$\sum_{i=1}^{Q_r} \underline{u}_i = \sum_{i=1}^{Q_r} \underline{Z}_{sc}\,\underline{i}_i = \underline{Z}_{sc} \sum_{i=1}^{Q_r} \underline{i}_i = 0 \tag{112}$$

The assumption that all the end-ring segments have equal impedances made in Eq. (112) gives the condition that the sum of the end-ring currents is zero. This means that the multiplication of the end-ring current vector by a matrix $\mathbf{K}_b$,

whose elements are all equal e.g. to one, gives the zero column vector. This zero vector is added to Eq. (79)

$$\mathbf{i}^r = -\underline{\mathbf{M}}^T \mathbf{i} = -(\mathbf{K}_b + \underline{\mathbf{M}}^T)\,\mathbf{i} \tag{113}$$

As a result, a nonsingular coefficient matrix is obtained and the end-ring current can be solved

$$\mathbf{i} = -(\mathbf{K}_b + \underline{\mathbf{M}}^T)^{-1}\,\mathbf{i}^r \tag{114}$$

The equation corresponding to Eq. (111) is obtained by substituting Eq. (114) in Eqs. (80) and (109)

$$\underline{\mathbf{M}}\,\mathbf{u}^r + \{\underline{\mathbf{M}}\,\mathbf{Z}_{be} + \mathbf{Z}_{sc}\,(\mathbf{K}_b + \underline{\mathbf{M}}^T)^{-1}\}\,\mathbf{i}^r = 0 \tag{115}$$

The expression in the parentheses is taken to mean the end-winding impedance of the rotor cage

$$\mathbf{Z}^r_b = \underline{\mathbf{M}}\,\mathbf{Z}_{be} + \mathbf{Z}_{sc}\,(\mathbf{K}_b + \underline{\mathbf{M}}^T)^{-1} \tag{116}$$

If the elements of the matrix $\mathbf{K}_b$ are defined

$$K_{b\,ij} = \begin{cases} 1 & \text{if} \quad \underline{h} = 1 \\ 0 & \text{otherwise} \end{cases} \tag{117}$$

Eq. (116) can be taken as a general expression for the end-winding impedance of a cage winding. The potential difference vector is eliminated from the voltage equation of the rotor cage by substituting the second equation in Eqs. (108) and Eq. (116) in Eq. (115)

$$\underline{\mathbf{M}}\,(\mathbf{Z}^{rs}\,\mathbf{i}^s + \mathbf{Z}^{rr}\,\mathbf{i}^r) + \mathbf{Z}^r{}_b\,\mathbf{i}^r = 0 \tag{118}$$

Taking the resistance and the end-winding inductance of the stator winding into account through the impedance matrix $\mathbf{Z}^s{}_b$ the voltage equation of the machine becomes

$$\begin{bmatrix} \mathbf{u}^s \\ \mathbf{0} \end{bmatrix} = \begin{bmatrix} \mathbf{Z}^{ss} + \mathbf{Z}^s_b & \mathbf{Z}^{sr} \\ \underline{\mathbf{M}}\,\mathbf{Z}^{rs} & \underline{\mathbf{M}}\,\mathbf{Z}^{rr} + \mathbf{Z}^r_b \end{bmatrix} \cdot \begin{bmatrix} \mathbf{i}^s \\ \mathbf{i}^r \end{bmatrix} \tag{119}$$

The impedance method is applied to Eq. (119). The n^{th} iteration step is

$$\begin{bmatrix} \mathbf{i}^s \\ \mathbf{i}^r \end{bmatrix}_{n+1} = \begin{bmatrix} \mathbf{Z}^{ss}+\mathbf{Z}^s_b & \mathbf{Z}^{sr} \\ \mathbf{M}\mathbf{Z}^{rs} & \mathbf{M}\mathbf{Z}^{rr}+\mathbf{Z}^r_b \end{bmatrix}_n^{-1} \cdot \begin{bmatrix} \mathbf{v}^s \\ \mathbf{0} \end{bmatrix} \tag{120}$$

The method described contains, as inner iteration loops, the solutions of the magnetic fields of the slices. The outer iteration loop consists of the solution of the voltage equations. As already mentioned such an iteration method is often slow to converge. Depending on the saturation level of the machine 5 - 10 outer iteration steps are usually needed to reach a result accurate enough. The inner iteration loops containing the Newton-Raphson solutions of the field are essentially similar to the solution of an unskewed machine. Thus the solution of a skewed machine takes considerably more computation time than the solution of an unskewed machine using a direct Newton-Raphson iteration. In order to reduce the amount of computation it is worth solving the field of an unskewed machine of the same cross sectional geometry and using it as the initial state in the iteration of the skewed machine.

In a linear case the impedance method gives the converged current vector at the first iteration step. If the method is used to solve an unskewed machine the results obtained are, of course, the same as the results obtained by the direct solution. An advantage of the method is that the impedance matrix obtained can be used in the evaluation of the parameters of the equivalent circuit of the machine (Section 2.4).

The equations were derived for sinusoidally varying fields. A similar method is possible in the connection of a step-by-step method, but the time consumption very soon becomes a limiting factor. In a step-by-step method the discretized field equations of the slices and the voltage equations of the windings should be solved in a same matrix equation, if only the memory capacity of the computer allows this. So far the method has not been implemented in the step-by-step routines.

2.4 Machine characteristics derivable from the field solution

The magnetic field, the currents and the potential differences of the windings are obtained in the solution of the coupled field and voltage equations of the machine as discussed in Section 2.3. Most of the other machine characteristics can be derived from these quantities. This section deals with the determination of the torque, resistive losses and the coefficients of the equivalent circuit.

Torque

Methods based on Maxwell's stress tensor are commonly used in the calculation of forces and torques in the finite element analysis of electrical devices (Reichert et al. 1976). The electromagnetic torque is obtained as a surface integral

$$T_e = \oint_S \mathbf{r} \times \boldsymbol{\sigma} \cdot dS$$

$$= \oint_S \mathbf{r} \times \left\{ \frac{1}{\mu_0} (\mathbf{B} \cdot \mathbf{n}) \mathbf{B} - \frac{1}{2\mu_0} B^2 \mathbf{n} \right\} dS \qquad (121)$$

where $\boldsymbol{\sigma}$ is Maxwell's stress tensor

$\mathbf{n}$ is the unit normal vector of the integration surface S.

When Eq. (121) is applied to the calculation of the torque of an induction motor, a closed integration surface that surrounds the rotor in free space must be chosen. In the two-dimensional model the surface integral is reduced to a line integral along the air gap. If a circle of radius r is taken as the integration path, the torque is obtained from the equation

$$T_e = \frac{l}{\mu_0} \int_0^{2\pi} r^2 B_r B_\varphi \, d\varphi \qquad (122)$$

where B_r and B_φ are the r- and φ-components of the flux density.

If the solution were exact, the value of the torque calculated from Eq. (122) would be independent of the radius r when r varies between the inner and outer radii of the air gap. However, in an approximate solution the integration path has an effect on the result. In practice, the variation of the torque as a function of the radius r may be as high as 50 % from the average value, when a typical finite element mesh like the one in Figure 2 is used. For linear elements Reichert et al. (1976) have suggested a zig-zag integration path through the midpoints of the elements and element sides.

Coulomb (1983) has presented a method based on the principle of virtual work, where the three-dimensional surface integral in Eq. (121) is replaced by a volume integral over a hollow shell in free space surrounding the moving body. In the two-dimensional model of an electrical machine a similar method can be derived

easily. As the true torque is independent of the radius, we obtain by integrating the expressions in Eq. (122) in the radial direction over the air gap

$$T_e\,(r_s - r_r) = \int_{r_r}^{r_s} T_e\,dr$$

$$= \frac{1}{\mu_0} \int_{r_r}^{r_s} \left\{ \int_0^{2\pi} r\,B_r\,B_\varphi\,r\,d\varphi \right\} dr$$

$$= \frac{1}{\mu_0} \int_{S_{ag}} r\,B_r\,B_\varphi\,dS \qquad (123)$$

where r_s and r_r are the outer and inner radii of the air gap respectively and S_{ag} is the cross sectional area of the air gap. From the equation above the torque is obtained as an integral over the air gap

$$T_e = \frac{1}{\mu_0\,(r_s - r_r)} \int_{S_{ag}} r\,B_r\,B_\varphi\,dS \qquad (124)$$

Eq. (124) has proven to give more reliable results than the expression in Eq. (122) (Chapter 3). The method is also very easy to implement in a finite element formulation because the same quadrature formulas can be used to compute the torque as are used in the computation of the residual vector and the Jacobian matrix.

If the air gap element is used, an analytical series expansion is obtained for the vector potential. The series derived for the torque from the series expansion of the vector potential is independent of the radius. The accuracy of the torque is related to the accuracy of the vector potential series in the air gap. The drawback of the method is the long computation time needed in the calculation of the coefficients of the series expansions.

In a general case the field and voltage equations are coupled through the electromagnetic torque to the equation of motion of the rotor

$$J_m \frac{d\Omega_m}{dt} = T_e - T_s \qquad (125)$$

where J_m is the moment of inertia of the rotor
Ω_m is the mechanical angular frequency of the rotor
T_s is the shaft torque.

The effect of friction losses is neglected. When Eq. (125) is used in the step-by-step method, the time derivative is replaced by a first-order difference ratio. At each time step the angular frequency and the rotation angle α are corrected by

$$\Omega_{m,k+1} = \Omega_{m,k} + \frac{T_{e,k} - T_{s,k}}{J_m} \Delta t$$
$$\alpha_{k+1} = \alpha_k + \Omega_{m,k} \Delta t \qquad (126)$$

The rotor is rotated by changing the finite element mesh in the air gap or with an air gap element to correspond to the value of the rotation angle.

Power balance and losses

At constant rotation speed a power balance exists in the model motor

$$P_{in} = P_{out} + P^s_{res} + P^r_{res} + \frac{dW_{em}}{dt}$$
$$= \Omega_m T_e + P^s_{res} + P^r_{res} + \frac{dW_{em}}{dt} \qquad (127)$$

where P_{in} is the input power of the stator winding
P_{out} is the output power on the shaft
P^s_{res} is the resistive losses of the stator winding
P^r_{res} is the resistive losses of the rotor cage
W_{em} is the electromagnetic energy of the fields.

As discussed in Section 2.2 the core material is treated as a non-conducting material without losses. The friction losses are also neglected in Eq. (127). The instantaneous input power of the motor is calculated from the potential differences and the currents of the stator windings

$$P_{in} = \sum_{i=1}^{m} u^s_i \, i^s_i \qquad (128)$$

In principle the resistive losses are calculated as a volume integral over the

conductor

$$P_{res} = \int_V \frac{1}{\sigma} \mathbf{J}^2 \, dV \tag{129}$$

However, as the circuit theoretical model is used for the stator windings the resistive losses of the stator are calculated from the resistances and the currents of the windings

$$P_{res}^s = \sum_{i=1}^{m} R_{si} \, (i_i^s)^2 \tag{130}$$

The resistive losses of the rotor cage are

$$P_{res}^r = \int_V -\mathbf{J} \cdot \frac{\partial \mathbf{A}}{\partial t} \, dV$$

$$= \sum_{i=1}^{Q_r} \int_{V_i} \sigma \left\{ \left(\frac{\partial A}{\partial t} \right)^2 - \frac{u_i^r}{l} \frac{\partial A}{\partial t} \right\} dV \tag{131}$$

where V_i is the volume of the i^{th} rotor bar inside the two-dimensional core region. The expressions in Eq. (131) also include the power fed to the ends of the rotor cage.

Eqs. (127) - (131) are expressions for instantaneous power. In a steady state average values are used. Expressions for the average powers are easily derived from the equations above. In the time-stepping method the average values are calculated by taking the time average of the power over a time interval long enough. If the assumption of sinusoidal time variation is made, average values are calculated as usual for the product of two phasors.

Eq. (127) gives a possibility to test the methods used in the calculation of the torque. In a steady state the time average of the change of the electromagnetic energy is zero if an integration time long enough is used. Thus an estimate for the average value of the electromagnetic torque is obtained from the average values of the powers. In Chapter 3 this method is used to check the reliability of the torque values obtained from Eq. (124).

Parameters of the equivalent circuit

The results of a conventional machine calculation method are often given as parameters of an equivalent circuit. It is also possible to obtain the parameters from the finite element analysis of an induction motor although some extra computation is needed. Figure 4 shows an equivalent circuit that is commonly used for induction motors.

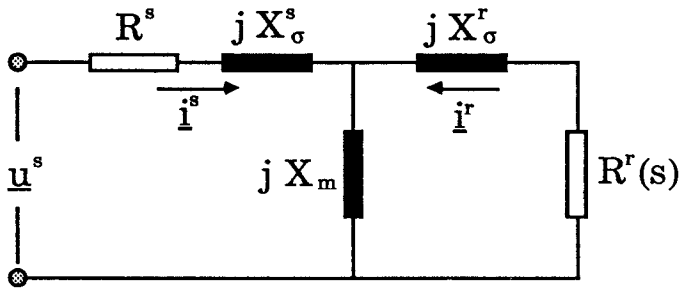

Figure 4. An equivalent circuit of an induction motor.

The iron loss resistance often connected parallel to the magnetization reactance X_m is not included in the circuit, as iron losses are neglected in the analysis. The components of an equivalent circuit are usually constants or at least independent of time. The motion of the rotor is taken into account in the rotor resistance R^r that is a function of the slip s. Thus equivalent circuits are related to the assumptions of sinusoidal time variation and a pseudostationary rotor.

The impedance method described in the previous section gives the coupling matrix between the line voltage and the stator and rotor currents. In a way Eq. (119) can be taken as the voltage equation of a complicated equivalent circuit. A method related to the theory of symmetric components is used to reduce the coupling matrix of the impedance method to the parameters of the simple equivalent circuit in Figure 4. If the stator winding has m phases and the rotor bars are taken to form a polyphase system with Q_r phases, the positive phase-sequence stator voltage, stator current and rotor current are defined

$$\underline{u}^s_+ = \frac{1}{m}\sum_{i=1}^{m} \underline{u}^s_i \, e^{j\frac{2\pi(i-1)}{m}}$$

$$\underline{i}^s_+ = \frac{1}{m}\sum_{i=1}^{m} \underline{i}^s_i \, e^{j\frac{2\pi(i-1)}{m}} \qquad (132)$$

$$\underline{i}^r_+ = \frac{1}{Q_r}\sum_{i=1}^{Q_r} \underline{i}^r_i \, e^{j\frac{2\pi(i-1)}{Q_r}}$$

The subscript + is used for positive phase-sequence quantities. Q_r is the number of rotor bars in the solution sector discretized by the finite element method. The equations are written for a solution sector containing an integer number of pole pairs. By substituting the stator potential differences in Eq. (119) to the first expression in Eq. (132) the positive phase-sequence voltage is obtained as a function of the currents

$$\underline{u}^s_+ = \frac{1}{m}\sum_{i=1}^{m}\sum_{k=1}^{m}(\underline{Z}^{ss}_{ik} + \underline{Z}^{s}_{b\,ik})\,\underline{i}^s_k \, e^{j\frac{2\pi(i-1)}{m}} + \frac{1}{m}\sum_{i=1}^{m}\sum_{k=1}^{Q_r}\underline{Z}^{sr}_{ik}\,\underline{i}^r_k \, e^{j\frac{2\pi(i-1)}{m}} \qquad (133)$$

The first sum in Eq. (133) is taken to be the voltage induced by the positive phase-sequence stator current and the second sum the voltage induced by the positive phase-sequence rotor current. From this basis the equation is written in the simple form

$$\underline{u}^s_+ = \underline{z}^{ss}\,\underline{i}^s_+ + \underline{z}^{sr}\,\underline{i}^r_+ \qquad (134)$$

where the impedances $\underline{z}^{ss}$ and $\underline{z}^{sr}$ are obtained by dividing the sum containing the stator currents by $\underline{i}^s_+$ and the sum containing the rotor currents by $\underline{i}^r_+$

$$\underline{z}^{ss} = \frac{1}{m\,\underline{i}^s_+}\sum_{i=1}^{m}\sum_{k=1}^{m}(\underline{Z}^{ss}_{ik} + \underline{Z}^{s}_{b\,ik})\,\underline{i}^s_k \, e^{j\frac{2\pi(i-1)}{m}}$$

$$\underline{z}^{sr} = \frac{1}{m\,\underline{i}^r_+}\sum_{i=1}^{m}\sum_{k=1}^{Q_r}\underline{Z}^{sr}_{ik}\,\underline{i}^r_k \, e^{j\frac{2\pi(i-1)}{m}} \qquad (135)$$

The zero vector in Eq. (119) may be taken as the potential difference vector of the rotor winding with Q_r phases. The positive phase-sequence rotor voltage is formed in a similar manner as the positive phase-sequence stator voltage above

$$\underline{u}_+^r = \frac{1}{Q_r}\sum_{i=1}^{Q_r}\sum_{k=1}^{m}(\underline{\mathbf{M}}\underline{\mathbf{Z}}^{rs})_{ik}\,\underline{i}^s{}_k\, e^{j\frac{2\pi(i-1)}{Q_r}}$$

$$+\frac{1}{Q_r}\sum_{i=1}^{Q_r}\sum_{k=1}^{Q_r}(\underline{\mathbf{M}}\underline{\mathbf{Z}}^{rr}+\underline{\mathbf{Z}}^r{}_b)_{ik}\,\underline{i}^r_k\, e^{j\frac{2\pi(i-1)}{Q_r}} = 0 \qquad (136)$$

or in a shorter form

$$\underline{u}_+^r = \underline{w}^{rs}\,\underline{i}_+^s + \underline{w}^{rr}\,\underline{i}_+^r = 0 \qquad (137)$$

The coefficients are given by

$$\underline{w}^{rs} = \frac{1}{Q_r\,\underline{i}_+^s}\sum_{i=1}^{Q_r}\sum_{k=1}^{m}(\underline{\mathbf{M}}\underline{\mathbf{Z}}^{rs})_{ik}\,\underline{i}^s{}_k\, e^{j\frac{2\pi(i-1)}{Q_r}}$$

$$\underline{w}^{rr} = \frac{1}{Q_r\,\underline{i}_+^r}\sum_{i=1}^{Q_r}\sum_{k=1}^{Q_r}(\underline{\mathbf{M}}\underline{\mathbf{Z}}^{rr}+\underline{\mathbf{Z}}^r{}_b)_{ik}\,\underline{i}^r_k\, e^{j\frac{2\pi(i-1)}{Q_r}} \qquad (138)$$

Eqs. (134) and (137) define the relation between the positive phase-sequence stator voltage and the positive phase-sequence stator and rotor currents. As the equations have been derived from the voltage equations of two magnetically coupled polyphase windings having different phase numbers, the coupling coefficients $\underline{z}^{sr}$ and $\underline{w}^{rs}$ are not equal as they should be in equations of an equivalent circuit. The equality is forced by rescaling Eq. (137)

$$\frac{\underline{z}^{sr}}{\underline{w}^{rs}}(\underline{w}^{rs}\,\underline{i}_+^s + \underline{w}^{rr}\,\underline{i}_+^r) = \underline{z}^{rs}\,\underline{i}_+^s + \underline{z}^{rr}\,\underline{i}_+^r = 0 \qquad (139)$$

where

$$\underline{z}^{rs} = \underline{z}^{sr}$$

$$\underline{z}^{rr} = \frac{\underline{z}^{sr}\,\underline{w}^{rr}}{\underline{w}^{rs}} \qquad (140)$$

Eqs. (134) and (139) define a simple equivalent circuit of the induction motor. However, if leakage reactances are used, the rotor quantities have to be reduced to the stator. The reduced rotor current in the stator winding should induce a

fundamental component of the air gap flux that is equal to the fundamental component of the flux induced by the original rotor current. Using this criterion a reduction factor $\underline{\kappa}$ is obtained

$$\underline{\kappa} = \frac{\underline{\Phi}^{s1}\, \underline{i}_+^{r}}{\underline{\Phi}^{r1}\, \underline{i}_+^{s}} \tag{141}$$

where $\underline{\Phi}^{s1}$ and $\underline{\Phi}^{r1}$ are the fundamental components of the air gap fluxes induced separately by the stator and rotor currents. The flux components are obtained as line integrals from the air gap. If a skewed motor is analyzed, the fluxes are the average values computed from the slices. The reduced parameters marked by an apostrophe are

$$\begin{aligned}
\underline{i}_+^{r\prime} &= \frac{1}{\underline{\kappa}}\, \underline{i}_+^{r} \\
\underline{z}^{ss\prime} &= \underline{z}^{ss} \\
\underline{z}^{sr\prime} &= \underline{\kappa}\, \underline{z}^{sr} \\
\underline{z}^{rs\prime} &= \underline{\kappa}\, \underline{z}^{rs} \\
\underline{z}^{rr\prime} &= \underline{\kappa}^2\, \underline{z}^{rr}
\end{aligned} \tag{142}$$

The stator current is not changed by the reduction. The components of the equivalent circuit in Figure 4 are obtained from the reduced impedances

$$\begin{aligned}
R^s &= \mathrm{Re}\{\underline{z}^{ss\prime}\} \\
X_m &= \mathrm{Im}\{\underline{z}^{sr\prime}\} \\
X^s_\sigma &= \mathrm{Im}\{\underline{z}^{ss\prime} - \underline{z}^{sr\prime}\} \\
X^r_\sigma &= \mathrm{Im}\{\underline{z}^{rr\prime} - \underline{z}^{rs\prime}\} \\
R^r &= \mathrm{Re}\{\underline{z}^{rr\prime}\}
\end{aligned} \tag{143}$$

As was emphasized in Section 2.3 the impedance matrix is associated with a given operation state of the machine. The circuit parameters obtained from the impedance matrix are, of course, associated with the same state. The method can be used to analyze e.g. the effects of saturation on the parameters of the equivalent circuit. Some results are given in the next chapter.

3 RESULTS

3.1 Test motors

The theory of the previous chapter is applied to the calculation of the operation characteristics of two induction motors. The first motor, whose reduced cross sectional geometry was already shown in Figure 1, is a three-phase cage induction motor. The second motor has a conventional three-phase stator, but a solid iron rotor. This motor type was chosen as a test motor because there are several methods applicable to the analysis of a non-slotted solid rotor. For instance methods based on coordinate transformations can be used. The cross section of the solid rotor machine is shown in Figure 5. The main parameters of the test motors are given in Table 1.

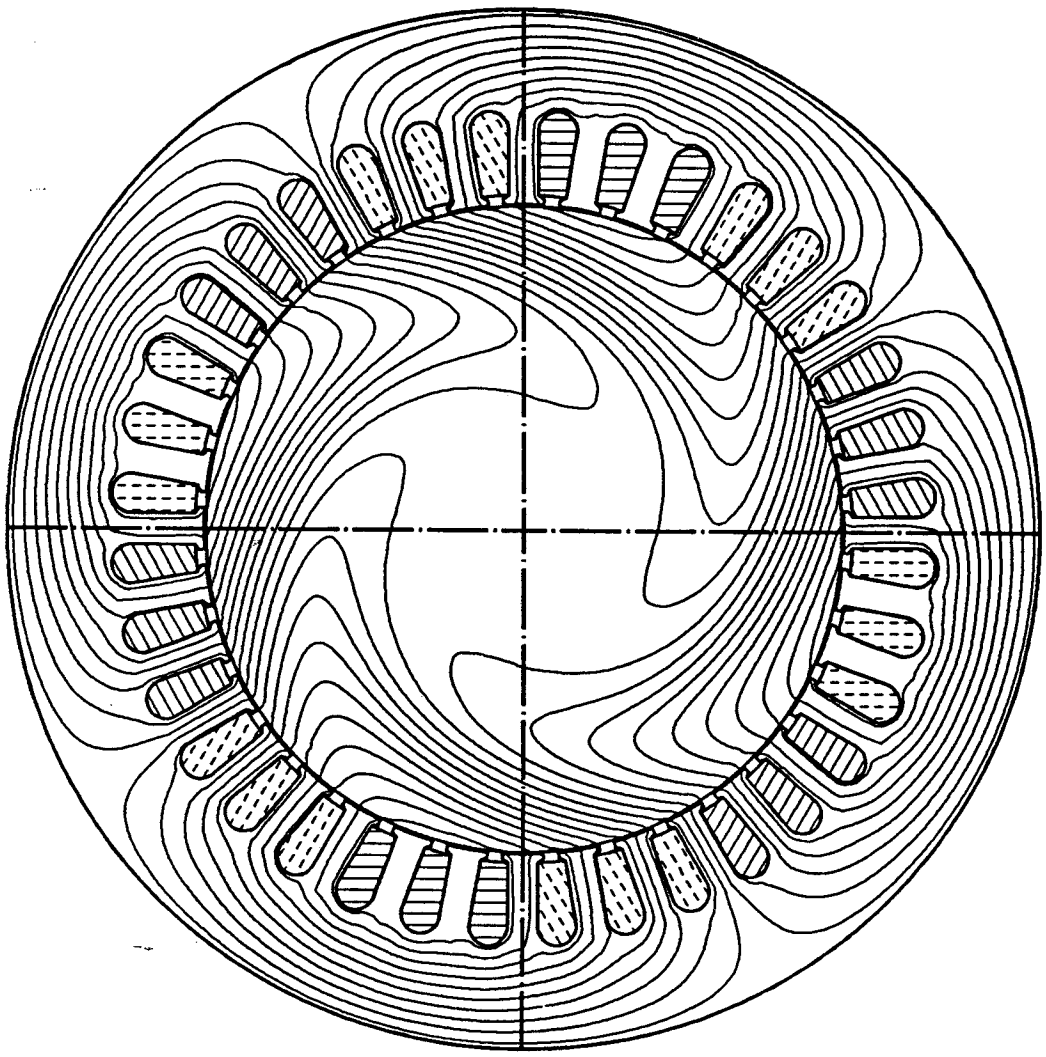

Figure 5. The cross section of the solid rotor machine. The equipotential lines of the vector potential correspond to the operation at the rated voltage at slip 0.01. Flux between two curves is 2.79 mWb/m.

Table 1. Parameters of the motors used in the testing of the validity of computed machine characteristics.

Machine type	Cage rotor machine	Solid rotor machine
Number of pole pairs	2	2
Number of phases	3	3
Number of stator slots	36	36
Number of rotor slots	34	0
Stator diameter [mm]	235	202
Rotor diameter [mm]	145	124
Air gap [mm]	0.45	0.38
Core length [mm]	195	145
Connection	delta	star
Rated voltage [V]	380	380
Rated frequency [Hz]	50	50
Rated current [A]	30	-
Rated power [kW]	15	-

The solid rotor was made of a shaft steel used in electrical machines. End rings made of copper were soldered onto the end surfaces of the rotor in order to obtain a more two-dimensional current distribution in the rotor. In the analysis the ends of the rotor are taken as equipotential surfaces of the scalar potential.

Two rotors were constructed for the 15 kW motor. The first one is the original rotor with 34 skewed slots. The skew is 1.2 stator slot pitches. The second rotor has the same cross sectional geometry, but the slots are unskewed. Thus there are actually three test motors, the two variants of the 15 kW motor and the solid rotor machine. The motors were tested in the Laboratory of Electromechanics. The measured and computed results are compared in the next sections. The measurement methods are discussed in these connections.

3.2 Locked-rotor characteristics

The locked-rotor condition is the easiest operation state to be analyzed by numerical field solution methods because there is no need to take the motion into account. However, the approximations used for modelling end windings and skewed rotor bars may cause errors because these three-dimensional features have especially large effects in the locked-rotor condition. An additional source of error is the reduction of the number of rotor bars that is made in order to obtain a smaller solution region. The effects of the reduced solution region are discussed

at the end of this section.

Figure 6 shows the magnetic field of the unskewed 15 kW motor in the locked-rotor condition at the rated voltage. The assumption of sinusoidal time variation has been used in the solution. It can be seen how the rotor cage restricts the penetration of the flux varying at 50 Hz frequency. The flux seems to accumulate into the teeth between the phase belts. The phenomenon can be explained by studying an ideal case in which the permeability of iron is assumed to be infinite and the rotor cage is assumed to form an ideal short circuit so that no flux can penetrate into the rotor. In this case the magnetomotive force of a slot current is spent in the leakage flux over the slot. If the currents in adjacent slots are equal, the leakage fluxes over the slots are also equal. There is no radial flux in the tooth between the slots. A radial flux can flow in a tooth only if the total currents in the slots at the sides of the tooth are different.

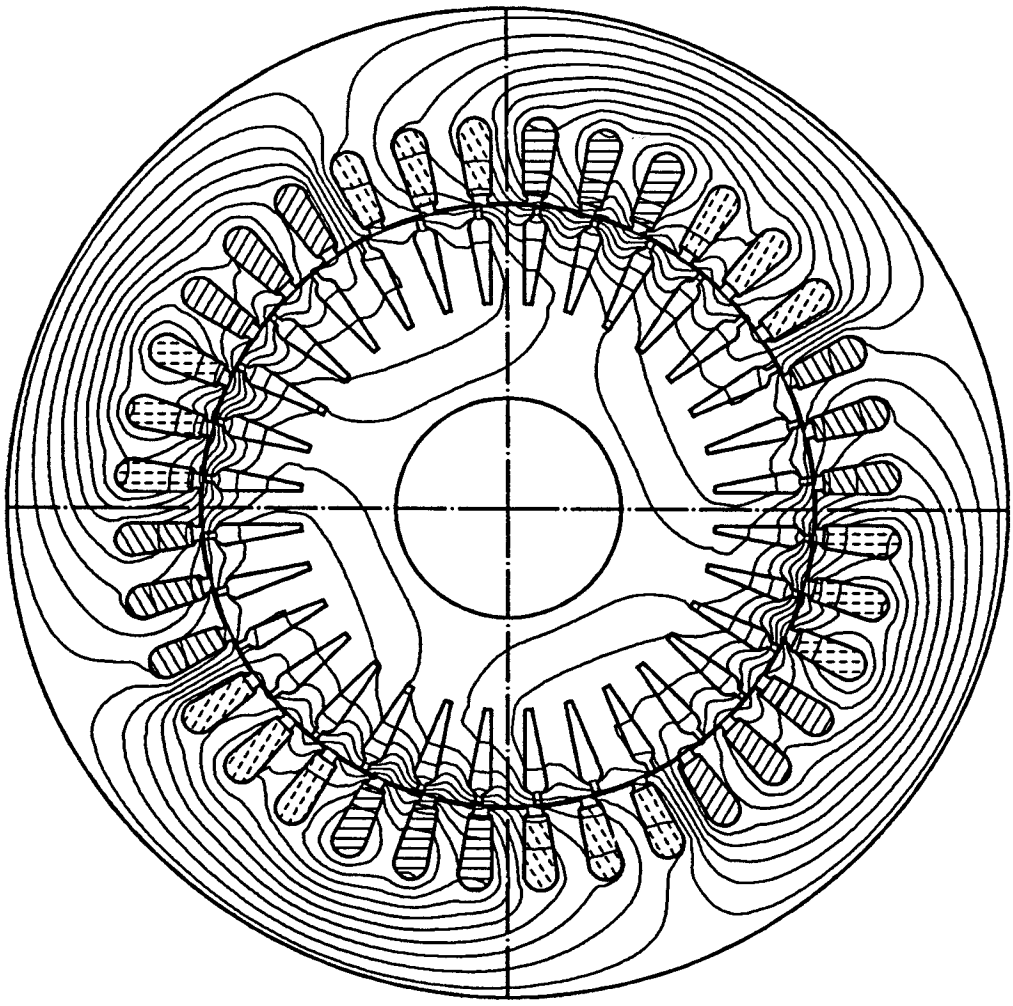

Figure 6. The magnetic field of the unskewed 15 kW motor in the locked-rotor condition at the rated voltage.

As the iron parts at the air gap region are strongly saturated, the choice of the effective reluctivity should be critical in the assumption of sinusoidal time variation. However, the results obtained by using different effective reluctivities seem to differ less from each other in the locked-rotor condition than in the no-load condition (Luomi et al. 1986). The starting currents and torques computed for the unskewed 15 kW motor using four different effective reluctivities are plotted in Figure 7. The results obtained by the step-by-step method are also shown.

The best agreement with the step-by-step method is obtained by the effective reluctivity defined by Eq. (47). Almost as good is the reluctivity defined by Eq. (49). As similar results were also obtained for other machines, the effective reluctivity defined by Eq. (47) was used when computing the results of this and the next sections with the sinusoidal approximation. Locked-rotor characteristics computed for various induction motors using the step-by-step method and the sinusoidal approximation are given in Table 2. The skew has not been taken into account.

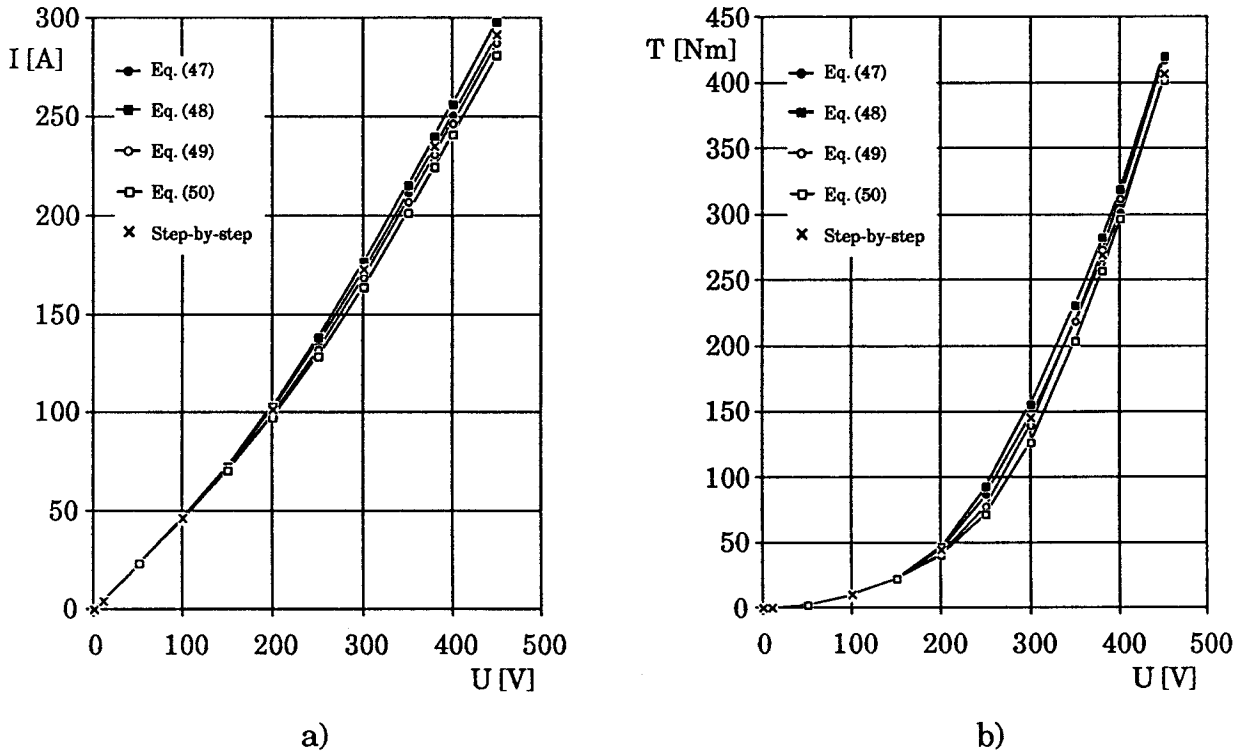

Figure 7. The starting current (a) and torque (b) computed for the 15 kW motor using different effective reluctivities. The definitions of the reluctivities are given by Eqs. (47) - (50). The results obtained by the step-by-step method are marked by crosses.

Table 2. Comparison between locked-rotor characteristics obtained by the step-by-step method and by the assumption of sinusoidal time variation. The values correspond to the rated voltages of the machines. The effective reluctivity used in the approximation of sinusoidal time variation is defined by Eq. (47).

Machine		Step-by-step method	Sinusoidal approximation
P = 7.5 kW p = 1 q = 6	Current [A] Torque [Nm] Power factor	111.7 80.22 0.594	111.7 79.15 0.592
P = 15 kW p = 2 q = 3	Current [A] Torque [Nm] Power factor	234.7 269.4 0.581	234.3 266.6 0.575
P = 110 kW p = 4 q = 3	Current [A] Torque [Nm] Power factor	1040 2159 0.361	1028 2132 0.356
P = 250 kW p = 3 q = 4	Current [A] Torque [Nm] Power factor	2259 2923 0.238	2251 2881 0.236
P = 350 kW p = 5 q = 3	Current [A] Torque [Nm] Power factor	244.8 5749 0.202	242.9 5553 0.201
P = 600 kW p = 4 q = 3	Current [A] Torque [Nm] Power factor	616.5 9683 0.131	606.7 9315 0.127
P = 800 kW p = 2 q = 5	Current [A] Torque [Nm] Power factor	593.1 4321. 0.149	586.9 4220. 0.146
Solid rotor machine p = 2 q = 3	Current [A] Torque [Nm] Power factor	63.10 146.2 0.755	65.23 142.9 0.718

The computed locked-rotor currents and torques of the three test motors are compared with the measured values in Figures 8 - 10. The computed values are within 15 % of the measured ones. The largest difference occurs in the case of the solid rotor machine. In a solid rotor the current distribution is clearly three-dimensional, especially at the ends of the rotor. A part of the difference between the measured and computed results is explained by the fact that the three-dimensional current and field are modelled by two-dimensional quantities.

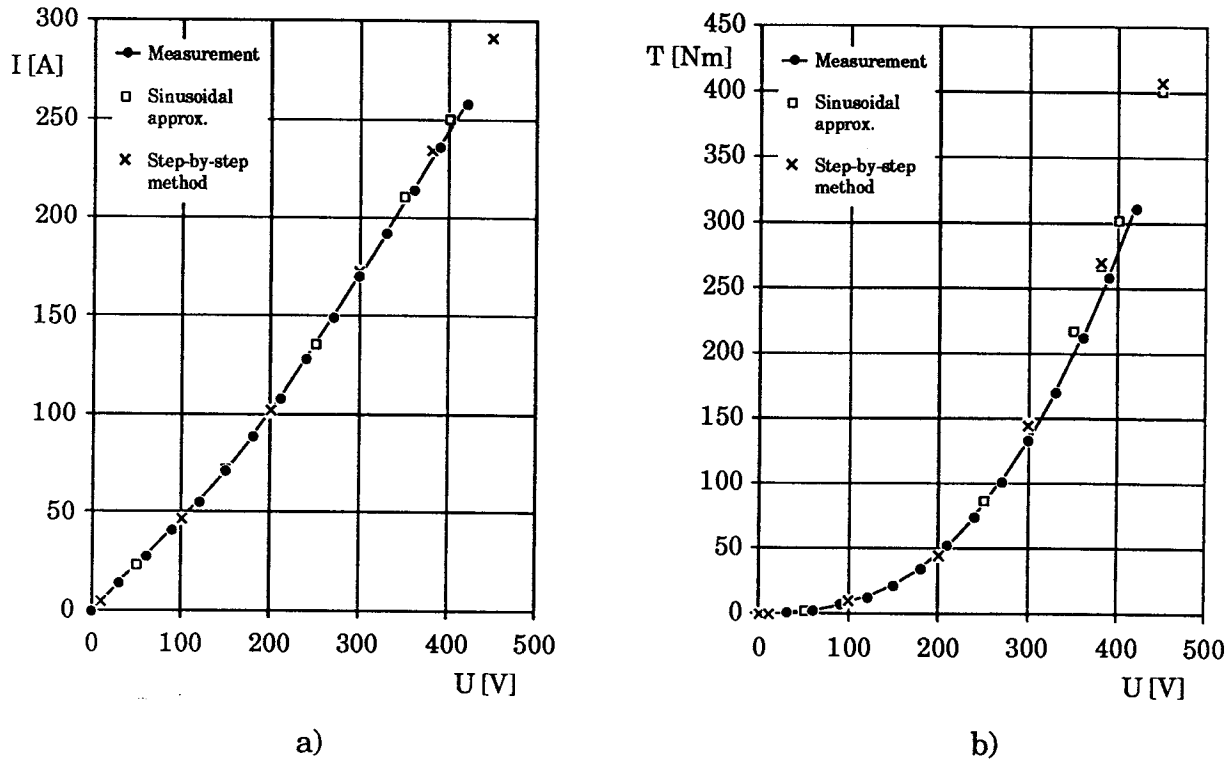

Figure 8. The locked-rotor current (a) and torque (b) of the unskewed 15 kW motor as functions of the supply voltage.

The locked-rotor characteristics were measured by raising the voltage linearly from zero to a value somewhat above the rated voltage. The voltage sweep lasted about 5 seconds. The RMS-value of the line current was measured with an RMS-amplifier, and the shaft torque was obtained from a torque transducer. The measured signals were recorded by a pen recorder.

The temperatures of the windings rise significantly in a locked-rotor test. If a new locked-rotor measurement was made immediately after a previous one, the current and torque values obtained at the rated voltage were 2 - 4 % lower than the values obtained at the previous measurement. Resistance values used in the computation correspond to a temperature of 80 °C.

The field of the skewed 15 kW motor was solved by the impedance method dividing the motor into three slices. It is seen by comparing the results in Figures 8 and 9 that the method gives satisfactory results. The division of the model motor into a larger number of slices is impractical as the results obtained differ only a little from the results obtained by the three slices.

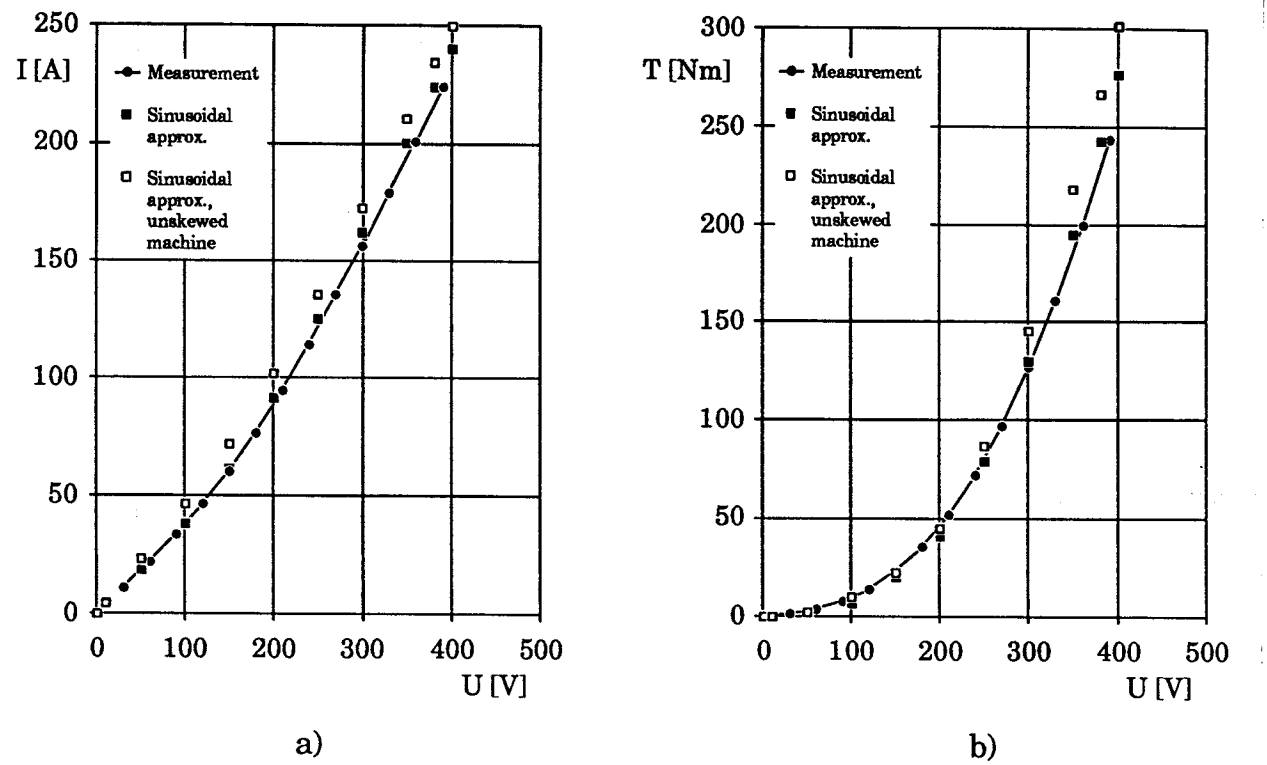

Figure 9. The locked-rotor current (a) and torque (b) of the skewed 15 kW motor as functions of the supply voltage. The values computed for the unskewed motor are also given (marked by non-colored squares) in order to show the effect of the skew.

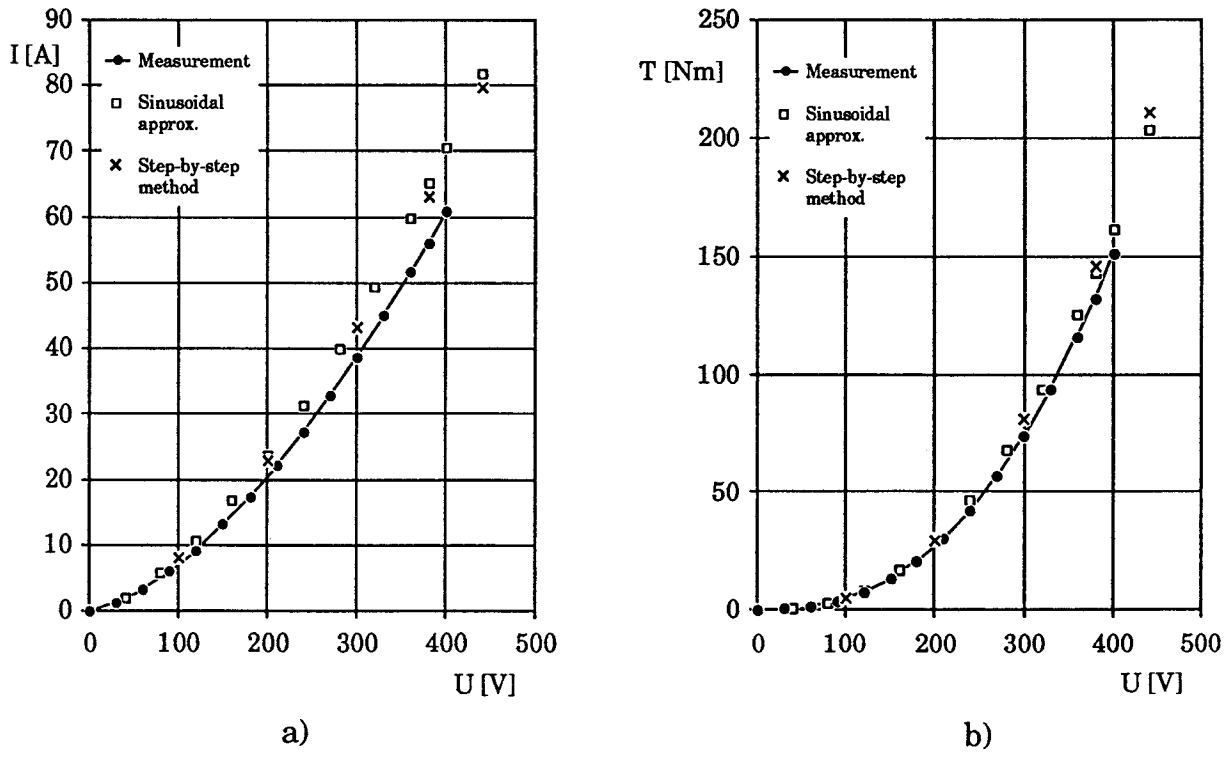

Figure 10. The locked-rotor current (a) and torque (b) of the solid rotor machine as functions of the supply voltage.

The relative values of the equivalent circuit parameters obtained for the skewed 15 kW motor are plotted in Figure 11 as functions of the supply voltage. The parameters have been computed from the results of the impedance method and they are associated with the locked-rotor condition.

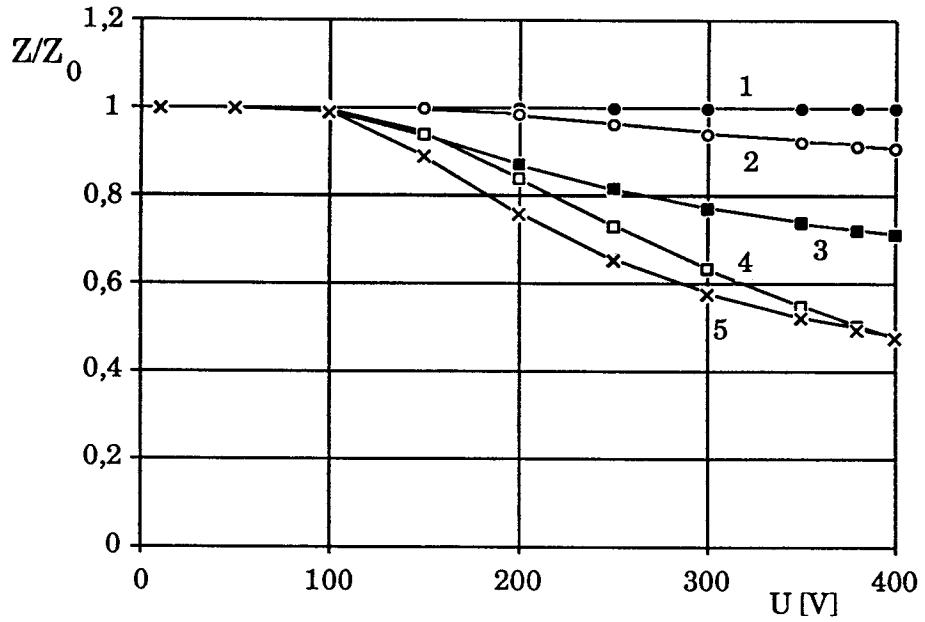

Figure 11. The parameters of the equivalent circuit computed for the skewed 15 kW motor in locked-rotor condition. 1) Stator resistance (0.830 Ω). 2) Rotor resistance (0.913 Ω). 3) Stator leakage reactance (1.53 Ω). 4) Rotor leakage reactance (2.84 Ω). 5) Magnetization reactance (61.4 Ω). The curves have been scaled with respect to the non-saturated values of the parameters given above in parentheses.

The computed results shown in Figures 6 - 11 were obtained by using isoparametric, triangular, second-order elements. The finite element mesh used for the 15 kW machines was shown in Figure 2. When third-order elements are used, the results are essentially equal to those obtained by second-order elements. If the same number of first-order elements is used in the discretization, the current and torque values obtained are 5 - 20 % higher than the values obtained by second-order elements. A closer agreement is obtained if the number of first-order elements is increased, especially at the air gap region. As the results obtained by second-order elements seem to match the measured results quite well, most of the computed results given in this and the next sections have been computed using second-order elements.

As mentioned in Section 2.1 an induction machine usually has such a symmetry that the solution sector contains two poles. If the number of slots per pole and

phase is large, the finite element mesh may contain so many nodes that the time needed for the solution becomes a problem. In such a case the geometry of the actual machine has to be reduced. This is done by reducing the number of rotor slots in order to obtain a solution sector that contains only one pole or one phase belt. The width of the rotor conductors is also changed in order to conserve the ratio between the conductor and core cross sectional areas. The results given above for the 15 kW motors have been computed for a reduced machine geometry, whose solution sector contains the cross sectional area corresponding to one pole pitch.

The change of the geometry affects the computed machine characteristics. This effect can be seen in the locked-rotor quantities computed for three variants of the unskewed 15 kW motor (Table 3). The motor variants have the same stator, but the rotors have different slot numbers. The symmetry sectors corresponding to the slot numbers 34, 32 and 36 contain one pole pair, one pole and one phase belt respectively. The effects of the change of geometry may be masked behind the averaging made in the calculation of the effective values, but they become very clear when the instantaneous values of step-by-step solutions are compared. Figure 12 shows the time variation of the locked-rotor torque computed for the three motor variants. First-order elements have been used in the computation.

Table 3. The effective values of the locked-rotor characteristics of the 15 kW motor having unskewed rotors of different slot numbers. First-order elements have been used in the computation.

Symmetry sector Number of rotor slots	One pole pair 34	One pole 32	One phase belt 36
Step-by-step method			
Current [A]	273.2	271.9	288.1
Torque [Nm]	303.6	307.9	81.17
Power factor	0.615	0.611	0.641
Sinusoidal approx. --			
Current [A]	273.9	272.6	289.0
Torque [Nm]	304.3	301.6	92.32
Power factor	0.610	0.606	0.639

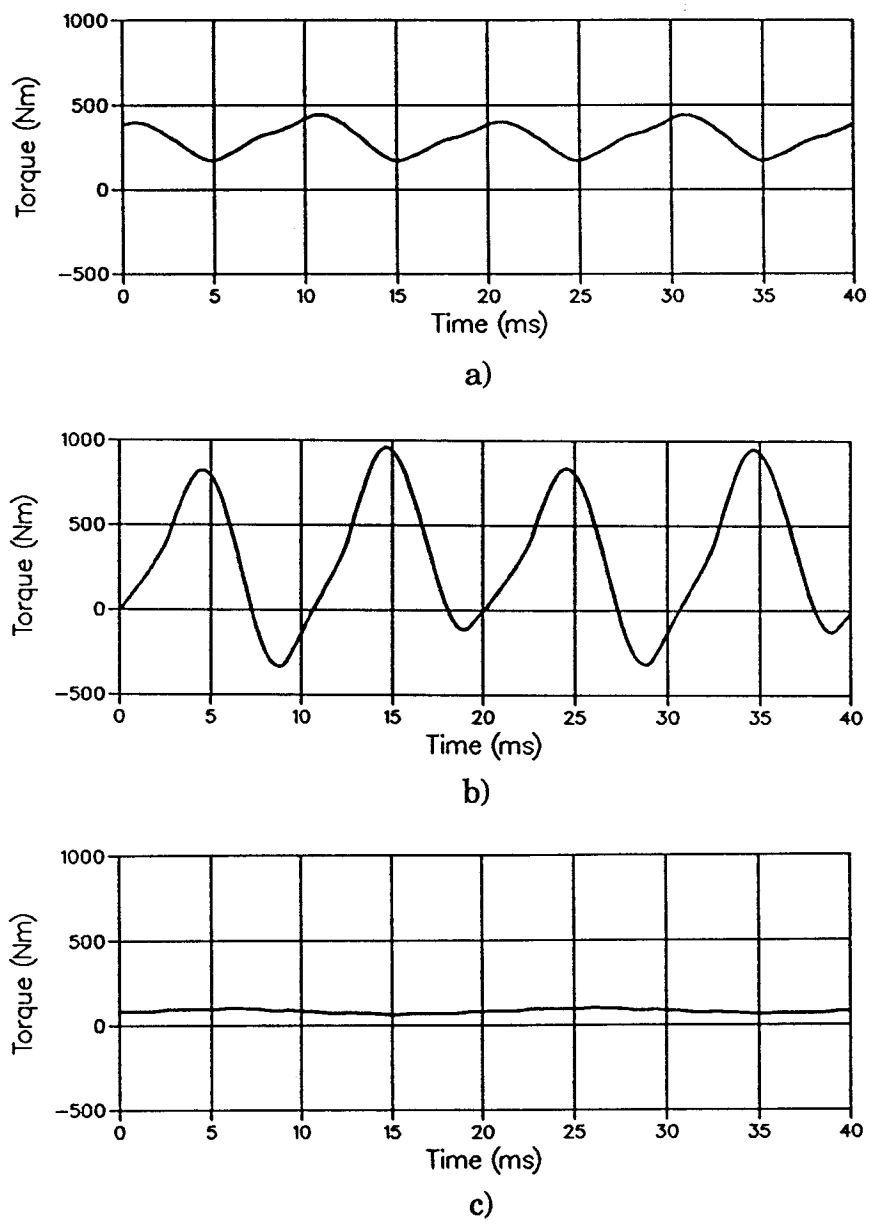

Figure 12. The locked-rotor torques of the 15 kW motor having unskewed rotors of different slot numbers. The curves have been computed using the step-by-step method. a) The original rotor geometry with 34 slots. In this case the symmetry sector contains two poles. b) A rotor with 32 slots. The symmetry sector contains one pole. c) A rotor with 36 slots. The rotor has the same number of slots as the stator and the symmetry sector contains one phase belt.

Only one particular case is treated in Table 3 and Figure 12. The results computed for other machine types, however, follow the same lines. The effective values of the operating characteristics are not greatly affected if the solution geometry is reduced from one pole pair to one pole as long as the stator and the rotor have different slot numbers. A further reduction to one phase belt may cause large errors in the effective values. The time-dependence of the quantities is changed radically in the reduction of the solution region from one pole pair to one pole.

3.3 Rotating machine

3.3.1 Rotor motion

The different ways of taking the motion of the rotor into account are compared in this section. The comparison is made by studying the results computed for the solid rotor machine. In order to eliminate the effect of nonlinearity the reluctivities of the materials have been fixed to their nonsaturated values. The two-dimensional field of the linearized machine satisfies Eq. (53). The results obtained by the coordinate transformation method are compared with the results obtained by the pseudostationary approximation and by the step-by-step method.

Figure 13 shows the current, torque and power factor computed for the linearized machine. The curves marked by non-colored circles are computed using the coordinate transformation method (Eq. (53)). The results obtained by using the approximation of a pseudostationary rotor are marked by black circles. The currents obtained by the two methods are so close to each other that it is not possible to distinguish them on the scale of the figure. The same applies to the power factor. On the other hand there is a large difference between the torques computed by the two methods. The same effect will also be seen in Section 3.3.3 when the computation of torque versus speed curves of true saturable machines is discussed. The errors due to the pseudostationary approximation are significant in the torque but smaller in the current.

If the step-by-step method with short enough time steps is used, the results are essentially the same as the results obtained by the coordinate transformation method. Table 4 gives the main characteristics of the linearized solid rotor machine computed using different step sizes. The column on the right hand side is obtained by using the coordinate transformation method.

It is seen by comparing the results (especially the torque values) obtained with different slip values that the step size must be shorter for a fast moving rotor. The effect is easily explained. If a too long step size is used, the magnetic field in the elements at the rotor surface changes quite discontinuously as the stator slots pass by. This induces unreal eddy-currents at the rotor surface of the model machine. The effect of the speed on the step size is also seen in Table 5, where the power balance of the linearized machine is given at different slips.

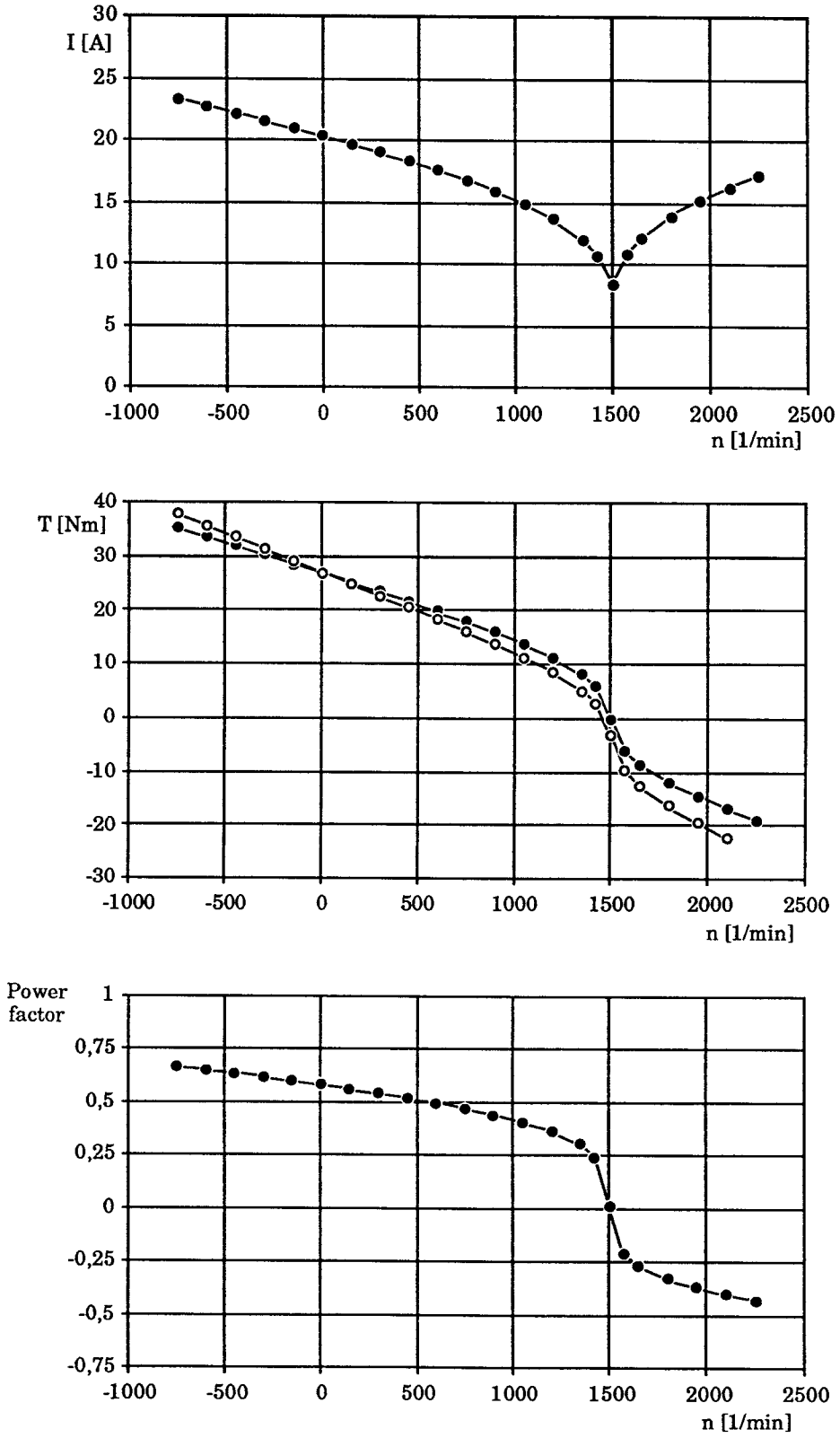

Figure 13. Comparison of the results obtained for the linearized solid rotor machine. The results of the coordinate transformation method are marked by non-colored circles connected by lines. The results obtained by the pseudostationary approximation are marked by black circles. The values obtained by the two methods for the current and the power factor are so close to each other that the difference is not distinguishable on the scale of the figure.

Table 4. The effect of step size on the results computed for the linearized solid rotor machine. The right hand column is obtained by using the coordinate transformation method.

	Step-by-step method				Sinusoidal time variation
Step size [ms]	0.2	0.1	0.05	0.025	-
Slip = 0.1					
Current [A]	12.000	11.993	11.992	11.992	11.995
Torque [Nm]	2.966	4.818	5.169	5.208	5.228
Power factor	0.308	0.308	0.308	0.308	0.308
Slip = 0.7					
Current [A]	18.357	18.354	18.353		18.336
Torque [Nm]	20.470	20.515	20.520	-	20.593
Power factor	0.522	0.522	0.522		0.523
Slip = 1.0					
Current [A]	20.350	20.346	20.345		20.344
Torque [Nm]	26.956	26.945	26.941	-	26.941
Power factor	0.583	0.583	0.583		0.583

The results given in Tables 4 and 5 show that relatively long time steps can be used in the computation of the stator current, the input power or the power factor. Short time steps must be used when the correct values of the torque and the rotor losses of a running machine are of interest.

As mentioned in Section 2.4 the power balance can be used to check the validity of the torque computation method. The input and resistive powers given in Table 5 have been computed from the currents and potential differences induced in the stator windings and in the solid rotor at each time step. The shaft power is the product of the mechanical angular frequency and the electromagnetic torque computed from the air gap using Eq. (124). The figures given are the steady-state average values integrated over one period of line frequency. The errors in the power balance become very small when the step size is decreased. This shows that the torque computation method is compatible with the method used in the field solution.

Table 5. The effect of step size on the power balance of the linearized solid rotor machine. The error in the power balance is obtained by subtracting the other power components from the input power. The error percentages have been calculated with respect to the input power.

Step size [ms]	0.2	0.1	0.05	0.025
Slip = 0.1				
Input power [W]	1408.139	1407.394	1407.187	1407.129
Shaft power [W]	419.308	681.129	730.750	736.264
Stator losses [W]	87.420	87.319	87.302	87.294
Rotor losses [W]	506.418	557.618	574.985	579.999
Error [W]	394.993	81.329	14.150	3.573
Error [%]	28.1	5.8	1.0	0.25
Slip = 0.7				
Input power [W]	3652.778	3653.128	3653.179	-
Shaft power [W]	964.626	966.747	966.982	
Stator losses [W]	204.556	204.466	204.453	
Rotor losses [W]	2480.594	2481.580	2481.804	
Error [W]	3.002	0.335	0.060	
Error [%]	0.082	0.009	0.002	
Slip = 1.0				
Input power [W]	4519.227	4519.391	4519.371	-
Shaft power [W]	0	0	0	
Stator losses [W]	251.383	251.269	251.241	
Rotor losses [W]	4267.875	4268.195	4268.211	
Error [W]	0.031	0.073	0.081	
Error [%]	0.001	0.002	0.002	

3.3.2 No-load operation

In no-load operation the three-dimensionality of the machine has only a small effect on the characteristics. On the other hand iron losses and eddy-current losses due to higher harmonic components should be taken into account. A step-by-step solution is needed if the effects of higher harmonics are studied properly. As discussed in the previous section a short step length should be used when computing a fast moving rotor. This means long computation times. Fortunately the pseudostationary approximation gives quite good results in the calculation of the no-load current, the most important no-load characteristic. Iron losses are neglected in the models used.

The no-load stator currents of the 15 kW and solid rotor motors are plotted as functions of the supply voltages in Figure 14. In the experiment the induction motor was driven by a synchronous motor. In this way the effect of friction losses is eliminated from the measured results. The computed results have been obtained by using the assumption of a pseudostationary rotor. At zero slip this means that the conductivity of the rotor bars is taken to be zero.

In the synchronous operation the field in the rotor is almost a DC field and varies nearly unidirectionally when the supply voltage is varied. The hysteresis of the rotor material is seen as the hysteresis between the no-load current and the stator voltage. The hysteresis loops, parts of which are shown in the figures, were obtained by starting from the maximum voltage, decreasing the voltage gradually to zero, changing the rotor angle 180 electrical degrees by reversing the magnetizing current of the synchronous machine and gradually raising the voltage of the induction motor back to the maximum value.

The solid rotor machine has a wider hysteresis loop in its magnetization current than the 15 kW motor. This is because of the rotor material. The solid rotor was made of a shaft steel that has much larger magnetic hysteresis than the electrical steel sheet used as the core material of the 15 kW motor.

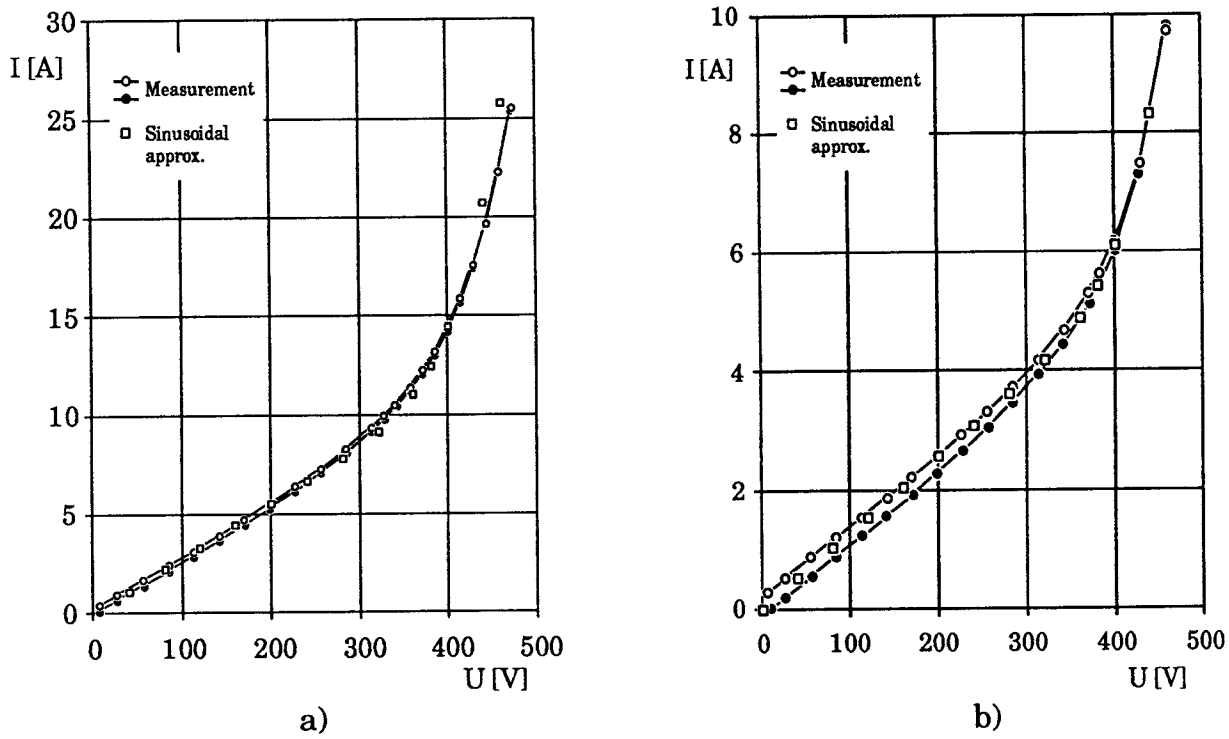

Figure 14. The no-load currents of the unskewed 15 kW motor (a) and the solid rotor machine (b) as functions of the supply voltage. The curves marked by circles are the two branches of the hysteresis loop due to the magnetic hysteresis of the rotor. The computed no-load currents are marked by squares.

At low saturation levels the computed results agree well with the measured ones. At supply voltages above the rated value the error increases. The approximation of sinusoidal time variation cannot model accurately the distorted current waveforms associated with high saturation levels.

Figure 15 gives the current waveforms of the unskewed 15 kW motor in no-load operation. The curves on the left hand side are computed by the step-by-step method and the curves on the right hand side are measured. The harmonic components due to the saturation and the slotting of the rotor can be clearly seen in the current waveforms.

The curves plotted in Figure 16 are the traces of flux density vectors in the core of the unskewed 15 kW motor at synchronous speed. The curves have been obtained by the step-by-step method. In the sinusoidal approximation the trace of a flux density vector is an ellipse. It can be seen that the assumption of sinusoidal time variation is a very rough approximation. It is also obvious that the iron loss

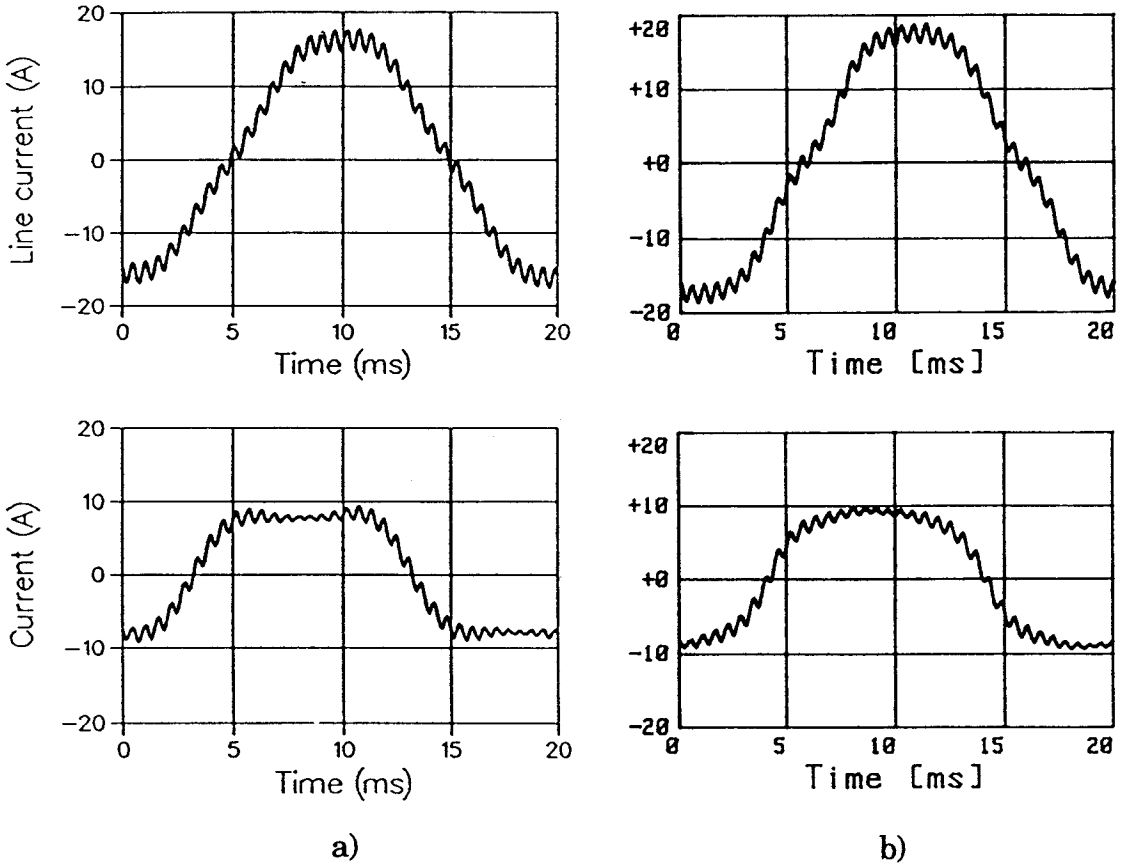

Figure 15. The waveforms of the line and winding currents of the unskewed 15 kW motor at no-load. The curves have been computed (a) and measured (b) for the delta connected machine running at synchronous speed and supplied by the rated voltage. The nonreduced rotor geometry of the 15 kW motor has been used in the simulation.

calculation methods based on the assumption of a magnetic field varying unidirectionally at a single frequency are not suitable for accurate loss analysis of induction motors.

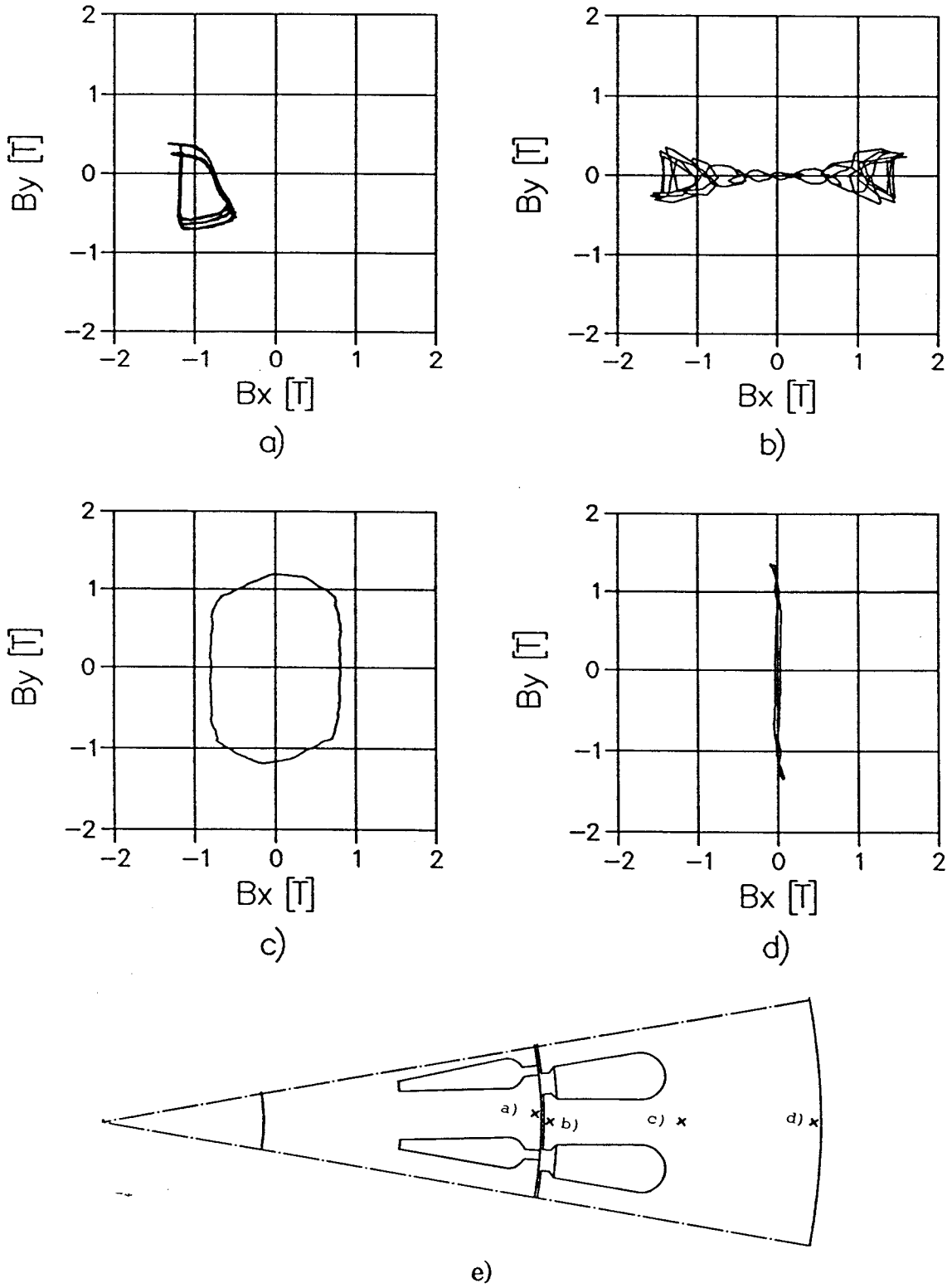

Figure 16. The traces of flux density vectors in the core of the unskewed 15 kW motor running at synchronous speed. The flux density vectors in the stator are given in the stator coordinate system and the one in the rotor is given in the rotor coordinate system. The points for which the curves have been computed are shown in figure e).

3.3.3 Loaded running motor

The main problem in the computation of a running induction motor is how to model the motion of the rotor accurately. The correct way is the step-by-step method in which the stator and rotor fields are solved in their own coordinate systems and matched with each other in the air gap. The method is, however, too slow to be used in the routine computation of e.g. torque versus speed curves of induction machines. The pseudostationary approximation on the other hand is too rough a simplification to give accurate torque values.

The current and torque of the 15 kW motor as functions of the speed at the rated voltage are shown in Figure 17. The currents obtained by both the step-by-step method and the pseudostationary approximation agree well with the measured values. The step-by-step method gives satisfactory torque values, too, but there are large errors in the torques obtained by the assumption of a pseudostationary rotor.

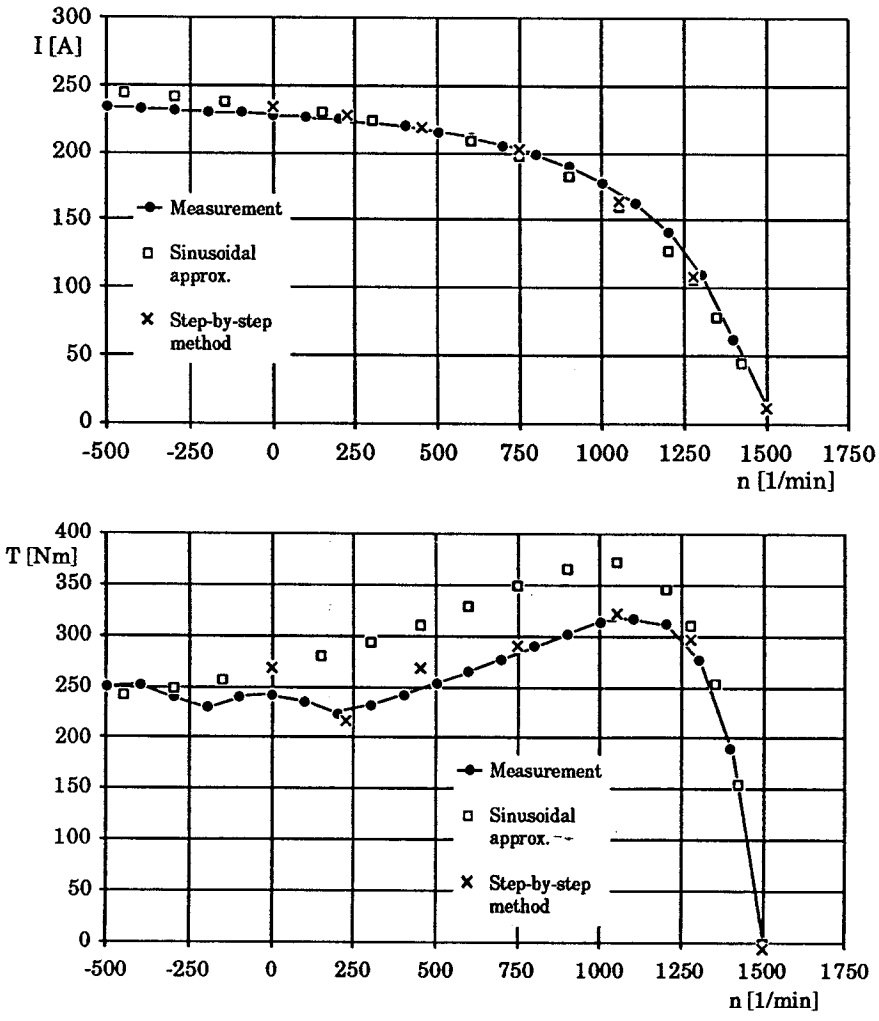

Figure 17. The current and torque computed and measured for the 15 kW motor as functions of the rotation speed.

Figure 18 shows the current and torque of the solid rotor machine as functions of the speed. In this case there are quite large differences between the measured and computed currents. The error can be partly explained by the fact that the three-dimensional effects at the ends of the solid rotor have been neglected. In the sinusoidal approximation the rotation of the motor has been modelled by the coordinate transformations. It is a correct method in the analysis of a linearized machine.

In a current versus speed or torque versus speed measurement the induction motor was driven by a DC motor supplied by a four quadrant thyristor converter. The induction motor was supplied by the rated line voltage. The rotation speed of the motors was controlled by the speed feedback circuit of the converter. In the measurement the rotation speed was swept linearly from a value somewhat above the synchronous speed down to a negative value. The time of the sweep was about 12 s. The line current was measured by an RMS-amplifier, and the shaft torque was obtained from a torque transducer. The measured signals were recorded by a pen recorder.

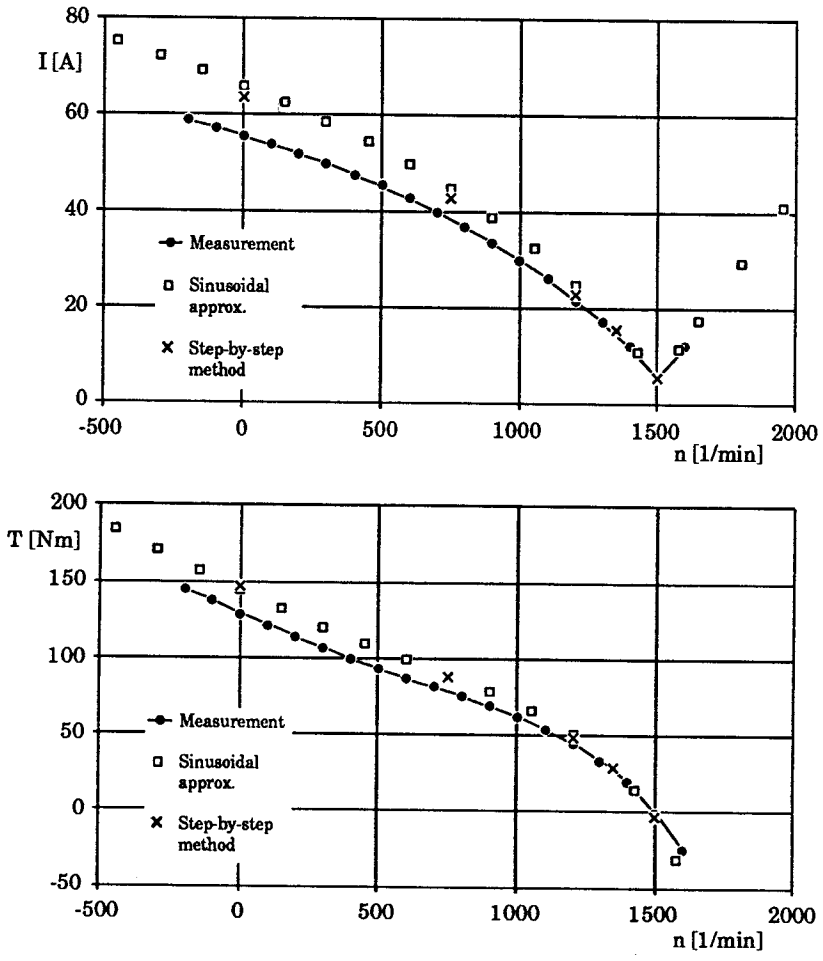

Figure 18. The current and torque computed and measured for the solid rotor machine as functions of the rotation speed.

Figure 19 is presented in order to demonstrate the flexibility of the step-by-step method. The computed and measured current and voltage waveforms of the solid rotor machine supplied by an inverter are shown. The curves have been computed for the solid rotor machine because in this case the symmetry sector of the actual machine contains only one pole pitch permitting a relatively small finite element mesh. The method is applicable to the computation of cage and wound-rotor machines, but they usually have symmetries that force the use of larger element meshes.

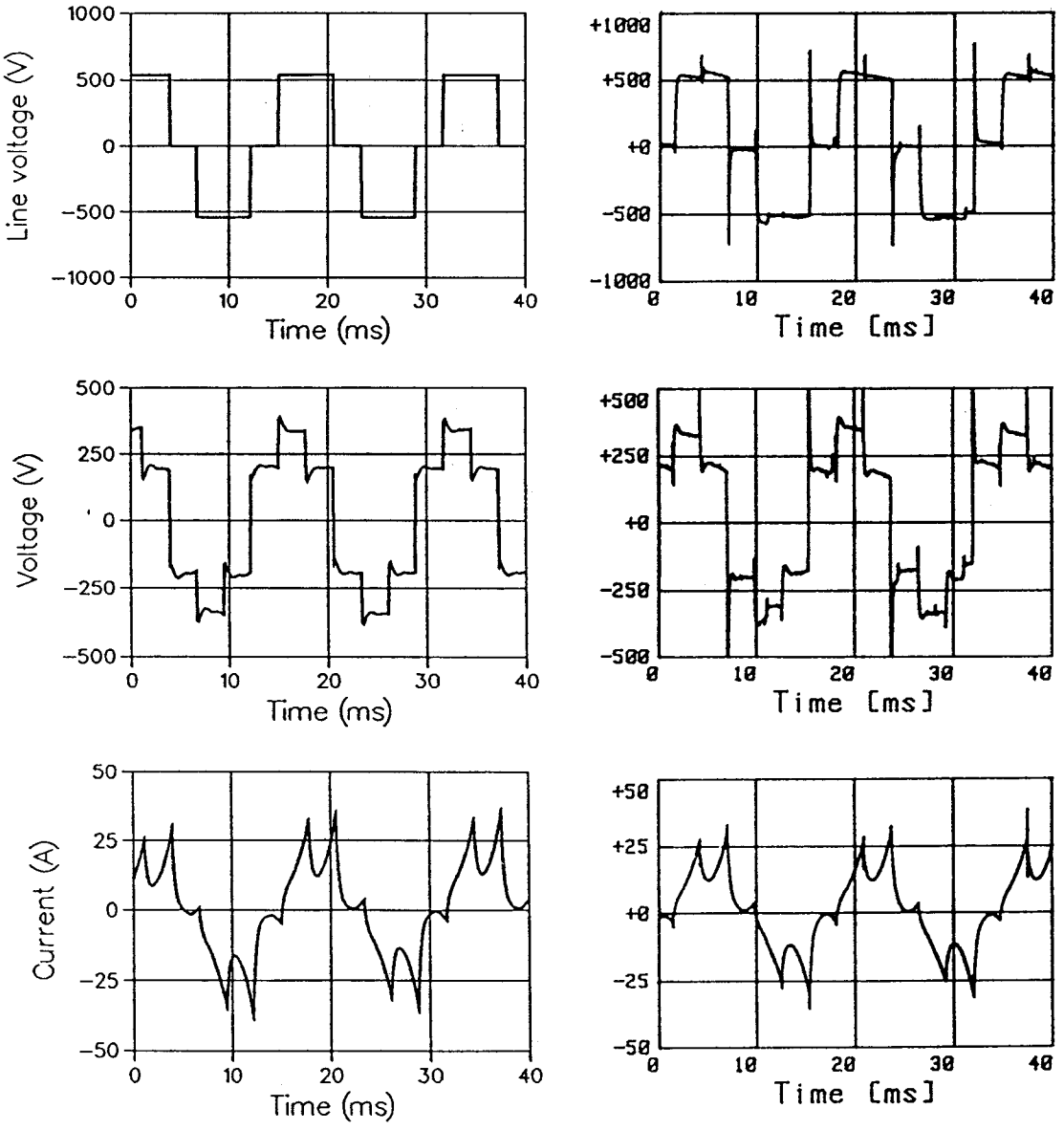

Figure 19. The current and voltage waveforms computed (a) and measured (b) for the star connected solid rotor machine in inverter supply. The frequency of the supply voltage is 60 Hz and the machine is running at slip 0.1. In the simulation the supply voltage has been modelled by square pulses shown in the first figure of column a). The middle figures give the voltage of a phase winding. The star point is not connected.

3.3.4 Transient phenomena

From the point of view of the step-by-step method it is quite the same whether the machine under simulation is in a transient state or in a steady state. Transients usually occur even in the simulation of a steady state as the available initial state is seldom the correct steady state.

Figure 20 shows the time variation of machine quantities during a starting of the unskewed 15 kW motor. At time t = 0 a sinusoidal voltage corresponding to the rated value of the machine has been connected to the delta connected stator winding. The shaft torque has been zero in the simulation. The motor reaches its rated speed in about 2.5 periods of the 50 Hz line frequency.

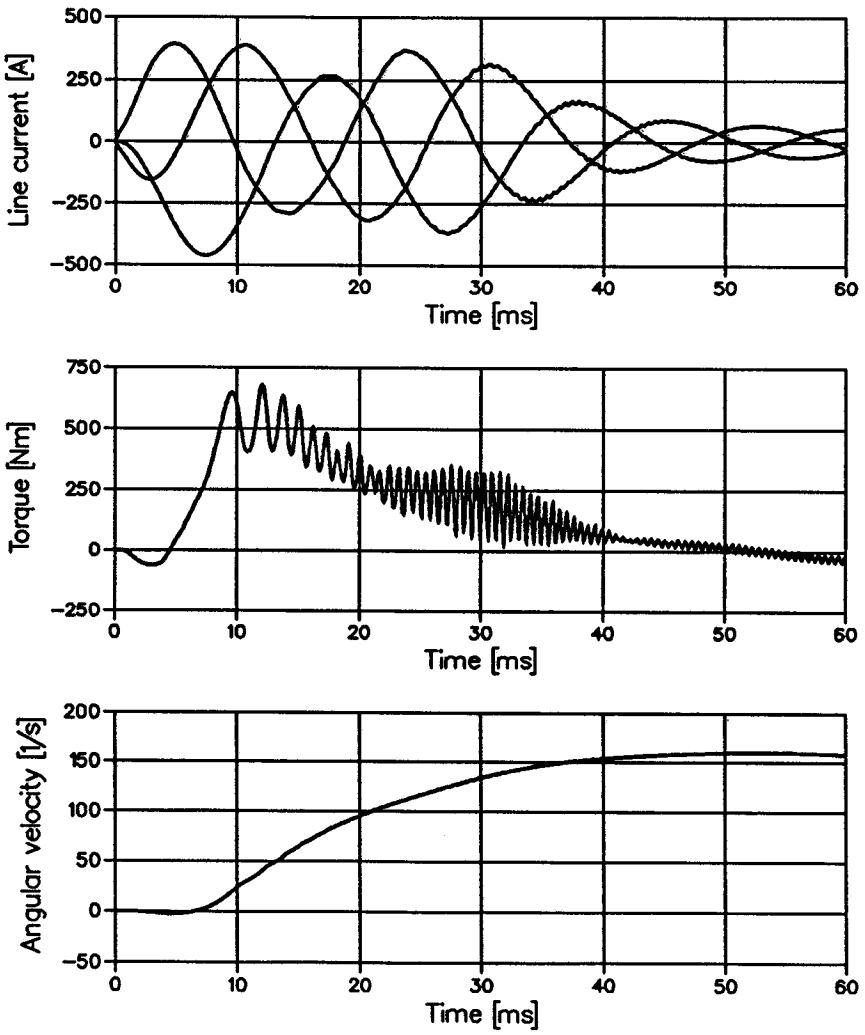

Figure 20. Starting of the unskewed 15 kW motor without a load torque. The motor is delta connected and supplied by the rated voltage. The line currents of the three-phase system are shown in the topmost figure and the electromagnetic torque acting on the rotor in the middle figure. The fluctuations in the torque are due to the unskewed stator and rotor slots moving passed each other. The nonreduced rotor geometry of the 15 kW motor has been used in the simulation.

3.4 Discussion about the results

The main factor that limits the use of numerical field solution methods in the routine calculation of electrical machines is the large amount of computation needed in the solution. Most of the simplifications discussed in Section 2.2 were made in order to decrease the computation time. As the use of a more precise method usually leads to longer solution times, a compromise between the accuracy and the solution time has to be made when choosing the method.

Solution times

Typical CPU times needed in the computation of the locked-rotor characteristics of the unskewed 15 kW motor are given in Table 6 for the different methods and for first-, second- or third-order triangular elements. The field analysis routines have been run on an IBM 3090-180 computer.

The solution times given for the sinusoidal approximation correspond to Newton-Raphson solutions with ten iteration steps. Usually a solution accurate enough is obtained in 4 - 7 iteration steps. The values given for the step-by-step method are the times needed in the simulation of one period of the AC cycle divided into 200 time steps. If a steady-state operation is simulated by the step-by-step method, the computation of two AC cycles is usually enough to reach

Table 6. The CPU times needed in the computation of the operating characteristics of the 15 kW motor in the locked-rotor condition. The values given for the step-by-step method are the times spent in the simulation of one AC cycle.

Element meshes	Sinusoidal approximation	Step-by-step method
904 first-order elements 474 node points	12.07 s (10 iteration steps)	236.4 s (200 time steps)
904 second-order elements 1851 node points	128.2 s (10 iteration steps)	2526 s (200 time steps)
904 third-order elements 3228 node points	650.6 s (10 iteration steps)	15800 s (200 time steps)

a steady state good enough. In this case the initial state has been obtained from the results of the sinusoidal approximation, as explained at the end of Section 2.3.3. The transients of an induction machine usually last much longer than two AC cycles. When transient phenomena are studied the simulation times are longer than the times given in Table 6.

The solution of the machine characteristics by the sinusoidal approximation is more than 20 times faster than the solution by the step-by-step method. Therefore the sinusoidal approximation is preferred in all cases where the results obtained by the method are reliable enough. The main shortage of the sinusoidal approximation is the lack of proper modelling for the motion of the rotor.

There are some possibilities for shortening the computation times. A large part of the Jacobian matrix remains unchanged during the Newton-Raphson iteration. Only the terms in the expressions of the matrix elements associated with the reluctivity and the matrix elements associated with the air gap nodes change from one iteration step to another. It would be economic to compute the constant part of the Jacobian only once and store it. At present the whole Jacobian is recalculated at each iteration step. Nyamusa et al. (1986) have described an accelerated Newton-Raphson method in which the elements of the Jacobian are recalculated only a couple of times during the iteration process. Most iteration steps are performed using an old Jacobian. Computer resources are saved both in the computation of the matrix elements and in the solution of the matrix equation as the triangular factor matrices used in the Gaussian elimination are computed only for a new Jacobian.

A short computation time is obtained by using a first-order finite element mesh containing the smallest number of elements needed to describe the geometry. The results obtained by the first-order discretization, however, differ significantly from the measured results and the results obtained by a second-order finite element approximation. A better accuracy is obtained if the number of first-order elements is increased, especially at the air gap region, but this also increases the solution time.

Accuracy

The absolute accuracy of the computation methods remains a little vague because of the small number of motors analyzed. The results computed for the 15 kW motors agree well with the measured results. There are larger differences between the measured and computed results for the solid rotor machine. At least

a part of the error can be explained by the neglection of the end effects of the solid rotor.

The statistical variation of the operating characteristics from one machine to another inside a machine series has to be taken into account when comparing computed results with the results measured from a single test motor. The variation is caused by irregularities in the dimensions of the construction parts, the variation of material properties of the electrical steel sheets, etc. Because of the variation results measured from a single motor cannot be taken as absolutely reliable reference values when the accuracy of a calculation method is considered.

According to the results obtained in the type and routine tests of induction motors at the Strömberg plants, a typical coefficient of variation (ratio between the standard deviation and the mean) of the no-load current is about 1 %. The corresponding value for the nonsaturated locked-rotor current is about 0.7 %. Deviations from the mean values occur that are larger than 5 %. The values given are based on quite a small number of tests (5-15 tested machines per a machine type, 8 machine types), but they show that mean values obtained from tests made for several machines of the same type would give a more reliable basis for the comparison.

Another factor that complicates the comparison between the measured and computed results is the temperature of the windings. The high currents in a torque versus speed measurement or in a locked-rotor test cause large resistive losses that rapidly raise the temperatures of the conductors. The temperature has a significant effect on the conductivities of the winding materials and thus on the performance of the machine. As it is impossible to measure the exact temperature distribution in the conductors during a test, the duration of the test should be as short as possible in order to limit the temperature rise. On the other hand, the machine should be in a steady state when measuring steady-state quantities. A compromise between the rise in temperature and the requirement of a steady state has to be made.

The time of the voltage sweep in a locked-rotor test was about 5 seconds and the time of the speed sweep in a torque versus speed measurement was about 12 seconds. If another test was made immediately after a previous one, the current and torque values obtained in the test were 2-4 % lower in the locked-rotor case and 5-15 % lower in the torque versus speed measurement. These figures give an idea of the amount of uncertainty in the results due to the unknown temperature.

In the computation a constant temperature of 80 °C was assumed.

For the test motors the differences between the measured machine quantities and the corresponding values obtained by the step-by-step method are less than 15 %. The same figure also applies to the sinusoidal approximation, except in the case of the torque of a rotating machine. Taking the various approximations made in the analysis into account, the computed results agree reasonably well with the measured ones. A larger number of motors should be carefully analyzed in order to get a more reliable judgement of the accuracy of the analysis methods.

Solution of different operation states

The sinusoidal approximation gives surprisingly good results in the computation of locked-rotor quantities when compared with the step-by-step method. Thus it is no use to spend computer resources on a step-by-step solution if only the effective values of locked-rotor quantities are of interest. The main error sources in the computation of locked-rotor operation are associated with the three-dimensionality of the machine.

The effective value of the no-load current is obtained accurately enough by the sinusoidal approximation. If the losses due to higher harmonic components or the waveforms of the quantities are studied, the step-by-step method has to be used. The neglection of iron losses is the main failing of the methods when computing no-load quantities. At present the solution routines are not applicable to the computation of the no-load losses of a machine. There is a research project going on in the Laboratory of Electromechanics, the aim of which is to develop a phenomenological model for the hysteresis of iron that could be implemented in the step-by-step solution routines. When such a model is obtained, the calculation of hysteresis losses will be included in the analysis method.

The failure in the calculations of the torque of a running motor is the main weakness of the sinusoidal approximation and the pseudostationary rotor model. The step-by-step method gives the torque of the 15 kW motor satisfactorily. The method is, however, too slow to be used in a detailed analysis of torque versus speed characteristics of induction motors. In the sinusoidal approximation the method used by Williamson & Ralph (1983) should give the torque more accurately. Some preliminary tests made using this method showed, however, that the computer time needed in the separate iterations of the field and voltage equations approaches the time of a step-by-step solution. The advantage of the method is, however, that skewed rotor slots are modelled without extra

computation.

The step-by-step method has to be used in the analysis of motors supplied by non-sinusoidal voltages or for the simulation of transient states. In the analysis of the inverter driven solid rotor machine the waveforms of the quantities obtained by the step-by-step method closely match the measured waveforms (Figure 19). The accuracy of the method in the simulation of transient phenomena has not been tested, but in principle there is no difference whether a steady state or a transient state is analyzed by the method.

4 SUMMARY

The analysis of induction motors is based on the numerical solution of the magnetic vector potential in the core region of the machine. The magnetic field is assumed to be two-dimensional. The two-dimensional field equation is discretized by the finite element method. The voltage equations of the stator and rotor windings are solved together with the discretized field equation.

The three-dimensional features of the machine are taken into account within the two-dimensional model. The end windings are modelled as constant impedances in the voltage equations of the windings. The skew is taken into account by dividing the machine into unskewed slices, the rotors of which have been rotated an angle corresponding to the skew. The currents of the conductors are assumed to be continuous from slice to slice. The magnetic field of each slice is solved separately by the two-dimensional model. The potential differences induced in the windings are summed from the slices and from the end windings.

The time-dependence of the field and the motion of the rotor are modelled correctly if the field is solved by the step-by-step method. It is, however, very time-consuming to use the step-by-step method in routine calculations. The computation time is reduced significantly if the time-dependence of the field quantities is assumed to be sinusoidal in spite of the nonlinearity of core materials and the rotation of the rotor. The pseudostationary approximation is used for modelling the effects of rotation. In the special case of a homogeneous solid rotor the motion is taken into account by using coordinate transformations.

Comparison between the results obtained by the step-by-step method and the simplified models shows that the sinusoidal approximation gives good results in the computation of locked-rotor characteristics of induction motors. The shortage of the pseudostationary approximation becomes clear when the method is used to compute torque versus speed curves. Large errors occur in the torque values. The current is obtained more accurately.

The computed and measured results agree within 15 %. Several simplifications are made in the analysis that can explain the differences. For instance the effect of end-region fields is approximated by a simple end-winding inductance. The currents in the laminated iron core of the machine are neglected and the magnetic properties of iron are approximated by a single-valued reluctivity curve. Taking the various approximations into account, the computed results agree reasonably well with the measured ones.

REFERENCES

Abdel-Razek, A. A. et al. 1982. **Conception of an air-gap element for the dynamic analysis of the electromagnetic field in electric machines.** IEEE Transactions on Magnetics **MAG-18**, 2, p. 655-659.

Andresen, E. and Müller, W. 1983. **Berechnung der Anlaufdaten von Asynchron-Käfigläufermotoren verschiedener Stabformen mit der Methode der finiten Differenzen.** Archiv für Elektrotechnik **66**, 3, p. 179-185.

Barnes, E. C. 1951. **An experimental study of induction machine end-turn leakage reactance.** AIEE Transactions **70**, p. 671-679.

Binns, K. J., Hindmarsh, R. and Short, B. P. 1971. **Effect of skewing slots on flux distribution in induction machines.** Proceedings IEE **118**, 3/4, p. 543-549.

Van Bladel, J. 1984. **Relativity and Engineering.** Berlin, Springer-Verlag. 402 p.

Bouillault, F. and Razek, A. 1983. **Dynamic model for eddy current calculation in saturated electric machines.** IEEE Transactions on Magnetics **MAG-19**, 6, p. 2639-2642.

Brandl, P., Reichert, K. and Vogt, W. 1975. **Simulation des Turbogenerators im stationären Lastfall.** Brown Boveri Mitteilungen **62**, 9, p. 444-449.

Brunelli, B. et al. 1983. **Transient and steady-state behaviour of solid rotor induction machines.** IEEE Transactions on Magnetics **MAG-19**, 6, p. 2650-2654.

Chari, M. V. K. and Silvester, P. 1971a. **Analysis of turboalternator magnetic fields by finite elements.** IEEE Transactions on Power Apparatus and Systems **PAS-90**, 2, p. 454-464.

Chari, M. V. K. and Silvester, P. 1971b. **Finite-element analysis of magnetically saturated d-c machines.** IEEE Transactions on Power Apparatus and Systems **PAS-90**, 5, p. 2362-2372.

Chari, M. V. K. et al. 1982. **Three-dimensional vector potential analysis for machine field problems.** IEEE Transactions on Magnetics **MAG-18**, 2, p. 436-446.

Chu, E. et al. 1984. SPARSPAK: **Waterloo sparse matrix package, User's guide for SPARSPAK-A.** University of Waterloo, Ontario, Canada, Research Report CS-84-36, 63 p.

Coulomb, J. L. 1983. **A methodology for the determination of global electromechanical quantities from a finite element analysis and its application to the evaluation of magnetic forces, torques and stiffness.** IEEE Transactions on Magnetics **MAG-19**, 6, p. 2514-2519.

Davat, B., Ren, Z. and Lajoie-Mazenc, M. 1985. **The movement in field modeling.** IEEE Transactions on Magnetics **MAG-21**, 6, p. 2296-2298.

Davey, K. R. and King, E. I. 1981. **A three dimensional scalar potential field solution and its application to the turbine generator end region.** IEEE Transactions on Power Apparatus and Systems **PAS-100**, 5, p. 2302-2310.

Ito, K. et al. 1980. **Simulation for design purposes of magnetic fields in turbine-driven generator end region.** IEEE Transactions on Power Apparatus and Systems **PAS-99**, 4, p. 1586-1596.

Ito, M. et al. 1981. **Analytical model for magnetic field analysis of induction motor performance.** IEEE Transactions on Power Apparatus and Systems **PAS-100**, 11, p. 4582-4590.

Konrad, A. 1982. **Integrodifferential finite element formulation of two-dimensional steady-state skin effect problems.** IEEE Transactions on Magnetics **MAG-18**, 1, p. 284-292.

Laursen, M. E. and Gellert, M. 1978. **Some criteria for numerically integrated matrices and quadrature formulas for triangles.** International Journal for Numerical Methods in Engineering **12**, 1, p. 67-76.

Lawrenson, P. J. 1970. **Calculation of machine end-winding inductances with special reference to turbogenerators.** Proceedings of IEE **117**, 6, p. 1129-1134.

Luomi, J. 1984. **Magnetic field analysis of superconducting homopolar machines.** Helsinki, Acta Polytechnica Scandinavica, Electrical Engineering Series No. 53. 109 p.

Luomi, J., Niemenmaa, A. and Arkkio, A. 1986. **On the use of effective reluctivities in magnetic field analysis of induction motors fed from a sinusoidal voltage source.** Proceedings of ICEM 86. München, 8-10 September 1986. Technische Universität München, Universität der Bundeswehr München. Vol. 2, p. 706-709.

Melcher, J. R. 1981. **Continuum Electromechanics.** Cambridge, Massachusetts, The MIT Press. 610 p.

Nakata, T. and Takahashi, N. 1982. **Direct finite element analysis of flux and current distributions under specified conditions.** IEEE Transactions on Magnetics **MAG-18**, 2, p. 325-330.

Niemenmaa, A. 1986. **The use of a complex valued vector potential in the numerical solution of magnetic fields of induction motors.** Master of Science thesis, Helsinki University of Technology, Faculty of Electrical Engineering, 51 p. (In Finnish)

Nyamusa, T. A., Demerdash, N. A. and Nehl, T. W. 1986. **An accelerated Newton-Raphson technique for finite element analysis of magnetic fields in electrical machines.** IEEE Transactions on Energy Conversion **EC-1**, 3, p. 122-128.

Reece, A. B. J. and Pramanik, A. 1965. **Calculation of the end-region field of a.c. machines.** Proceedings of IEE **112**, 7, p. 1355-1368.

Reichert, K., Freundl, H. and Vogt, W. 1976. **The calculation of forces and torques within numerical magnetic field calculation methods.** Proceedings of COMPUMAG. Oxford, 31 March - 2 April 1976. Rutherford Laboratory. p. 64-73.

Richter, R. 1954. **Elektrische Maschinen**, Vol. 4, Die Induktionmaschinen. 2nd Edition, Stuttgart, Verlag Birkhäuser. 440 p.

Shen, D. et al. 1985. **Solution of magnetic fields and electrical circuits combined problems.** IEEE Transactions on Magnetics **MAG-21**, 6, p. 2288-2291.

Shen, D. and Meunier, G. 1986. **Modelling of squirrel cage induction machines by the finite elements method combined with the circuits equations.** Proceedings of the International Conference on Evolution and Modern Aspects of Induction Machines. Torino, 8-11 July 1986. Associazione Elettrotecnica ed Elettronica

Italiana. p. 384-388.

Sikora, R., et al. 1986. **Magnetic field computation in the end-region of electric machines using various boundary conditions on iron surfaces.** IEEE Transactions on Magnetics **MAG-22**, 3, p. 204-207.

Silvester, P., Cabayan, H. S. and Browne, B. T. 1973. **Efficient techniques for finite element analysis of electric machines.** IEEE Transactions on Power Apparatus and Systems **PAS-92**, 4, p. 1274-1281.

Strangas, E. G. and Theis, K. R. 1985. **Shaded pole motor design and evaluation using coupled field and circuit equations.** IEEE Transactions on Magnetics **MAG-21**, 5, p. 1880-1882.

Strangas, E. G. 1985. **Coupling the circuit equations to the non-linear time dependent field solution in inverter driven induction motors.** IEEE Transactions on Magnetics **MAG-21**, 6, p. 2408-2411.

Tandon, S. C., Armor, A. F. and Chari M. V. K. 1983. **Nonlinear transient finite element field computation for electrical machines and devices.** IEEE Transactions on Power Apparatus and Systems **PAS-102**, 5, p. 1089-1096.

Vogt, K. 1983. **Elektrische Maschinen, Berechnung rotierender elektrischer Maschienen.** 3rd Edition, Berlin, VEB Verlag Technik. 500 p.

Wallenius, A. 1983. **Computation of the magnetic field and the iron losses of an induction motor using the finite element method.** Master of Science thesis, Helsinki University of Technology, Faculty of Electrical Engineering, 49 p. (In Finnish)

Weiss, J. and Csendes, Z. J. 1982. **A one-step finite element method for multiconductor skin effect problems.** IEEE Transactions on Power Apparatus and Systems **PAS-101**, 10, p. 3796-3803.

Williamson, S. and Ralph, J. W. 1982. **Finite-element analysis for nonlinear magnetic field problems with complex current sources.** IEE Proceedings A **129**, 6, p. 391-395.

Williamson, S. and Ralph, J. W. 1983. **Finite-element analysis of an induction motor fed from a constant-voltage source.** IEE Proceedings B **130**, 1, p. 18-24.

Williamson, S. and Begg, M. C. 1985. **Analysis of cage induction motors - A combined fields and circuits approach**. IEEE Transactions on magnetics **MAG-21**, 6, p. 2396-2399.

Zienkiewicz, O. C. 1983. **The finite element method**. 3rd Edition, New York, McGraw-Hill. 787 p.

APPENDIX A. ROTATING CONDUCTING CYLINDER IN A TRANSVERSE MAGNETIC FIELD

Let us consider a circular cylinder having thin conducting walls and rotating around its axis at the mechanical angular frequency Ω_m in a transverse magnetic field. The time variation of the magnetic field observed in a stationary coordinate system is sinusoidal at the angular frequency ω. The magnetic field induced by the currents in the cylinder and by exterior sources can be derived from a complex vector potential $\underline{\mathbf{A}}$

$$\mathbf{A} = \sum_{n=-\infty}^{\infty} \left\{ \underline{A}_n(r)\, e^{-j(np\varphi - \omega t)} \right\} \mathbf{e}_z = \underline{A}(r,\varphi,t)\, \mathbf{e}_z \tag{A1}$$

where r and φ are the cylindrical coordinates

t is time

$\underline{A}_n(r)$ is a complex r-dependent Fourier-coefficient

$\mathbf{e}_z$ is the unit vector parallel to the axis of the cylinder.

The coefficient p in Eq. (A1) corresponds to the number of pole pairs in the analysis of electrical machines. Periodic symmetry in the azimuthal direction is associated with this parameter. If there is no periodic symmetry, p is equal to 1.

If the ends of the cylinder are assumed to be perfectly short circuited, the electric field strength $\underline{\mathbf{E}}'$ in the cylinder is

$$\underline{\mathbf{E}}' = -\frac{\partial \underline{\mathbf{A}}'}{\partial t} - \nabla \underline{\Phi}' = -\frac{\partial \underline{\mathbf{A}}'}{\partial t} \tag{A2}$$

where $\underline{\Phi}'$ is the scalar potential. The quantities in Eq. (A2) are observed and the differentiations are made in the rotating coordinate system fixed to the cylinder. The term on the right hand side of Eq. (A2) can be expressed with the aid of the quantities observed in the stationary coordinate system

$$\frac{\partial \underline{\mathbf{A}}'}{\partial t} = \frac{\partial \underline{\mathbf{A}}}{\partial t} + (\mathbf{v} \cdot \nabla)\, \underline{\mathbf{A}} \tag{A3}$$

where $\mathbf{v}$ is the velocity of the cylinder wall. The electric field induces a current density according to Ohm's law

$$\underline{\mathbf{J}} = \sigma \underline{\mathbf{E}}' = -\sigma \frac{\partial \underline{\mathbf{A}}'}{\partial t} \tag{A4}$$

where σ is the conductivity of the cylinder. The velocity of the cylinder wall written in circular cylindrical coordinates is

$$\mathbf{v} = \Omega_m \, r \, \mathbf{e}_\varphi = (1 - s) \frac{\omega}{p} r \, \mathbf{e}_\varphi \tag{A5}$$

The velocity has been expressed as a function of the slip s, the angular frequency ω and the number of pole pairs p as is the habit in the analysis of electrical machines. When Eqs. (A3), (A5) and (A1) are substituted in Eq. (A4), the equation of the current density becomes

$$\begin{aligned} \underline{\mathbf{J}} &= \sigma \left\{ -\frac{\partial \underline{\mathbf{A}}}{\partial t} - (1 - s) \frac{\omega}{p} \frac{\partial \underline{\mathbf{A}}}{\partial \varphi} \right\} \mathbf{e}_z \\ &= \sigma \left\{ -js\omega \, \underline{\mathbf{A}} + j\omega (1 - s) \sum_{n=-\infty}^{\infty} (n - 1) \, \underline{A}_n(r) \, e^{-j(np\varphi - \omega t)} \right\} \mathbf{e}_z \end{aligned} \tag{A6}$$

In the pseudostationary approximation the equation for the current density is

$$\underline{\mathbf{J}}_{ps} = -j \sigma s \omega \underline{\mathbf{A}} \tag{A7}$$

Comparison between the equations (A6) and (A7) shows that the pseudo-stationary approximation gives the right current density only when the slip is equal to one (stationary cylinder). If the magnetic field consists of the first harmonic component only, Eq. (A7) gives the right current density at all values of the slip.

The torque acting on the cylinder is obtained from the equation

$$\mathbf{T} = \int_V [\mathbf{r} \times (\mathbf{J} \times \mathbf{B})] \, dV = r \, \Delta r \, l \int_0^{2\pi} J \frac{\partial A}{\partial \varphi} \, d\varphi \, \mathbf{e}_z \tag{A8}$$

where Δr is the wall thickness of the cylinder and l is the length of the cylinder. After the substitutions the average value of torque is obtained from the equation

$$\mathbf{T}_{av} = \pi \sigma \omega p \, \Delta r \, l \, r \sum_{n=-\infty}^{\infty} \left\{ [1 - (1 - s) \, n] \, n \, \underline{A}_n \, \underline{A}_n^* \right\} \mathbf{e}_z \tag{A9}$$

where $\underline{A}_n^*$ is the complex conjugate of $\underline{A}_n$. The torque of the pseudostationary approximation is

$$T_{ps\,av} = \pi \sigma \omega p \Delta r\, l\, r\, s \sum_{n=-\infty}^{\infty} (n \underline{A}_n \underline{A}_n^*) e_z \qquad \text{(A10)}$$

The pseudostationary approximation gives the right value of torque only when the slip is equal to one.

The derivations given above are also valid for solid conducting cylinders of magnetically linear materials. The torque equations (A9) and (A10) must be integrated over the volume of the cylinder.